INNOVATIVE COMPOSITE MATERIAL PRODUCTION, RARE EARTH ELEMENT AND RECYCLING OF INDUSTRIAL WASTE



EDITORS

Prof. Dr. Şeref TURHAN

Prof. Dr. Aybaba HANCERLIOGULLARI

Assoc. Prof. Dr. Mehmet AKKAŞ

DUVAR

INNOVATIVE COMPOSITE MATERIAL PRODUCTION, RARE EARTH ELEMENT AND RECYLING OF INDUSTRIAL WASTE

Editors

Prof. Dr. Şeref TURHAN

Prof. Dr. Aybaba HANÇERLİOĞULLARI

Assoc. Prof. Dr. Mehmet AKKAŞ

Innovative Composite Material Production, Rare Earth Element and Recyling of Industrial Waste
Editors: Prof. Dr. Şeref TURHAN, Prof. Dr. Aybaba HANÇERLİOĞULLARI Assoc. Prof. Dr. Mehmet AKKAŞ

Editor in chief: Berkan Balpetek
Cover and Page Design: Duvar Design
Printing: November-2025
Publisher Certificate No: 49837
ISBN: 978-625-8734-21-8

853 Sokak No:13 P.10 Kemeraltı-Konak/İzmir
Tel: 0 232 484 88 68
www.duvaryayinlari.com
duvarkitabevi@gmail.com

TABLE OF CONTENTS

Chapter 1

PROPERTIES, ENRICHMENT, APPLICATION FIELDS AND INDUSTRIAL RESOURCES OF RARE EARTH ELEMENTS

Aybaba HANÇERLİOĞULLARI[1], Şeref TURHAN[2], Aslı KURNAZ[3]

1. INTRODUCTION

Rare Earth Elements (REEs) have become the unseen driving force of modern technology. They are used in the production of high-tech products that are resistant to high temperatures, abrasion, and corrosion. They are listed as critical raw materials due to their high economic value and the risk of supply [1]. The word "rare" actually refers to the fact that these elements are generally found dispersed in low concentrations and are chemically very similar, making separation difficult and costly. They require environmentally polluting mining and refining processes. REEs consist of the lanthanide series with atomic numbers 57-71 (15 metallic elements), as well as yttrium (Y) and scandium (Sc). They are strategically important in everything from electric vehicles and wind turbines to nuclear reactors and medical imaging systems. REEs are essential components in more than 200 products across a wide range of applications, including computer hard drives, mobile phones, electric and hybrid vehicles, and high-tech consumer products such as flat-screen monitors and televisions. Important defense applications for REEs include electronic displays, guidance systems, lasers, radar, and sonar systems. While the amount of REE used in such technological and electronic products may not constitute a significant portion of the product by weight, value, or volume, it is essential for the device's operation. REEs dont occur naturally as elements in the Earth's crust and are found in mineral forms such as phosphates, silicates, carbonates, oxides, and halides. The primary economic sources of REEs are the minerals bastnasite, monazite, and loparite, as well as lateritic ion-sorption clays. Due to the 4f orbitals in their electron configurations, they exhibit high magnetic

[1] Prof. Dr., Department of Physisc/Faculty of Science, Kastamonu University, Turkey, serefturhan63@gmail.com, (ORCID: 0000-0000-1700-8480)
[2] Prof. Dr., Department of Physisc/Faculty of Science, Kastamonu University, Turkey, aybaba@kastamonu.edu.tr, (ORCID:0000-0005-5303-3680)
[3] Prof. Dr., Department of Physisc/Faculty of Science, Kastamonu University, Turkey, akurnaz@kastamonu.edu.tr, (ORCID: 0000-0002-7910-3461)

moment, luminescence, catalytic activity, and alloy strength properties [2]. REEs hold a significant place globally and also encompass future policies in the context of a sustainable circular economy in our country. The high-technology and energy applications of the REEs have increased significantly in diversity and importance since the 1960s. Furthermore, because many of these applications are highly specific and substitutes for REEs are of lower quality or unknown, REEs have acquired a much greater technological importance than might be expected from their relative obscurity. Despite being more abundant than similar industrial metals, rare earth elements are less likely to be concentrated in exploitable ore deposits. As a result, most of the world's REEs supply comes from just a few sources that can be depleted within a short timeframe. For example, the United States generally had a sufficient REE supply for a decade, but has since become dependent on imports from China, changing the strategic landscape. Some REEs are currently used to generate electricity in nuclear power reactors. Many of the popular rare earth oxides with significant mercial, industrial, space, and defense applications are identified, including the following [3,4]. Common rare earth isotopes and applications of rare earth oxides, alloys, and compounds; yttrium oxide (Yb_2O_3), cerium oxide (Ce_2O_3), dysprosium oxide (Dy_2O_3), gadolinium oxide (Gd_2O_3), lanthanum oxide (La_2O_3), europium oxide (Eu_2O_3), neodymium oxide (Nd_2O_3), praseodymium oxide (Pr_2O_3), samarium oxide (Sa_2O_3) [3,5-8]. It shows that Turkey can be not only a raw material but also a strategic technology producer. In our study, we particularly aim to define the physical and chemical properties of REEs, explain the enrichment methods, reveal the recovery potential in industrial wastes and propose a sustainable model with environmental, economic and strategic aspects [6-10]. As a result of the experimental studies carried out with the physical, chemical and magnetic properties of REEs, high amounts of La, Ce, Nd, Sm and Dy were detected in waste materials such as phosphogypsum, redmud and fly ash

2. PROPERTIES AND USAGE AREAS OF REEs

REEs are a group of elements that are of extreme strategic importance in terms of industry, technology, and defense. REEs are known as lanthanides. These are La, Ce, Pr, Nd, Pm, Sm, Eu, Gd, Tb, Dy, Ho, Er, Tm, Yb, Lu, Sc and, Y. REEs are distinguished by their physical, chemical, and magnetic properties. They are silvery-gray in color, ductile, and malleable. Density varies between 5.0 and 9.3 g/cm³. Gd behaves ferromagnetically, while Dy and Tb are paramagnetic. Their melting points range from 800 to 1660 °C. They are generally in the (+3) oxidation state, which is explained by the decreasing ionic radius as we progress through the

series. The order of reactivity is ranked as La > Ce > Nd > Gd. The order of solubility is listed as HCl > HNO_3 > H_2SO_4. Their Curie temperatures are 293 K (Gd), 219 K (Tb), 88 K (Dy). Eu^{3+} and Tb^{3+} ions have high luminescence efficiency. They readily react with oxygen in the air to form oxides, which have high electrical and thermal conductivity. They are moderately dense and soft, with moderate density and hardness, and are easily processed. Rare earth elements are the fundamental building blocks of high technology and the defense industry. Due to their strong magnetic, optical, nuclear, and chemical properties, they are used in a wide range of applications. They are strategic resources for the global economy and geopolitical balances. REEs are quite difficult to separate. The difference in ionic radius is only 2–3%. They are divided into light and heavy groups. Commercial applications and uses of rare earth elements are summarized in Table 1 [9,1,17]. REEs are widely used in nuclear power reactors, aerospace systems and components, jet engines, scramjets, battery electrodes for high-power batteries, and many other aerospace products. Samarium-cobalt magnets are most suitable for high-power radio frequency sources and microwave filters [4,9,13,17]. Yttrium-iron-garnet filters are widely used in satellite and airborne systems, where a sharp cutoff frequency, minimal pass-band loss, and high attenuation in the stop-band region are key design requirements. High-performance diode-pumped solid-state infrared lasers use rare earth elements such as holmium, thulium, yttrium, and erbium to achieve superior laser performance at infrared frequencies.

Table 1. Examples of commercial products utilizing rare earth element

REE	Commercial product
Neodymium (Nd), praseodymium (Pr), terbium (Tb) dysprosium (Dy)	Mobile phones, computer hard drives, cameras
Nd, Pr, Dy, La, Ce	Hybrid electric vehicles, high-capacity batteries, infrared lasers
Eu, Y, Tb, La	Energy-efficient light bulbs
Ce, La, Neodymium (Nd), Eu	Glass additives
Eu, Y, Er	Fiber-optic lines, fiber-optic amplifiers
Promethium (Pm)	Portable x-ray equipment
Scandium (Sc)	High-intensity flood lights for stadiums
Samarium (Sm)-cobalt (Co)	Permanent magnets for electric motors, widely deployed in hybrid electric vehicles

REE are considered strategic elements due to their use in many different sectors inthe production of advanced technological materials resistant to high temperatures, abrasion, and corrosion [1,5,6]. NdFeB (Neodymium-iron-boron) magnets, in particular, are the backbone of modern green technologies. NdFeB magnets are used in wind turbines due to their high energy density. In PV/T systems with CO_2 doping, the electrical efficiency has increased by 11% and the thermal efficiency by 14%. $LaNi_5$ alloys increase the cycle life of Li-ion batteries to 2400 cycles. Dy and Tb elements provide high temperature resistance. Sc-doped aluminum alloys offer both lightness and strength in aircraft fuselages [9]. Gd-based contrast agents are used in MRI; Sm-153 and Lu-177 isotopes are used in cancer treatment [13]. CeO_2 nanoparticles have antioxidant and antimicrobial properties. Table 2 lists the main reserves by some countries [14].

Table 2. World REE reserves and production amounts [14-16]

Country	Reserve (REO) (million tons)	Global share approx (%)
China	44	49
Brazil	21	23
India	6.9	7.7
Australia	3.4	3.8
Russia	6.0	6.7
Vietnam	3.5	3.9
USA	2.0	2 0

3. SECONDARY RESOURCES AND ENRICHMENT PROCESSES OF RREs

REEs can be obtained not only from primary sources extracted from the ground but also from various secondary sources. With regard to REEs, examining their secondary sources (recycling, tailings, etc.) and enrichment processes (separation and purification techniques from the ore) is crucial for both economic value and the valorization of industrial wastes. The recovery of REEs from secondary sources is the most important step in sustainable mining. The main secondary sources of REEs are red mud, phosphogypsum, coal fly ash, blastfurnace slag, and electronic waste. Türkiye [3,12]. Economic recovery of REEs from secondary sources is given in Table 3. Furthermore, Table 4 shows the comparative characteristics of secondary by-products by waste type. The recovery of these wastes both reduces the environmental burden and creates

economic value [11,15]. China accounts for 60% of global production, followed by the US, Australia, and Myanmar [14]. The Critical Raw Materials Act, published by the European Commission in 2024, classified REEs as elements at high risk of strategic dependency. Turkey's waste stock potential is worth approximately 1.8 billion USD/year [16]. Utilizing these resources reduces both environmental risks and import dependency. The enrichment processes for REEs generally include hydrometallurgical, acid (HCl, H_2SO_4) dissolution, ion exchange, and solvent extraction. REEs do not occur in nature as pure metals; they are generally carbonate, silicate, phosphate, or oxide minerals. Therefore, reserve, production, and commercial values are given in oxide equivalents (REOs) rather than pure metals. For example, 1000 tonnes of Nd_2O_3 is the REO equivalent of the rare earth element neodymium. REO is a technical term used to indicate the amount of rare earth elements in their oxide form. Production and reserve data are generally given in oxide equivalents because this form is the most common in nature and the most stable and measurable form used commercially. Generally, by country, China is reported to produce approximately 270,000 tonnes of REO equivalent in 2024, while the US is estimated to produce approximately 45,000 tonnes. These figures clearly demonstrate China's dominant position in global production.

Table 3. Economic recovery of REEs / secondary sources [4-6,17,22]

Source	REE_2O_3 (%)	Major Elements	Method	Economic Value (USD/t)
Red mud	0.10–0.30	La, Ce, Nd	H_2SO_4 leaching + ion exchange	1750
Phosphogypsum	0.05–0.20	Ce, La, Sm	HCl leaching + Cyanex 272	1200
Coal fly ash	0.05–0.10	Nd, Dy	Na_2CO_3 leaching	900
NdFeB (magnet)	25–30	Nd, Dy, Sm	Mechanical + bioleaching	25000

Secondary by-products (wastes) generated during the extraction of REEs or similar industrial processes can pose serious environmental problems. In some cases, these wastes can be recycled and utilized. Three important secondary byproducts in this context are as follows. General principles for environmental management strategies include: source reduction; reduction of waste production

(process optimization); waste characterization; identification of risks through chemical analysis; storage management; red mud should not be stored directly without neutralization; phosphogypsum requires radioactive monitoring; and fly ash should be stored in a closed environment due to the risk of dust generation. However, leaching, water pollution, and soil impact must be continuously monitored for reuse/recycling, waste recycling through the aforementioned practices, and monitoring and control.

Table 4. Comparative characteristics of REE by-products [7-15,23- 26]

	Red Mud	Phosphogypsum	Coal Fly Ash
Source	Aluminum production (Bayer)	Phosphoric Acid Production	Thermal power plants (Coal)
Chemical structure	Fe_2O_3, Al_2O_3, TiO_2, Na_2O	$CaSO_4 \cdot 2H_2O$, F^-, U, Th	SiO_2, Al_2O_3, CaO, Fe_2O_3
pH	11–13 (very basic)	5–7 (neutral-acid)	8–9 (slightly basic)
Physical Structure	Muddy, fine-grained	Powdery, moist,	Lumpy very fine, spherical particles
Color	Red /Brown	White / Gray / Yellow	Gray
REE Potential	Scandium, yttrium	Thorium, uranium, REE	Lanthanides, cerium etc.
Environmental Risk	Alkali hazard	Radioactivity	Heavy metal leakage

The choice of each method depends on the type of waste and economic/environmental factors. Common mechanisms for recovering REEs from red mud, phosphogypsum, and fly ash include

a) *Acid leaching:* waste is treated with strong acids (usually sulfuric, nitric, or hydrochloric). The acid dissolves the REEs, allowing them to pass into the liquid phase. The resulting solution is further processed to separate the REEs.

b) *Alkaline leaching*: Some wastes, especially red mud, are treated with alkali (e.g. sodium hydroxide) to solubilize the REEs.

c) *Precipitation and solvent extraction*: REEs are purified from the solutions

obtained after acid or alkaline leaching by precipitation (e.g., oxalate or carbonate precipitation) or solvent extraction.

d) *Ion exchange resins:* REEs can be separated and collected using resins that selectively retain REEs in solution.

e) Pyrometallurgical methods: REEs can be separated from the waste matrix by high-temperature melting or thermal treatments.

3.1 Red Mud

Its source is formed as a result of the Bayer process used in the production of aluminum from bauxite ore. In this process, rare earth elements can also be found in bauxite and migrate to the red mud. Its properties; high alkalinity (pH > 12), it can contain iron oxide, titanium dioxide, alumina and trace amounts of REE, it is very fine grained and has a mud consistency. In terms of REE potential, it may contain scandium, cesium, yttrium. Recovery studies are being carried out for this by-product. It is the waste generated during the production of aluminum oxide (Al_2O_3) from bauxite ore by the Bayer process during the formation process, bauxite is digested with sodium hydroxide (NaOH); insoluble residues are separated, this residue is called red mud. In terms of chemical properties, the content of red mud as the main components is Fe_2O_3 (iron oxide); 30-60%, Al_2O_3 (alumina), 10-20%, TiO_2 (titanium dioxide); 2-10%, SiO_2 (silicon dioxide); 3-50%, Na_2O (sodium oxide); 2-10% (alkaline). Its pH value is quite high and poses an environmental riskIn terms of physical properties, red mud has reddish-brown (high iron oxide) color tones. Structurally and geometrically, it is fine-grained and muddy, and can turn into powder when dried over time. Its material density is in the range of 2.7–3.3 g/cm³. After processing, its content is around 20-30%. It may contain trace amounts of rare earth elements such as scandium and yttrium, and may also deteriorate soil and water quality due to its sodium content [4-10,22-30]. Let me explain the recycling (utilization) methods of wastes such as red mud, phosphogypsum and coal fly ash, as well as the recovery technologies and environmental management strategies of REE; the areas of use of red mud are especially cement production (additive material thanks to its Fe_2O_3, Al_2O_3, TiO_2 content), road filling, brick production, soil improvement (by neutralization), iron recovery (by pyrometallurgical methods. In terms of REE recovery methods, acid leaching uses sulfuric acid (H_2SO_4) or nitric acid (HNO_3) to dissolve REEs. It is the most common method, especially effective for scandium. Pressure leaching provides more efficient REE recovery under high temperature and pressure. Ion exchange and solvent extraction separate REEs from the acid solution.

3.2 Phosphogypsum

Its source is formed as a byproduct during the production of phosphoric acid by treating phosphate rocks with sulfuric acid. Based on calcium sulfate, it can contain the radioactive elements uranium and thorium and is generally stockpiled or discarded in large quantities. Regarding its REE potential, it can contain trace amounts of thorium and other REEs. Although REE recovery for this byproduct is challenging, research is ongoing. Phosphoric acid (PA) is an environmental waste and an important industrial chemical used as an intermediate in the fertilizer industry, in metal surface treatment in the metallurgical industry, and as an additive in the food industry. The use of phosphate compounds in the detergent industry is significantly restricted. In terms of its formation process, it is formed as a byproduct in the production of phosphoric acid by treating phosphate rocks with sulfuric acid. It is usually stored in large piles, and its recovery and use are limited due to radioactivity, making it of limited use in construction, road construction, and agriculture. Phosphogypsum is obtained by chemical reaction as follows;

$$Ca_5(PO_4)_3F + 5H_2SO_4 + 10H_2O \rightarrow 3H_3PO_4 + 5CaSO_4.2H_2O + HF$$

where $CaSO_4 \cdot 2H_2O$, namely phosphogypsum, is the waste of the process. In terms of chemical properties, the main component is calcium sulphate dihydrate ($CaSO_4 \cdot 2H_2O$) 85–95% and in terms of other contents, it contains P_2O_5, F^- (fluorine), heavy metals (Cd, As, Pb, Hg). In terms of radioactive elements, it has trace amounts of U, Th, Ra-226 [1-9,23,24]. In terms of physical properties, they are light gray, white, or slightly yellow. In terms of mechanical and structural geometry, phosphogypsum generally has a lumpy structure with a powder-clay consistency. Its material density is in the range of 2.3–2.4 g/cm³, and its moisture content is generally high (20–30%). However, with increasing storage time, it can harden over time. Let me explain in detail the recycling methods, REE recovery technologies, and environmental management strategies for phosphogypsum waste. In terms of its uses, it is used in agriculture as a soil conditioner and source of calcium sulfate. In the construction sector, it is used as a drywall, cement additive, road base filler, and also as a mine drainage control. Recycling in terms of REE method is carried out as follows; thorium, uranium and trace REEs can be recovered by precipitation method but the economic efficiency is low and the process is complicated due to radioactivity. Bioleaching (digestion with bacteria) method is being studied as a new method. REE recovery is shown in Table 5. Final product characterization of phosphogypsum is done by XRF, ICP-MS, and ICP-OES [13-24,26].

3.3 Coal Fly Ash

Its source is a by product of the burning of coal in thermal power plants. It is in fine particle form and collected from chimneys by electrostatic filters. Its properties include silica, alumina, iron oxide, and it has a light, glassy structure. Some coals may contain REEs and other heavy metals. In terms of REE potential, trace amounts of elements such as yttrium, lanthanum, and cerium can be found, and various solutions for their recovery are being investigated. The formation process is fine particles formed by the combustion of coal in thermal power plants, and after combustion, they are collected from chimneys by electrostatic filters. In terms of chemical properties and main components, SiO_2 (silicon dioxide) 40-60%, Al_2O_3 (alumina) 20-30%, Fe_2O_3 (iron oxide) 4-10%, CaO (calcium oxide) and 5-20% (high calcium ash), and also the Ph is slightly basic (8-9) and in terms of heavy metals (As, Pb, Cr), Comparative properties of secondary by-products of REEs (lanthanides, scandium, etc.) are shown in Table 3 in terms of waste type. In terms of mechanical structure, it contains spherical, glassy particles with a very fine grain (cement-like) density of 2.1–2.6 g/cm³ and a particle size of around 1–100 μm. It exhibits pozzolanic properties and can harden like cement by reacting with water and calcium hydroxide. It is widely used in concrete and building materials. It may contain trace amounts of rare earth elements. Let me explain the recycling (recycling) methods for wastes such as coal fly ash, as well as REE recovery technologies and environmental management strategies. In terms of its applications, fly ash is used as an additive in cement and concrete, and its pozzolanic properties increase durability. It can be used in road fills, dam fills, the ceramic and glass industries, and those with high carbon content in carbon capture systems. In terms of REE recovery methods; acid leaching: REEs such as lanthanides (La, Ce, Nd, Pr) and cerium are dissolved using H_2SO_4, HCl. Froth flotation and concentration methods are applied. Thermal treatments leaching method is also used to break the glass phase and release the elements [4-9,23-29]. Some images of the REE minerals formed are shown in Figure 1 [1,6].

Figure.1 Visual of main REE minerals [1,4,22]

REEs show their existence in the Earth's surface at various stages in terms of geological processes. Igneous processes; the condensation of ree during the crystallization of magma; hydrothermal processes; the movement of hot fluids through rocks and the accumulation of ree in veins; metamorphic processes; ree are mobilized and re-condensed during rock metamorphism. Sedimentary processes; weathering, erosion and deposition; ree concentrate in sedimentary environments. Lateritic processes; intense weathering in tropical climates enriches ree in residual soils [1,9,23-28]. REEs are currently commercially extracted from hard rock, typically bastnäsite or monazite, marine placers, and ionic clays. Hard rock ores above grade 5 must be ground in a closed-circuit using screens or mechanical classifiers that separate liberated grains before over-grinding occurs. Over-grinding wastes energy and can also reduce the recovery of brittle minerals that can be ground too finely for efficient enrichment. The ore is often "de-sluiced," a step that typically involves mechanical washing to break up small particle aggregates. Heavy mineral sands from both old and fresh placer deposits may require feed preparation such as abrasion washing and de-sluicing, but comminution is not necessary. Figure 2 is a simplified diagram of the REE ore process, illustrating the processing of REE Significant academic research and moderate commercial process innovations in REE processing have been ongoing for decades. The largest demand for rare earth elements in the global market comes from the Chinese economy. With changing living conditions, demand for rare earth elements is likely to increase depending on developments [7]. The last few years have seen exponential growth in research due to the increasing demand for REE, threatened by supply risks and environmental barriers [3,16-20,23-28]. Some of the standard

measuring instruments listed in Table 6 can be used in laboratory analyses of REEs [6-12,30].

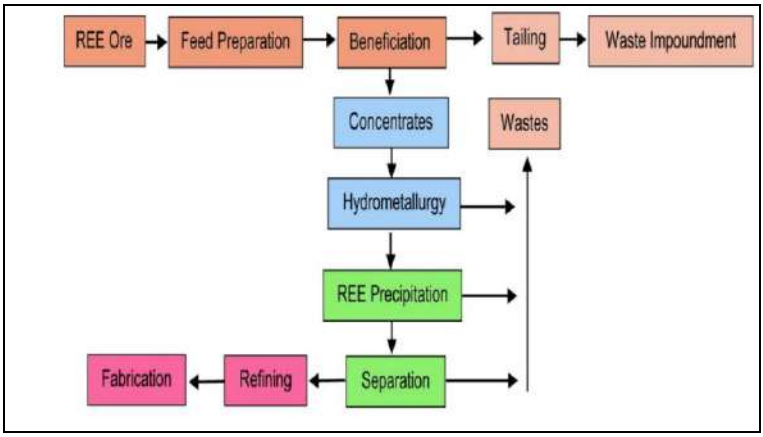

Figure 2 Processing of rare earth element ores [18-25,31]

Table.5 Rare earth elements (REE) recovery [1,4,5,18]

Waste type	Recyclable materials	Recycling methods	Environmental risks
Red Mud	Alumina, Iron, TiO_2, SC, Y	Acid Leaching, Pyrometallurgy	High alkalinity
Phosphogypsum	$CaSO_4$, Thorium, Uranium, RREs	Acid Leaching, Biolixiviation	Radioactivity, fluoride leakage
Fly Ash	SiO_2, Al_2O_3, lantanitler	Acid Leaching, Thermal Activation	Dust contamination, heavy metal

5. CONCLUSION AND DISCUSSION

One of the biggest challenges associated with REE mining and processing is that all deposits contain Th and U, but in lower concentrations in ionic clays. On-site disposal options are generally limited and subject to strict regulations [5,6,18-24]. REE is a key component in technology and industry, including hydrogen storage, superconductivity, photovoltaic conversion, and nuclear neutron control systems. NdFeB magnets provide a 25% higher energy density in wind turbines. Waste-based REE production could generate an annual economic gain of $400–500 million. Carbon emissions are reduced by 60% [16-24,31]. Significant support should be provided to individuals working in this field at the Turkish REE Technology Institute and universities, and advanced

research centers should be established. Microorganism genetics should be investigated for biotechnological processes. Artificial intelligence-supported process optimization models should be developed. Turkey's REE policy should be planned in three stages: short-term (2025-2030), a waste inventory should be created, and an REE-TR database should be created. medium-term (2030-2035), pilot facilities (Bandırma, Seydişehir) should be established. R&D clusters should be established through university-industry collaboration. long-term (2035-2045). Entirely domestic REE refining facilities, NDFEB, and SMCO alloy production lines should be established. AI-based enrichment software should be used. Scientific studies indicate that Türkiye has the potential to produce 9,000 tons of REE annually from its red mud, phosphogypsum, and fly ash reserves. This amount could cover 70% of the country's REE imports. It is known that consumption in developed countries will increase in parallel with REE production in the coming years. The evaluation of discovered deposits is increasing according to the supply-demand balance in the global market. In our country, the evaluation of REE in recent years, particularly in the Eskişehir-Beylikova Basin in the Central Anatolia region, has been reported by the MTA as having potentially significant reserves.

REFERENCES

1. Celep, O., Yazıcı, E. Y., & Deveci, H. (2021). Production of rare earth elements from primary and secondary sources. *Gümüşhane University Journal of Science*, 11(1), 264-280.
2. Bünzli, J. C. G. (2022). Handbook on the physics and chemistry of rare earths. 34, *Elsevier*.doi: 10.1016/S0168-1273(04)34006-7
3. MTA (2023). *Türkiye Rare Earth Elements Potential Report*, general directorate of mineral research and exploration, Ankara.
4. Turkish Ministry of Energy (2024).
5. Zdzisław A.(2024).Distribution of rare earth elements in ash from lignite combustion in polish power plants, *Materials* 17(18), 4477.
6. I.M.S.K. Ilankoon, N.P. Dushyantha, N. et al. (2022). Constraints to rare earth elements supply diversification: Evidence from an industry survey, *Journal of Clearner Production,* 331, 10.
7. M. Schlumbohm, L. Muñoz-Giraldo, E. Barth, J.,at al.(2021).Statista Global *Business Cities Report 2021* (Statista, Hamburg, Germany)
8. McCarthy, G. I. & Rhyne, J.J. (1977). The Rare Earths in Modern Science and Technology, *New York: Plenum Press*, USA.
9. Kim, J., & Lee, D. (2022). Microstructural behavior of Sc and Y reinforced aluminum alloys for aerospace applications. *Materials Science and Engineering A*, 846, 143404. https://doi.org/10.1016/j.msea.2022.143404
10. K.R. Long, B.S. Van Gosen, N.K. Foley, D. Cordier, The Principal Rare Earth Ele ments Deposits of the United States: A Summary of Domestic Deposits and a Global Perspective (*US Geological Survey Scientific Investigations Report* 2010-5220,
11. VA, (2010), U.S. Geological Survey, *Reston* , 96
12. Yang, X., Zheng, Y., Le Bas, M.J. (2003). *Mineral Petrol.* 78(1–2), 93
13. Turhan, Ş., Duran, C. et al. (2023). Impact of toxic metal pollution on surface water pollution: a case study of tohma stream in sivas, Turkey. *International Journal of Environmental Analytical Chemistry*,103(14), 3224-3234.
14. USGS (2023). Mineral commodity summaries: rare earths, Washington D.C. U.S. *Geological Survey, USA.*
15. Kurnaz, A., Turhan Ş, et al. (2020). Natural radioactivity, radon emanating power and mass exhalation rate of environmental soil samples from Karabük province, Turkey., *Radiochim Acta* 108(7), 573–579.
16. OECD, (2022). Circular economy and critical raw materials: *Policy Directions. Paris: Oecd Publishing.*

17- IAEA (2022). Measurement of radionuclides in environmental samples. vienna: *International Atomic Energy Agency*

17.Jha, A. R (2014). Handbook of rare earth materials properties and applications,crp press,Taylor&FranciGroup,http://www.crppress.com.*International Standard Book*, Number-13: 978-1-4665-6403-9 .

18.IEA (2023). Global critical minerals outlook 2023. paris: *International Energy Agency.*

19 .Shulan, S. (2023) Bioleaching of rare earth elements: perspectives from mineral characteristics and microbial species, minerals13(9):1186 doi:10.3390/min13091186

20. Imperl J, Kolar M, Petrova P, Chochkova M. (2023).Mineral content Estimation of black Cumin seeds. *J Chem Technol Metall.* ,58(5),859.

21.ERMA (2024). European raw materials alliance: *Annual Report 2024*. erma@eitrawmaterials.eu, Brussels

22. J.E. Sutton, S. Roy, A.U. Chowdhury, L. Wu, A.K. at al.(2020), ACS Appl. Mater. Interfaces 15- S.B. Caster, J.B. Hedrick, (2006), Rare Earth Elements, Industrial Minerals Volume, 7th edn. *(Society for Mining, Metallurgy & Exploration, Littleton, CO, pp. 769–792 12.*

23.Balaram,V.(2022). Rare earth element deposits: sources, and exploration strategies,*Jour. Geol. Soc. India* (2022) 98:1210-121.

24.McNulty,T.(2022).Processing the ores of rare-earthelements,*Mrs.Org/Bulletin*, 47 https:// doi:10.1557/s43577-022-00288-4

25.Binnemans, K., & Van Gerven, T. (2021). Towards sustainable recovery of rare earth elements from industrial waste. *Journal of Cleaner Production,* 298, 126890.

26.Binnemans, K. (2020). Recycling of rare earths: a critical review. *Journal of Cleaner Production,* 264, 121573.

27.Wildenboer R.A & Sandenbergh R.F. (2024).Extraction of rare earth elements from phalaborwa phosphogypsum, *Journal Of The Southern African Institute Of Mining And Metallurgy*,124(10)10.

28.European Commission (2023). Report from the commıssıon to the european parlıament and the councıl Progress on competitiveness of clean energy technologies *Eu Critical Minerals Review*, Brussels.

29.B. Lehmann, Euro. *Geol.* 37, 21 (2014)

30. Imholte, D.D., Nguyen, R. T., et al. (2018).W. Collins, C.G. Anderson, B. O'Kelley, *Energy Policy* 113, 294 (2018)

31-Y. Kanazawa, M. Kamitani, J. *Alloys Compd.* 408, 1339 (2006)

Chapter 2

PERLITE MINERAL PROPERTIES AND APPLICATIONS: (Elemental Properties, Perspectives Industrial Using)

Şeref TURHAN[1], Aybaba HANÇERLİOĞULLARI[2], Aslı KURNAZ,[3] Savaş TÜRKDOĞAN[4]

1.INTRODUCTION

Minerals, naturally occurring in the Earth's crust, are homogeneous, usually solid, inorganic substances with a specific chemical composition and a regular atomic structure. Minerals have certain distinguishing properties. The best way to accurately identify a mineral is to examine its chemical composition. Rocks, on the other hand, are formed by geological processes, with multiple elements combining to form a mineral complex [1]. Mountains and continents are also formed by the aggregation of rocks. However, in rare cases, some rocks consist of only a single mineral. Turkey is a country rich in mineral diversity, and since 1939, mineral exploration has been underway [2]. More than 80 different mineral species have been discovered. Turkey is one of the world's leading producers of many minerals, particularly boron, perlite, sepiolite, chromium, trona, feldspar, graphite, barite, bentonite, and zeolite. In our study, we focused on perlite. Turkey has significant potential as a country with one of the world's leading perlite mines. Perlite is a versatile material due to its chemical and physical properties (low density, high porosity, chemical inertness, etc.) and is widely used as a filler raw material in many sectors, especially construction [3]. Perlite is a naturally occurring volcanic glass with unique physical properties, making it extremely useful in a variety of applications. Table -1 lists some of the physical and chemical properties of perlite [4-6]. Perlite is an amorphous volcanic glass with a relatively high water content, typically formed by the

[1] Prof. Dr., Department of Physisc/Faculty of Science, Kastamonu University, Turkey, serefturhan63@gmail.com, (ORCID: 0000-0005-5303-3680)
[2] Prof. Dr., Department of Physisc/Faculty of Science, Kastamonu University, Turkey, aybaba@kastamonu.edu.tr, (ORCID:0000-0000-1700-8480)
[3] Prof. Dr., Department of Physisc/Faculty of Science, Kastamonu University, Turkey, akurnaz@kastamonu.edu.tr, (ORCID: 0000-0002-7910-3461)
[4] Lecturer (Phd)., Department of Physisc/Faculty of Science, Kastamonu University, Turkey, savasturkdogan74@gmail.com,(ORCID:0009-0004-7243-7268)

hydration of obsidian. Figure -1 shows the general distribution of perlite minerals in Turkey and around the world [3].It occurs naturally and has the unusual property of expanding significantly when heated sufficiently. It is a suitable industrial mineral for use as a ceramic flux to reduce sintering temperatures and is a commercial product due to its low density after processing [5].Perlite is an amorphous volcanic glass with a relatively high water content.Mineral formations are found in nature, particularly in volcanic regions. More than 5,400 minerals have been identified worldwide, and Turkey is among the richest countries in terms of this mineral diversity. China, Turkey, and Greece lead global production, with Türkiye's share at approximately 28% [6,7]. This strengthens Turkey's mineral-material integration and strategic position in the domestic composite/insulation market. In figure-1 show that the general distribution of perlite minerals worldwide [8].

Table 1 Physical and chemical properties of perlite mineral [4].

Physical Properties		**Chemical Properties**			
Property	Value	Element composition(%)		Chemical composition(%)	
Color	white/grey	Si	33,8	SiO_2	72,08
Brightness (% GE)	70-80	Al	7,2	Al_2O_3	12,92
Density (kg/m^3)	50-300	K	3,5	TiO_2	0,90
Hardness index (mohs)	5,0-5,5	Na	3,4	Fe_2O_3	1,50
Specific gravity	2,2 - 2,4	Fe	0,6	MgO	0,63
Ph	6,0- 8.5	Ca	0,6	CaO	0,88
Water absorption, % of mass	200-600	Mg	0,2	Na_2O	3,76
Thermalconductivity, (W/m.K)	0,043-0,093	Mica	0,2	K_2O	4,33
Melting point(c°)	980	O	47,5	H_2O	3,0
Thermal diffusivity (m^2)	0,632-0,330	-	-	-	-
Humidity (%)	up to 1,0	-	-	-	-

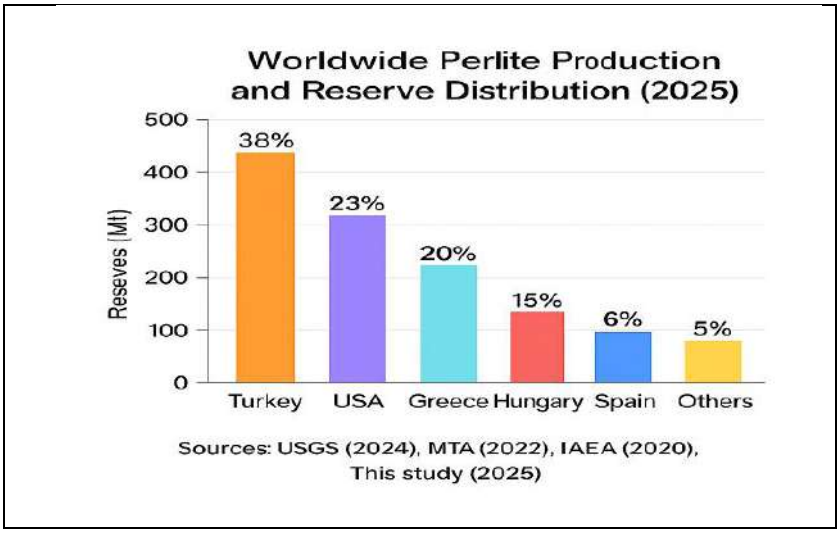

Figure 1. General distribution of perlite minerals in worldwide [8].

2. PROPERTIES AND USES OF PERLITE MINERALS

2.1 Properties of perlite mineral

Perlite mineral contains between 2% and 6% crystalline water. When the natural rock form is heated sufficiently, this water is lost and the resulting water vapor pressure causes it to expand significantly. Expanded perlite is generally known as a siliceous volcanic material that tends to expand in size when exposed to temperatures of 900 to 1200°C [9,10]. Expanded perlite, used in the production of building materials, generally has a brittle structure due to its expanded nature at high temperatures. It exhibits crumbling properties in mortar and/or dough mixtures prepared for product production, or due to the influence of other mixture components, depending on the mixing method. This causes the coarse-sized expanded perlite aggregate entering the mixture to transform into smaller aggregates within the product matrix. This reduction in expanded perlite particle size both increases the density of the material and results in a smaller than expected volume of the resulting fresh mortar. This volume reduction in mortar generally results in the use of more mortar material in the production of building materials, thus further increasing consumption. To achieve a mortar with optimal conditions and volume, the particle size, expansion temperature, and aggregate structure of the expanded perlite used in the mixture are crucial. Expanded perlite, which does not fragment or lose volume during mixing and has high aggregate strength, is critical in this regard. Panagiotopoulou and colleagues found that the crushing strength of expanded perlite aggregate increases with increasing bulk density [9,10]. However, a literature review

reveals that due to the delicate structure of expanded perlite, the changes induced by this aggregate during mixing and placement of cementitious products are poorly understood. Water trapped in the material's structure escapes by evaporation, causing the material to expand up to 7-25 times its original volume [11]. The expanded material is bright white in color due to the reflective properties of the trapped bubbles. The bulk density of unexpanded raw perlite is approximately 1100 kg/m3, while the bulk density of typical expanded perlite is approximately 30-150 kg/m3 [12]. Perlite is a non-renewable resource [13,14]. World perlite reserves are estimated at 700 million tonnes, with confirmed perlite resources in Armenia amounting to 150 million m^3, and the total estimated resources reach 3 billion m^3.After crushing, grinding, and classifying, perlite undergoes expansion. Perlite is most commonly used in the construction sector [13,14]. Therefore, demand for perlite parallels the developments and stagnation in the construction sector. In commercial use, perlite is a naturally occurring acidic glass of volcanic origin; when heated to a suitable temperature, it expands and becomes porous. When perlite is heated between 900-1100°C in special forms with a specific grain size, its volume expands approximately 25-fold, popping like popcorn, and its density becomes much lighter. Porosity is defined as the average ratio of the void volume in perlite grains to the total grain volume. Porosity gives perlite its absorbency and surface cooling properties and is therefore important in applications where this property is required. Water absorbency is undesirable in water pollution removal efforts and thermal insulation. This is because filling the pores with water increases thermal conductivity. In this case, perlite becomes hydrophobic by passivating the pores with silicone or a substance. Raw perlite has a medium hardness (5,5-7,0). This means that perlite glass cannot be scratched with a fingernail, but it can be scratched with a steel nail or knife. The degree of hardness is important. The hardness of a mineral is one of the fundamental physical properties that directly affects its use in engineering, industry, and geology. The material density of perlite is around 2.2-2.4 g/cm^3. Perlite is a natural volcanic aluminosilicate glass (rhyolitic rock) formed by the rapid cooling of lava or magma [14,15]. Heavy metals (HMs), which can be carcinogenic, cytotoxic, and mutagenic, can pose a threat to fauna, flora, and humans. In the mining industry, large amounts of HMs are released uncontrolled as a result of activities such as ore extraction, grinding, ore aggregation, and dumping of waste in open areas. Perlite is a naturally occurring glassy volcanic alumina silicate rock that is mined and used worldwide. Perlite is used in the construction, agriculture, food, pharmaceutical, and chemical industries. Perlite is found in many countries worldwide. Turkey

is one of the world's leading perlite producers [14]. Confirmed reserves in Armenia reach 165 million tons. Perlite is a natural mineral composed of volcanic glass with a high water content and exhibits the property of expanding when heated. This property makes it attractive for lightweight construction materials, insulation, filtration, and agricultural applications. Turkey holds 30% of the world's perlite reserves and plays a strategic role in terms of exports. The main perlite deposits in Türkiye are located in Bergama, Manisa, Bitlis, Kars, and Erzincan. It is estimated that 30% of the world's perlite reserves are in Türkiye. Other important producers include the United States, Greece, and Hungary [7]. The world perlite reserves are approximately 700 million tons. Other reported reserves are; Greece (120 million tons), Turkey, USA and Hungary approximately 49-57 million tons [15]. World perlite production, led by China, Turkey, Greece, USA, Armenia and Hungary, reached 4.6 million tons in 2018 [14,15]. In India, the Osham Hills in Patanvav city of Gujarat state are the only perlite mineral source in India, USA, Armenia, Japan, Italy, Turkey, Greece and Hungary are rich countries in terms of perlite resources [5,14]. Türkiye's proven perlite reserves are 30 million tons, and the total probable perlite reserves are 4.5 billion tons [5,14]. Figure 2 shows the general grain structure and different forms formed by the processing of perlite mineral [5,14,15].

Figure 2. General grain structure formed by processing perlite mineral [1,5]

The naturally occurring perlite mineral is an amorphous volcanic alumino-silicate rock mined and used worldwide [12,16-18]. When heated to 1100 0C, perlite converts natural water (3.5% total weight) into vapor and expands and becomes porous, expanding up to twenty times its original volume [12,16,17]. Expanded perlite has attractive physical properties for commercial applications, such as high surface area, low thermal conductivity, high heat resistance, low sound transmission, and chemical inertness [12].

2.2 Geological formation of perlite mineral

The geological formation of perlite is closely linked to volcanic activity and the resulting interaction with water. Perlite, of volcanic origin, typically begins as siliceous lava (rich in SiO2) with a rhyolitic composition and cools rapidly at or near the Earth's surface. This rapid cooling prevents crystallization, forming a dense volcanic glass known as obsidian. Over time, hydration causes the obsidian to absorb meteoric water from the surrounding environment. This process, known as hydration, involves the diffusion of water into the glassy structure. The absorbed water is stored within the glassy structure, giving perlite its characteristic water content. This hydration process leads to the formation of characteristic concentric cracks in the glass (known as pearlitic structure), which cause the rock to fragment into small, pearl-like masses, giving perlite its name. Perlite originates from hydrated rhyolitic magma. Formation involves volcanic eruption and lava flow, rapid cooling to obsidian, hydration (2-6% H_2O uptake by weight), vesiculation, and fracturing. Mineralogically, perlite consists of 70-90% amorphous glass with minor inclusions of feldspar, quartz, hematite, and amphibole. Turkish perlite compositions closely follow global rhyolitic trends. Slightly higher SiO_2 indicates advanced polymerization. Perlite is hydrous volcanic glass that, when rapidly heated at 760-1000°C, expands its volume 25-fold, resulting in a highly porous and lightweight structure. This unique microstructure lowers thermal conductivity, reduces density, and provides perlite with a wide range of applications including insulation,lightweight aggregate, filtration, and composite reinforcement [18,19]. The combined evaluation of radiometric (Ra-226, Th-232, K-40), elemental (especially traces of Na, K, Fe in Si-Al matrix) and RREs (non-thermal emission behavior due to surface defects/odors) properties of perlite provides rational design inputs for building materials, nuclear protection, environmental engineering and energy systems (PV/T, heat storage, flame retardant composites, etc.) [20,21]. The glass phase of perlite contains high SiO_2 (70-75%) and Al_2O_3 (12-15%); alkali oxides (Na_2O, K_2O), Fe_2O_3 and trace elements vary depending on the mining site. A detailed characterization study

on Izmir-Bergama perlite confirmed the glassy structure, limited crystalline phase and large specific surface area using xrf, xrd, sem, BET and ftır measurements [20-24]. These findings directly affect the expansion behavior associated with heat treatment conditions and industrial classification.

3. MATERIAL AND METHODS

Türkiye's perlite mineral reserves are approximately 4.5 billion tons, which constitutes a significant portion of the estimated world reserves [1,10-14]. Perlite samples from the Turkish provinces of Erzurum, Izmir, Ankara, and Nevşehir were brought to the sample preparation laboratory in plastic bags. 10 perlite quarries are P1(Pasinler), P2 (Erzincan,Mollaköy),P3 (İzmir, Mezarkaya), P4 (Ankara, Çubuk), P5 (Nevşehir, Karapınar), P6 (Nevşehir, Acıgöl), P7 (Nevşehir, Göllü Mountain), P8 (İzmir, Bergama, Koyuneli), P9 (İzmir, Bergama,) and P10 (Nevşehir, Nenezi Mountain). The locations of important perlite quarries in Türkiye are shown in detail in Figure- 3 [1,3,23]. Significant perlite reserves in Turkey are concentrated in Tertiary-Early Middle Quaternary volcanic provinces [1,14]. Perlite reserves in Eastern Anatolia were formed by these flows directly related to young Neogene rhyolitic volcanism and are distributed over wide areas within rhyolite lavas, rhyolitic tuffs, and other volcanic deposits [1,14].

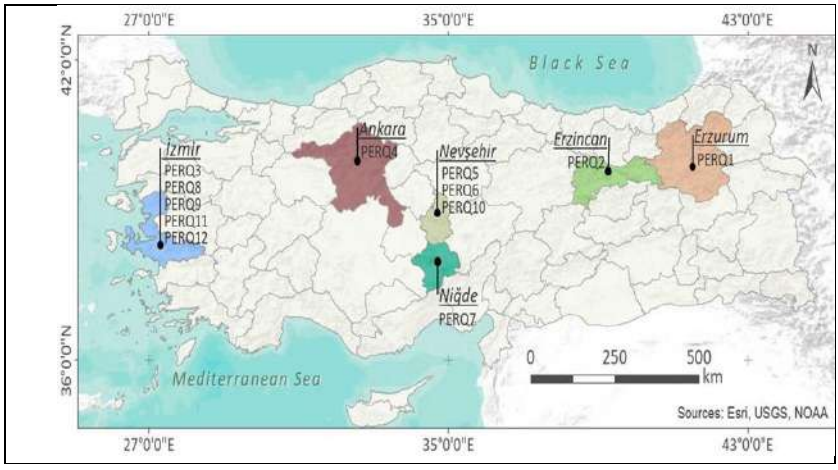

Figure.3 Locations of perlite quarries in Türkiye [1,8]

The overall uncertainty of the analytical procedure varied between 0.1% and 16.6%. The detection limit (DL) was calculated as follows

$$DL = \frac{3 \times C_i}{N_C} \times \sqrt{\frac{N_B}{t}} \quad (1)$$

Where, Ci is the ith element concentration, NB is the background count rate, NC is the net count rate and t is the counting time [24-27]. XRF spectrometry, which performs simultaneous qualitative and quantitative multi-element determinations, is an accurate, fast, sensitive, reliable, simple and systematic analysis technique [24-27]. The analysis of HMs (As, Cu, Co, V, Ni, Pb, Zn, Cr, Zr, Mn, Ti and Fe) in perlite samples was carried out using an EDXRF spectrometer (Spectro Xepos Ametek) with an X-ray tube (50 W, 60 kV) with a double-thickness Pd/Co mixture anode. The detection limits of analyzed HMs were found as 0.5 (As), 0.5 (Cu), 3.0 (Co), 0.5 (V), 0.6 (Ni), 0.8 (Pb), 0.7 (Zn), 0.3 (Cr), 1.0 (Zr), 1.1 (Mn), 2.0 (Ti), 0.8 (Fe), 2.0 (Cd) and 1.0 (Hg) mg/kg.

4. CALCULATION OF ENRICHMENT FACTOR

In this study, Toe's such as inhalation of particles emitted from perlite, incidental ingestion of perlite particles, and dermal contact with perlite were primarily considered to estimate direct exposure to perlite samples. Within the PHHR assessment model recommended by the USEPA, the mean daily intake of these TOEs (in mg/kg.d, ADD per day) was calculated for PERQ workers using the following equations [8,24-31].

$$ADD_{Inh} = \frac{C \times InhR \times EF \times ED}{PEF \times BM \times AT} \quad (2)$$

Additionally, hazard coefficient (HQ) and hazard index (HI) were used to estimate non-carcinogenic PHHR ,HQ was estimated as follows [24-27,31-34].

$$HI = \sum_{i=1}^{n} HQ_i \quad (3)$$

The hazard index (HI) is obtained by summing the estimated HQi values for each HM in the PERM sample as follows [3,24-34]. Where n is the number of HMs analyzed in the perlite samples. If the HI values are less than 1, there is a negligible level of non-carcinogenic PHHR. However, if the HI values are higher than 1, non-carcinogenic PHHR may occur with a probability that tends to increase as the HI value increases [29-34]. The enrichment factor (EF) was

used to determine the contamination level and to infer the distribution of elements of anthropogenic or natural origin from the positions determined by individual elements in the environmental samples. EF calculated as follows [17,18] at equations 4.There are according to EF values five contamination factors [23-26].

$$EF = \frac{\left(C_n / C_{Ref}\right)_{Sample}}{\left(C_n / C_{Ref}\right)_{Backgroun\ (Earth)}} \qquad (4)$$

5. RESULTS AND DISCUSSION

While radiogenic heat affects subsurface temperatures, radiometric analyses are mandatory for the safe extraction of perlite. Radioformic formations are used in geological mapping. Radioactivity is the radiation from natural isotopes; radiotoxicity is related to biological effects on human health. The internal energy of the Earth is approximately 12.6 x 10^{24}Joule, and most of this energy originates from radiogenic decay [23-26]. In Table 2 show that some properis of statıcal data.The geological layers are; Lithosphere (0-100 km), Asthenosphere (100-300 km), Mantle (300-2900 km), Outer Core (2900-5100 km), Inner Core (5100-6371 km). The geological environments in which perlite is found may contain natural radiogenic elements. Some descriptive statistical data regarding the NORE concentrations measured in all perlite samples are presented in Table 2.

Table 2. Some descriptive statistical data regarding perlite mineral [35].

HM	Concentration (mg/kg, dw)								EUC (mg/kg)
	Average	Median	SD	SE	Kurtosis	Skewness	Min	Max	
Ti	528.3	515.4	214.3	19.1	0.1	0.7	117.1	1361.0	3931
V	7.1	6.9	3.5	0.3	0.4	-0.8	< DL	14.7	97
Cr	64.9	50.1	57.6	5.1	1.2	1.2	< DL	247.1	92
Mn	383.5	378.8	73.5	6.5	0.4	-0.2	257.3	640.9	774.5
Fe	6585.4	6255.5	1626.3	144.9	0.6	0.2	3914.0	12730.0	32041
Co	7.0	6.4	1.8	0.2	2.4	5.9	< DL	13.9	17.3
Ni	19.8	16.4	15.7	1.4	1.8	3.4	4.6	77.7	47
Cu	4.3	3.4	3.4	0.3	2.5	6.7	1.1	19.7	28
Zn	31.1	31.8	6.4	0.6	-0.4	-0.8	17.0	45.7	67
As	4.2	3.5	2.3	0.2	0.4	-1.3	< DL	9.0	4.8
Pb	26.4	24.4	7.2	0.6	0.4	-1.1	15.1	41.6	17
Zr	93.7	88.0	28.3	2.5	0.2	-0.9	40.5	163.1	193

* SE: standard error; SD: standard deviation

The average concentrations of U, Th and K measured in perlite samples are listed are shown in Table 3, and Figure 4 shows the trace amounts of rare earth elements (ppm) in perlite mineral [35]. The measured U concentrations in perlite samples value are approximately twice the average of 2.5 mg/kg for the Earth's crust [35].The geological environments where perlite is found may contain naturally occurring radiogenic elements.Radiogenic heat affects subsurface temperatures, and radiometric analysis is essential for the safe extraction of perlite. Radioformic formations are used in geological mapping. Radioactivity is the emission from natural isotopes; radiotoxicity relates to biological effects on human health.

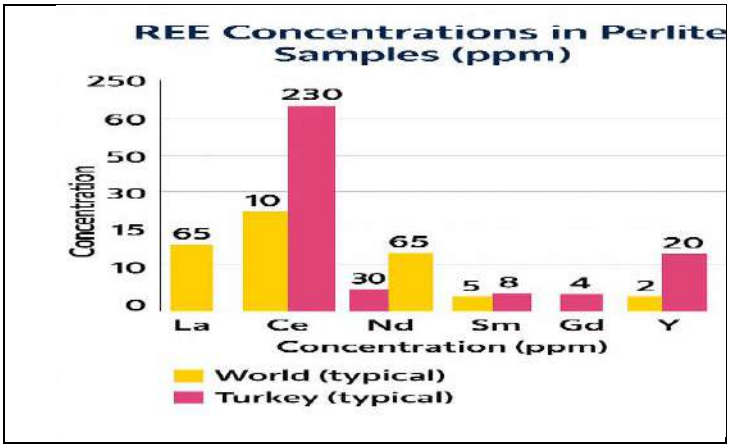

Figure 4. Distribution of RREs in perlite in the world and Türkiye

Table 3. Comparison of radionuclide elements [35]

Element	Earth (Bq/Kg)	Türkiye (Bq/Kg)	Radiogenic Source	Cardiotoxicity
U-238	35–45	40–90	high	high
Th-232	30–40	35–100	high	middle - high
K-40	400–500	450–850	middle	low-medium
Ra-226	25–35	40–70	high	high
Pb-210	5–15	10–30	middle	high

5. CONCLUSIONS

This study comprehensively examines the geochemical, radiometric, radiotoxic, and ecological properties of perlite deposits in Turkey and worldwide. The heavy metals, radionuclide elements, radiogenic heat production (RHP) and environmental risks contained in perlite are evaluated

using scientific data, mathematical models, and comparative analyses. Furthermore, health effects related to radioactivity, perlite's applications, and occupational safety measures are discussed. Analyzing of RHP is crucial for shedding light on abnormally high thermal regimes in any given region. Knowing the chemical composition of perlite samples is crucial and directly related to their intended uses. Therefore, it plays a key role in the effective and efficient use of perlite [1,8,35]. In this study, the distribution of ten major and minor oxides and twelve heavy metals in twelve commercially operated perlite mines in Türkiye was determined for the first time using EDXRF spectrometry. Furthermore, based on the heavy metal contents analyzed in perlite samples, potential carcinogenic and non-carcinogenic health risks to adult quarry workers assessed for the first time. Average SiO_2, Na_2O, and K_2O concentrations found to be higher than those in the Earth's upper crust. [1,8,35].

REFERENCES

1- Turhan, Ş., Tokat, S., Kurnaz, A., Altıkulaç, A. (2022). Distribution of elemental compositions of zeolite quarries and calculation of radiogenic heat generation.*Int. J. Environ. Anal. Chem.* 109(19), 7851–7862.

2- MTA, (2023). Türkiye rare earth elements potential report, general directorate of mineral research and exploration, *Mining Technical Exploration Institution*,Ankara-Türkiye.

3- Turhan, Ş., Altuner, E.M., Bakır, T.K., Duran, at al. (2024). Assessment of human health risk caused by heavy metals in kiln dust from coal-fired clay brick factories in Türkiye. *Expo Health*,

4- Samar, M., and Saxena,S.(2016).Study of chemical and physical properties of perlite and its application in India. *International Journal of Science Technology and Management* 5(4), 70-80.

5- Turp, M.S. (2019). Adsorption kinetics and isotherms of Ni (II) and Zn (II) heavy metals onto a natural adsorbent: expanded perlite, desalin. *WATER TREAT*. 142, 205–21.

6- USGS.(2024).A centralized archive for land treatment tabular and spatial data ver., *Land Treatment Digital Library Data Release*,https://ui.adsabs.harvard.edu/link_gateway/2019usgs.data..265P,doi: 10.5066/P98obols.

7-USGS.(2025).USGS national and global oil and gas assessment project-gulf coast mesozoic province, lower cretaceous travis peak and hosston formations: assessment unit boundaries, *Assessment Input Data*, *And Fact Sheet Data Tables*,10.5066/p1jpwray.

8- Turhan, Ş., Altuner, E.M., Ayata, A., Gezer, F., at al. (2025). Dispersion of oxides, heavy metals, and natural radionuclides in phosphogypsum stockpiles of the phosphate industries in Türkiye. *ENVIRON. SCI. POLLUT. RES.*, https://doi.org/10.1007/s11356-025-36180-2

9- Gündüz, L.& Kalkan,O.Ş.(2023).An ınvestıgatıon on the effects of temperature change on aggregate characterıstıcs ın perlıte expansıon - a new approach, *konya Journal Engineeringsciences,*11(1),2140.,https://doi.org/10.36306/konjes.1088530.

10-Ibrahim,M.(2022).Durability of structural lightweight concrete containing expanded perlite aggregate11-panagiotopoulou*, İnternational Journal Of Concrete Structures and Materials.,* 14(50)

11-Turhan,Ş.(2023).Heavy metal contamination and health risk evaluation of chestnut (*castanea sativa* miller) consumed in turkey, *Internatıonal Journal Of*

*Environmentalhealthresearch,*33(11),https://doi.org/10.1080/09603123.2022.2073984

12-Maxim, L.D., Niebo, R., McConnell, E.E. (2014). Perlite toxicology and epidemiology-a review. *Inhal. Toxicol*. 26(5), 259–270.

13- Chung, J.Y., Yu, S.D., Hong, Y.S. (2014). Environmental source of arsenic exposure. *J. Prev. Med. Public Health* 47(5), 253–257.

14- DPT (2001). Mining Specialization Commission Report. Industrial Raw Materials Sub-Commission Building Materials III (Pumice-Perlite-Vermiculite-Phlogapite-Expanding Clays) *Working Group Report.* 2617-ÖİK: 628, Ankara.

15- Angelopoulos, P.M. (2024). Insights in the physicochemical and mechanical properties and characterization methodology of perlites. *Minerals* 14(1), 1–25.

16- Vijayaraghavan, K., Raja, F.D., (2014). Experimental characterisation and evaluation of perlite as a sorbent for heavy metal ions in single and quaternary solutions. *J. Water Process. Eng*. 4, 179–184.

17- Khoshraftar, Z., Masoumi, H., Ghaemi, A. (2023). On the performance of perlite as a mineral adsorbent for heavy metals ions and dye removal from industrial wastewater: A review of the state of the art. Case Stud. *Chem. Environ. Eng.* 8, 1–17.

18- Petrella, A., Spasiano, D., Rizzi, V., Cosma, P., Race, M., De Vietro, N. (2018). Lead ion sorption by perlite and reuse of the exhausted material in the construction field. *Appl. Sci*. 8(10), 1–13.

19- Najafi, P., Asgari, K., Samadi, N.(2016). Heavy metal elimination from industrial wastewater using natural substrate on pitcher irrigation. *Int. J. Recycl. Org. Waste Agricult.* 5, 333–337.

20-Kayakökü,H.(2016).Measurements of radioactivity and dose assessments in some building materials in Bitlis, *Turkey Applied Radiation and Isotopes*

115, P172-179

21- Jiang, W., Meng, L., Liu, F., Sheng, Y., Chen, S., Yang, J., Mao, H., Zhang,J., Zhang, Z., Ning, N. (2023). Distribution, source investigation, and risk assessment of topsoil heavy metals in areas with intensive anthropogenic activities using the positive matrix factorization (PMF) model coupled with self-organizing map (som). *Environ. Geochem. Health* ,45(8), 6353–6370.

22- Togun,H.(2025).Advancing photovoltaic thermal (pv/t) systems: Innovative cooling technique, thermal management, and future prospects, *Solar Energy,*291,113402, https://doi.org/10.1016/j.solener.2025.113402.

23- Turhan,Ş.(2020). The natural radioactivity in drinking water by gross alpha and beta measurements and radiological quality assessment, *Radiochimica Acta,*108(6),491-498.

24- Van Grieken, R., Markowicz. A. (2001). *Handbook of X-Ray Spectrometry. CRC press.*

25- Baltas, H., Sirin, M., at al. (2020). A case study on pollution and a human health risk assessment of heavy metals in agricultural soils around Sinop province, Turkey. *Chemosphere*, 241, 1–10.

26- Altıkulaç, A., Turhan, Ş. (2023). Assessment of the levels of potentially toxic elements contained in natural bentonites collected from quarries in Turkey. ACS Omega 8(23), 20797–20986.

27-USEPA. (1989). Risk assessment guidance for superfund. volume i: *human health evaluation manual (part a),* epa/540/1–89/002, washington, dc.

28-USEPA. (2004). risk assessment guidance for superfund. *volume 1: Human Health Evaluation Manual (Part E*, *Supplemental Guidance ForDermal Risk Assessment).* epa/540/r/99/005, office of superfund remediation and technology innovation, u.s. environmental protection agency washington, dc.

29-USEPA. (2011). exposure factors handbook (final report). *Chapter 5: Soil And Dust Ingestion. U.S. Environmental Protection Agency, W*ashington, Dc.

30-USEPA.(2014). epa positive matrix factorization (pmf) *5.0* Fundamentals and User Guide. U.S. Environment Protection Agency, Washington, Dc.

31-USEPA.(2024). updated dermal exposure assessment guidance. region 3 ,*Technical Guidance Manual, Risk Assessment.,*https://www.epa.gov/risk/updated-dermal-exposure-assessment-guidance.

32- Miletić, A., Lučić, M., Onjia, A.(2023). Exposure factors in health risk assessment of heavy metal(loid)s in soil and sediment. *Metals* 13(7), 1–28.

33- Ma, J., Chen, L., Chen, H., Wu, D., at al.(2023). Spatial distribution, sources, and risk assessment of potentially toxic elements in cultivated soils using isotopic tracing techniques and Monte Carlo simulation. *Ecotoxicol. Environ. Saf.* 259, 1–12.

34- Hao, W., Liu, H., Hao, S.at al. (2024). Characterization of heavy metal contamination in groundwater of typical mining area in Hunan Province. *Sci. Rep.* 14, 1–12.

35- Yaroshevsky, A. A. (2006) Abundances of chemical elements in the Earth's crust. *Geochemistry International*, 44 (1) 48-55 doi:10.1134/s001670290601006x

Chapter 3

NUMERICAL AND EXPERIMENTAL INVESTIGATION OF SPATIOTEMPORAL DISCHARGE CHARACTERISTICS OF ZNSE-AR MICROPLASMA SYSTEM

Hatice Hilal YÜCEL[1], Erhan ONGUN[2], Selçuk UTAŞ[3]

1.INTRODUCTION

In today's world, the infrared-visible (IR-VIS) image converter technology is used in many potential applications and is a constantly evolving technological field. Some potential applications of the IR-VIS image converter systems include detecting heat sources for defense industry applications, laser source spectrophotometric process monitoring for industrial applications, laser beam profile analysis, early detection of fire (eg.; T=800 K; λ=3.62 μm), gas absorption spectroscopy in sample testing and analysis studies, and in non-destructive testing and inspection processes.

Microplasmas, which have become the focus of increasing interest in the plasma science and technology, are nonthermal, high-energy-density, and unstable reactive gas discharge systems in the micrometer range [1]. Many research studies were reported in the field of microplasma science and technology for advanced materials and devices such as multi-purpose light sources, efficient ultraviolet (UV) light sources for photochemical material processing, spectroscopic material analysis, surface disinfection, water purification, microplasma-optics based artificial electromagnetic devices [2], microplasma field effect transistors [3], miniature plasma sources for electric micropropulsion [4], field emission discharges in microcombustion [5], microplasma thruster powered by X-band microwaves [6] and microplasma technology-based functional nanomaterial synthesis [7]. Their electrical and

[1] Prof. Dr., Gazi University, Institute of Science, Department of Physics, Ankara, hkurt@gazi.edu.tr, (ORCID: 0000- 0002-1277-5204)

[2] Ph:D., Gazi University, Institute of Science, Department of Physics, Ankara, erhan_ongun@hotmail.com (ORCID: 0009-0007-4966-1044)

[3] Ph:D. Student, Gazi University, Institute of Science, Department of Physics, Ankara, selcuk.utas@gmail.com (ORCID: 0000-0002-9709-516X)

optical properties also make the microplasma systems attractive for the design of “Gas Discharge-Semiconductor Microplasma (GDSμP)” systems in the field of infrared photodetection and infrared-visible wavelength conversion applications [8,9]. Microplasma systems require advanced characterization of the spatio-temporal dynamics of the plasma formation at the microscale [10]. The discharge characteristics of gas discharge-semiconductor microplasma (GDSμP) systems were examined in detail using experimental and numerical methods. Numerical analyses were carried out by FEM solver COMSOL Multiphysics simulation program. In GDSμP system; zinc selenide (ZnSe) compound semiconductor and indium tin oxide (ITO) thin-film coated silica (SiO2) substrate were used as cathode and anode electrodes, respectively. In adition, the dielectric barrier discharge (DBD) system was designed in a cell model with rectangular geometry in two-dimensional planar topology. Interplanar electrode gas discharge gap (d) was spaced at the mm-scale for the DBD system. Argon (Ar) gas system was introduced in the gap. Gas pressures (P) were defined at above atmospheric levels. The GDSμP systems were operated in the normal glow DC discharge regime. Spatiotemporal distributions of the dynamic discharge parameters, including surface ion current density (ICD), migrative electron flux (MEF), reduced electric field (REF) and capacitive power deposition (CPD) were analyzed in 2D- color graphical media. It is figured out that GDSμP and DBD system models can be used to manufacture high-end and miniature infrared-to-visible image conversion microplasma devices for a wide range of industrial, aerospace and defense applications.

2.GAS DISCHARGESEMICONDUCTOR MICROPLASMA(GDSMP)

Various numerical and experimental studies were reported on the DC-driven GDSμP systems [11, 12] to investigate the electrical charge transport properties in gas discharge-semiconductor optoelectronic devices. Experimental studies on the GaAs, GaP, and ZnSe semiconductor -coupled Ar gas microplasma systems were reported [13,14].The electrical properties of ZnS and ZnSe semiconductor materials were investigated in the gas discharge-semiconductor microplasma system The infrared photosensitivity of ZnSe semiconductor material was investigated experimentally [15].

2.1 Electrical discharge in gases

Detailed research on the electrical breakdown phenomena in gases from macro to micro scale was reported [16]. The electrical breakdown phenomena in gases are governed by Townsend avalanche reactions through a combination of

electron emission and ionization mechanisms, including thermionic electron emission, ion-induced secondary electron emission, and field electron emission. The transitions between electron emission mechanisms and Townsend avalanche formation across discharge gap are introduced in detail [17]. The microscale electrical breakdown mechanism based on the ion-enhanced field emission has been extensively studied [18].Theoretical and computational techniques provide valuable insights into the microscale electrical breakdown mechanisms and kinematic behavior of gases. To put it plainly, FEM-based space-time simulation programs are just one example. This allows us to theoretically analyze many plasma parameters in a virtual laboratory [19].Figure 1(a) shows Paschen's curve, which defines conduction state (discharge) and insulation state (cutoff/non-discharge) regions in a gas medium [3]. Paschen's multiplier (p.d) is defined by the gas pressure (p) and the interelectrode distance or discharge gap (d). Paschen's multiplier determines the electrical breakdown voltage (Vdc) of gas medium. Each gas has a characteristic electrical breakdown voltage and a specific Paschen's curve. Paschen's curves of He, Ne, Ar, H_2, N_2 gases are shown as examples in Figure 1(b).

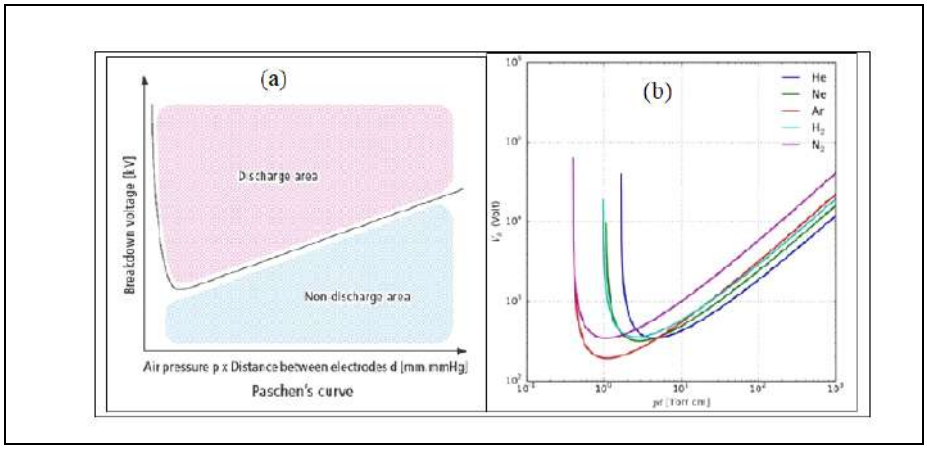

Figure 1. (a) Discharge and non-discharge on the Paschen's curve, (b) Paschen's curves of He, Ne, Ar, H_2, N_2 [35].

At large p.d values, the number of collisions in the gas discharge gap is also high. At small p.d values, the electrical breakdown voltage increases because the collisions in the plasma region are very few. Below this value, electrical breakdown does not occur. The reactions of electron-impact ionizations of Ar gas are given in Table 1 [20].

Table 1. Electron-impact ionizations of Ar [20].

Reaction	Formulas	Type	Δε (Ev)	
1	$e + Ar \longrightarrow e + Ar$	Elastic	0	Boltzmann
2	$e + Ar \longrightarrow 2e + Ar+$	Direct ionization	15.824	Boltzmann
3	$e + Ar \leftrightarrow e + Ar*$	Excitation	11.424	Boltzmann
4	$e + Ar \leftrightarrow e + Ar$	Excitation	13.1	Boltzmann
5	$e + Ar* \longrightarrow 2e + Ar+$	Stepwise ionization	4.3997	Boltzmann
6	$2Ar* \longrightarrow e + Ar+ + Ar$	Penning ionization	-	6.2×10^{-10} cm^3 s^{-1}
7	$Ar* \longrightarrow h\nu + Ar$	Radiation	-	$1.0\times10^{7}s^{-1}$

Electrons gain very little kinetic energy during collisions, thus reducing the probability of ionization of Ar atoms. To compensate, the interelectrode voltage is increased. In Figure 2, gas discharge regimes under DC supply are defined in the current/voltage (I/V) graphical medium.

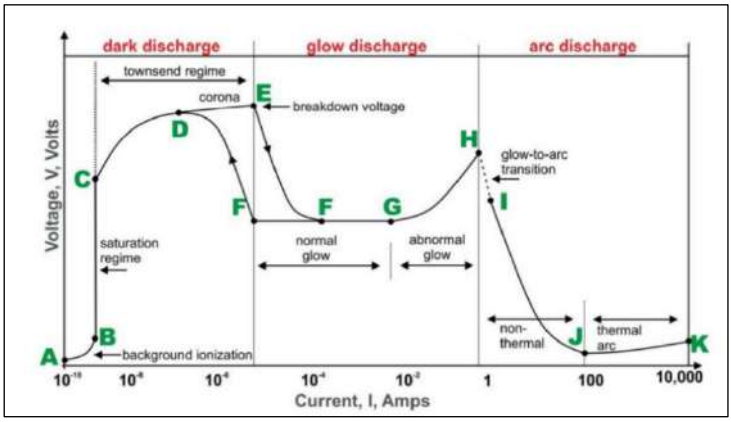

Figure 2. DC Gas Discharge Regimes (I/V graph) [35].

In this study, it is aimed to investigate the nonlinear and fast transient electrical discharge characteristics of unary Ar gas media, which is coupled to semiconductor cathode element across a micro discharge gap, operating in the normal glow discharge regime F-G.

2.2 Zinc selenide (ZnSe) semiconductor

Infrared spectral bands are defined as shortwave infrared (SWIR) in the wavelength range of 1-3 μm, midwave infrared (MWIR) in the wavelength range of 3-5 μm, and longwave infrared (LWIR) in the wavelength range of 8-14 μm [21]. For infrared detection and visible wavelength conversion systems, the appropriate semiconductor material selection depends on the application. Semiconductor materials with direct and indirect band gaps are used. The

resistivity value should be a minimum of 1E7 ohm.cm. Silicon and other indirect narrow-band gap semiconductors require special integrated cooling equipment when used as infrared photodetection devices. Various alternative materials are being studied to support the continued development of infrared photodetection technology [22, 23]. The physical and material properties of semiconductors have been reported in detail [24].Group II-VI compound semiconductors offer alternative solutions in the field of infrared sensing technologies and applications. Uncooled infrared photodetection devices have the potential use in a variety of specialized applications, such as early fire detection and remote warning, remote object detection for drivers in low-illumination environments, handheld night vision imagers, and security surveillance. The binary compound semiconductor ZnSe [25], with a direct band gap of ~2.7 eV at 300 K, has attracted considerable attention from researchers working in the field of thermal imaging applications [26] due to its properties such as fast spectral response in the long-wave infrared band, excellent electronic charge transport properties, and optical transparency in the visible spectrum. Electrical and optical properties of ZnSe semiconductor material have been reported for infrared sensitivity in the range of 0.5–15 μm in gas discharge-semiconductor microplasma systems for night vision devices due to its high resolution. In Figure 3, the valence and conduction electronic band structures of CdSe, ZnSe and ZnTe binary compound semiconductors from Group II-VI, which have high intrinsic absorption coefficients, are introduced on a diagram [27].

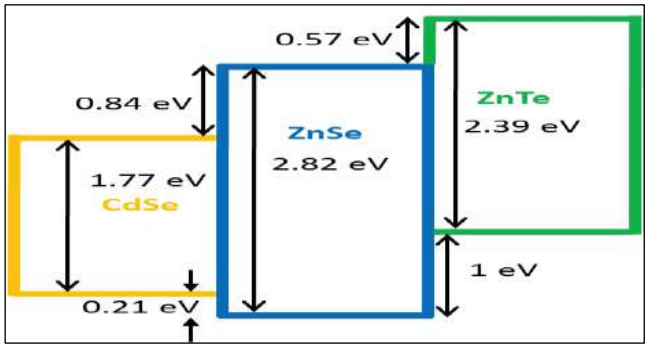

Figure 3. Electronic band structure of CdSe, ZnSe and ZnTe [27].

In the numerical investigations part of this study, the effects of the cathode electron emission surface on the discharge parameters of the microplasma system were also investigated by modeling simple planar DBD with ZnSe cathode elements across Ar gas gap. It is known from the literature that the

effects of microscale artificial surface patterning such as the fabrication of concentric multiple surface protrusions [28], the decoration of plasmonic metallic nanoparticles (Ag, Au) [29, 30] on the electrical breakdown of the gas discharge medium, the effects of natural surface morphology such as surface waviness and roughness on the work function of the photocathode semiconductor material [31] and electron emission mechanisms were reported in detail [32].

3.MATERIAL AND METHOD

In the experimental studies; (1) elemental analysis, (2) optical analysis, (3) electrical analysis, and (4) microplasma analysis techniques were utilized for investigation of ZnSe-Ar system. Discharge parameters were explored at atmospheric and subatmospheric pressure levels under infrared illumination at varying irradiance intensity levels.Energy dispersive X-ray (EDAX) spectroscopy and atomic force microscopy (AFM) techniques were used in the analysis of microstructural and elemental properties of ZnSe semiconductor sample. The energy dispersive X-ray spectroscopy (EDAX) graph of ZnSe sample is given in Figure 4.

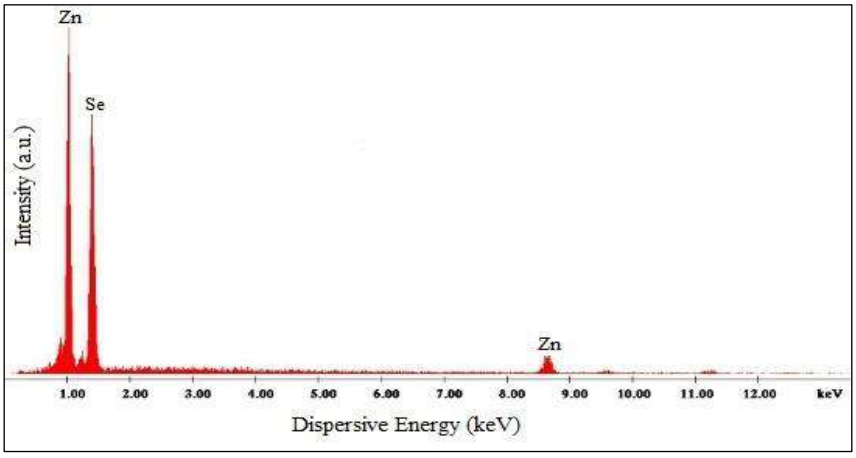

Figure 4. EDAX for ZnSe [42].

Data on the stoichiometric ratios of ZnSe sample were obtained by the EDAX analysis. It was determined that sample consists of 65.04% selenium (Se) and 34.96% zinc (Zn) by weight.

Figure 5 shows a photograph of Gas Discharge Semiconductor System (GDSS-lab) utilized for the experimental works in the Microplasma Research Laboratory of the Physics Department at Gazi University.

Figure 5. GDSS-lab setup.

Spectrophotometric absorption measurements were performed for ZnSe sample. Visible-near infrared absorption of uncoated ZnSe sample in the wavelength range of 800-1500 nm spectra is given in Figure 6.

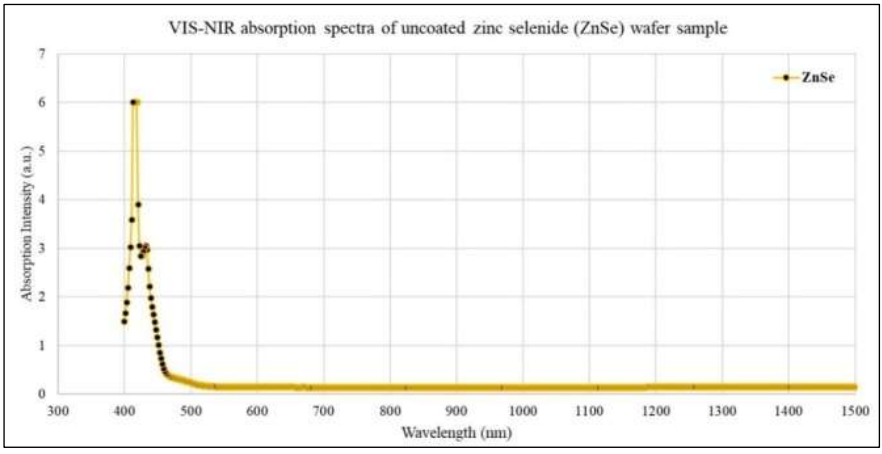

Figure 6. Absorption spectra for ZnSe [42].

Electrical measurement setup of GDSS-lab is schematically presented in Figure 7(a). A Keithley 199 multimeter and a Stanford PS DC power supply were used in the measurements. Electrical equivalent circuit model of GDSS-lab is given in Figure 7(b). The microplasma cell is formed by direct coupling of semiconductor photocathode electrode and gas discharge gap to define the nonlinear current (I) and voltage (V) characteristics of the gas discharge system. The glow discharge light emissions (DLE) in the microplasma medium were excited at three different infrared illumination intensity levels (dark, weak, strong), and measured using a photomultiplier tube. The schematic representation of GDSS-lab cell module with a photomultiplier tube is shown in

Figure 8. A 40 nm thick gold (Au) film was used as IR-transparent electrical contact on the photocathode side. An 80 nm thick indium tin oxide (ITO) film was used as VIS-transparent electrical contact on the anode side.

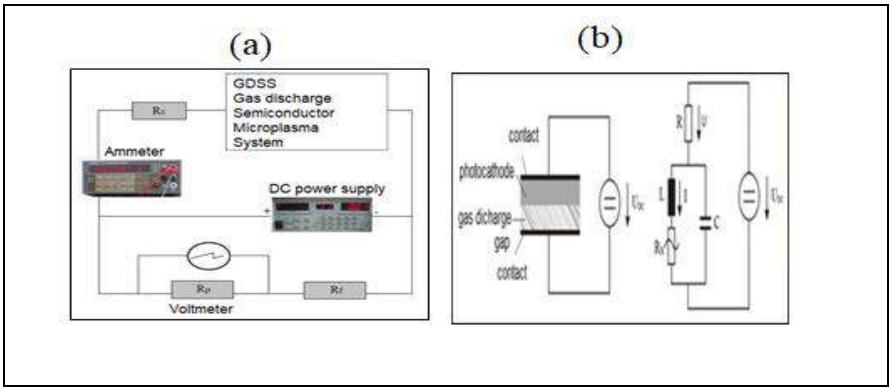

Figure .7(a) Electrical measurement setup,
(b) Equivalent circuit model of GDSS-lab cell
(Rs=1.0 kΩ, Cp=1.0 pF).

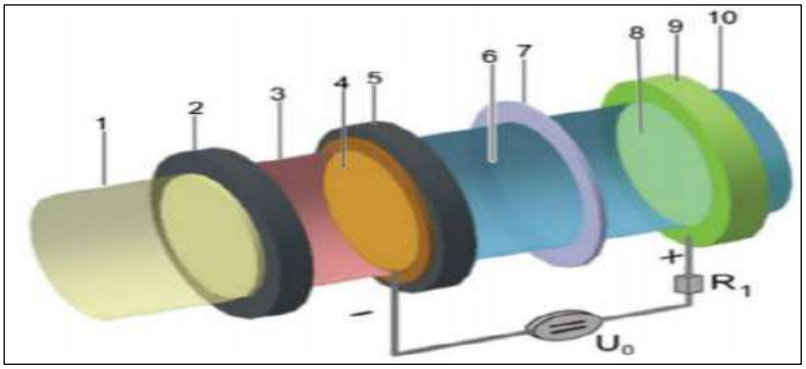

Figure 8. Schematic of GDSS-lab cell module: (1) light source, (2) Silicon filter, (3) IR light input, (4) IR-transparent Au-film contact, (5) ZnSe photocathode disc, (6) Gas discharge microgap, (7) Mica dielectric separator, (8) VIS light output, (9) VIS-transparent ITO-film contact, (10) Silica disc.

The schematic of the GDSμP system is given in Figure 9(a), and aims to convert IR-to-VIS wavelength at the micro scale. The incident IR radiation is efficiently absorbed by high specific resistivity (ρ>E5 ohm.cm) semiconductor photocathode material (ZnSe), Figure 9(b). Photoelectrons are ejected to micro-gap under DC field induced between anode and cathode planar electrode pair.

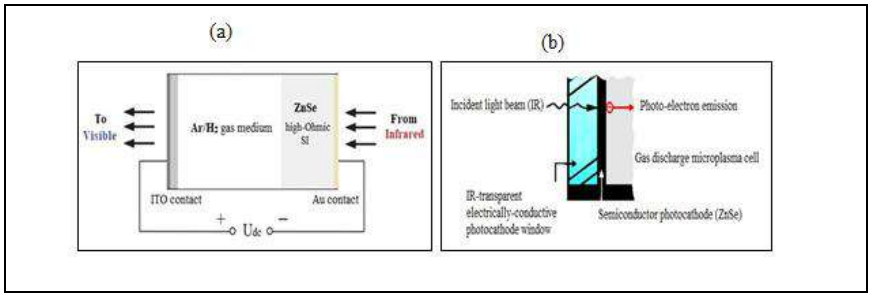

Figure .9 (a) GDSμP system model,
(b) Photocathode structure and operating principle

The effect of infrared illumination intensity on discharge light emission (DLE) was analyzed for Ar gas at above atmospheric pressures in the the cell module. Figure 10(a-b) shows the DLE graphs of the cell module in Ar gas media with 50 μm and 330 μm discharge gaps at 810 Torr and 900 Torr pressures, respectively, coupled with a 12 mm diameter (D) ZnSe cathode.

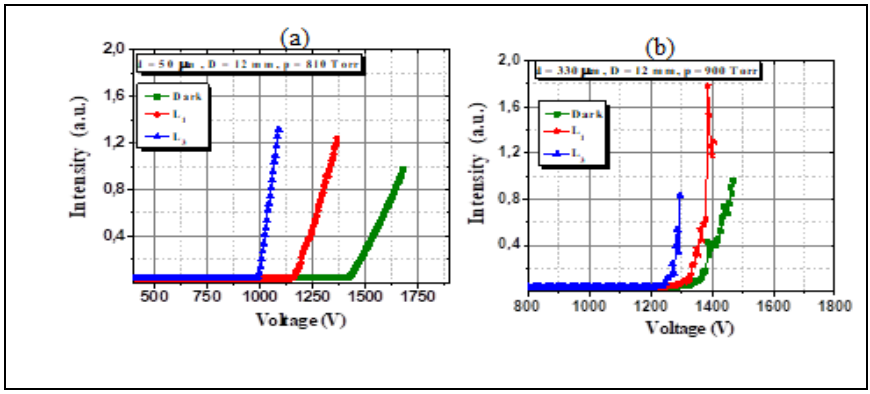

Figure. 10 (a-b)(DLE) of ZnSe-Ar cell module with discharge gap of: (a) 50 μm, b) DLE for 330 μm.

Glow discharge light emission measurements of ZnSe-Ar cell, illuminated under different IR radiation intensities (weak, medium, strong), were performed. Ar gas pressure was set at 810 Torr. First, the cell was evacuated to 10 mTorr using a mechanical vacuum pump. Then, Ar gas was introduced into the evacuated cell. Glow discharge light emission measurements were performed through photomultiplier tube. Thus, the electrical gas discharge dynamics of GDSS-lab cell module were analyzed at different gas pressure levels. While Ar gas medium is in an electrically-insulating state before reaching the electrical breakdown voltage (BDV) point, it is made electrically-conductive by increasing the infrared

illumination intensity on ZnSe photocathode.The plasma radiation (DLE) in the cell module shows instantaneous increases as a function of DC supply voltage rate and the infrared illumination intensity. The electrical breakdown voltage (BDV) of the microplasma cell was measured at around 1000 VDC for strong illumination (L_3), 1180 VDC for medium illumination (L_1), and 1450 VDC for weak illumination (dark) at 810 Torr Ar gas pressure. The electrical breakdown voltage (BDV) of the microplasma cell was measured at around 1220 VDC for strong illumination (L_3), 1330 VDC for medium illumination (L_1), and 1380 VDC for weak illumination (dark) at 900 Torr Ar gas pressure. DLE plots showed a multifilament form for Ar gas system with discharge gap of 330 μm, and a homegeneous form for that with gap of 50 μm. As a result of illuminating ZnSe cathode under increasing infrared radiation intensity, the number of electrons emitted into the micro gap also increases, thus decreasing the static electrical breakdown voltage (BDV).The wavelength and intensity of infrared radiation incident on the photocathode surface play a critical role in the electrical triggering of the microplasma reactor module and the initiation and development of the microplasma reaction sequence process.Electrical breakdown in gases is one of the most important phenomena governed by the reciprocal balance between the production of electrically charged particles and their loss through the processes of recombination and diffusion throughout the microplasma cell.It was understood that the collision ionization effect, which causes an increase in the number of electrons, plays an important role in field emission in microscale discharge gaps. Therefore, type of semiconductor cathode material, microstructure of electron emission's surface, and other electro-optical properties are critical in determining the infrared operating wavelength range of the microplasma reactor cell, and thus the electrical operating point of the system. It is aimed to detect low-energy, low-number photons in the infrared spectrum and convert them into high-energy, high-number photons in the visible spectrum.

4.NUMERICAL ANALYSIS

Numerical analysis, including modeling and simulation efforts, provides important data on the spatio-temporal variations of gas discharge dynamic parameters in the DBD systems. The microscale 2D-models of DBD system were numerically analyzed using FEM solver COMSOL Multiphysics AC plasma simulation program to investigate the spatiotemporal discharge parameters, including surface ion current density (ICD), migrative electron flux (MEF), capacitive power deposition (CPD), and reduced electric field (REF). The simulation results were presented in the color graphical media.Numerical calculations are based on (1) Mixture-averaged diffusion drift theory, (2) Maxwell

electron energy distribution function, (3) Townsend electron avalanche reactions, and (4) Low-pressure normal glow gas discharge process. Computational simulations are performed based on a boundary-separated structure to visualize the spatiotemporal distribution of gas discharge parameters in the cell. In the comparative models of the system, 2D- DBD cells coupled with ZnSe planar anode/cathode electrode pairs across a gas discharge gap were introduced in the simulations. Ar gas was used in the simulations at above atmospheric pressures. The electrical equivalent circuit (EEC) of the models was driven by an AC source in the simulations.These free electrons are accelerated towards anode electrode across gas medium of Ar. High-kinetic-energy free electrons collide with neutral gas molecules, initiating ionization reactions. Townsend avalanche (TA) mechanism causes the gas medium to transition from an insulating (cutoff) to a conducting (discharge) state. A self-sustaining microplasma is formed in the normal glow discharge regime under AC electric field in the gas medium. In The table-2 show that simulation of modeling parameters 2D-DBD cell.The glow radiation emitted along the optically transmissive and electrically conductive planar anode electrode (ZnSe) is amplified in intensity using a photoelectron multiplier tube, making it electronically detectable and processable.In this section of this study, we presented simulation results obtained theoretically, but could not be found experimentally. Our results were obtained for 20 kHz with ZnSe cathode in Ar gas discharge medium. DBD is a type of discharge used to produce stable plasma at room temperature, at least one electrode consisting of a dielectric material that limits the current. In this discharge, wo electrodes are separated by a dielectric barrier. The process uses high-voltage alternating-current (HV-AC) with different frequencies.

Table .2 Parameter definition of the simulation study

Parameter	**Description**
GDSS (Gas Discharge Semiconductor System)	ZnSe-Ar
Cell structure	Two-dimensional DBD reactor
Cell Supply voltage	V = 20.0 kV AC sinusoidal
Plasma process gas type	Ar
Plasma process gas pressure	P = 810 Torr
Distance between electrodes (discharge gap)	d = 0.300 mm (300 μm)
Photocathode electrode material	ZnSe (Adachi and Taguchi, 1991)
Photocathode electrode radius	r = 0.2 mm
Frequency	20 kHz
Initial (seed) electron density in the gas medium	$n_{e,o} = 1.0x10^9 (1/m^3)$
Paschen's Eq.	P.d = 810 Torr.300 μm = 24.3 Torr.cm
Cell operating ambient temperature	T = 300 K

In this discharge, the distance between the DBD electrodes can vary from micrometers to centimeters, depending on the type of gas used. One of the most distinctive features of this discharge is its symmetrical structure, making it an effective tool for surface modification. In this discharge, it is possible to achieve a higher electron structure plasma by using a double electrode structure as the power electrode instead of conventional electrodes. Dielectric barriers are used in all DBD outputs. These are the most important elements of a power system acting as a power source. The simulation model of the 2D-DBD cell is shown in Figure 11.

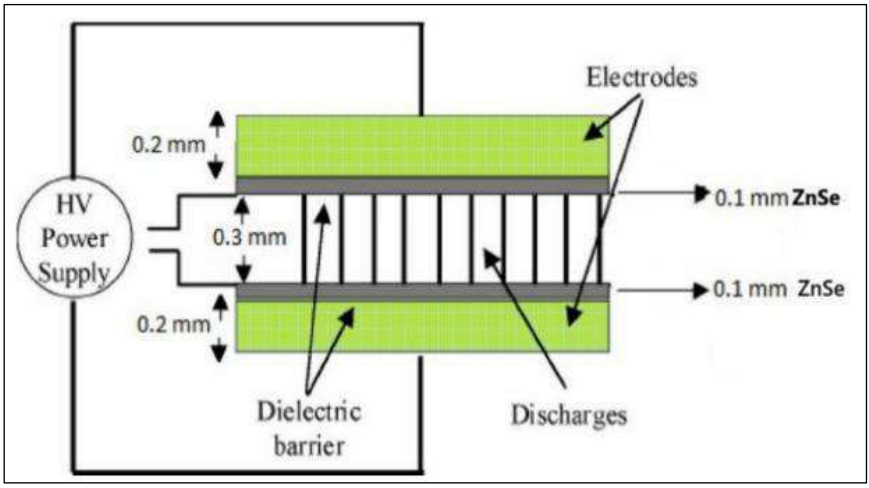

Figure .11 DBD cell with ZnSe cathode electrode

In Figure -12 show that the simulation results for DBD discharges, including (a) reduced electric field, (b) ion current density, (c) capacitive power deposition, and (d) migrative electron energy flux parameters visualized in 2D color graphical media. Reduced electric field (REF) was recorded at a peak value of 3.34×10^{-19} (Vm^2). Although background ionization reactions continue at the beginning (t_0=3.1623×10^{-14} s), ED shows an unstable and average distribution in the cell since Townsend (TA) ionization reaction has not yet started and the electrical breakdown of the gas medium has not occurred. The microplasma reaction sequence was completed in the simulation time scale at 1.4125×10^{-10} s in Ar gas system. Ion current density (ICD) was measured at a peak value of 11.2 A/m^2. Capacitive power deposition (CPD) analyses were also studied. The 2D- spatial distribution of CPD was observed in a filament form for 330 mm of discharge gap, and its peak was recorded at 6.59×10^7 (W/m^3). The fast and complex spatiotemporal variation of the microplasma is

directly related to the homogeneity of electric potential distribution in the cell. If this distribution is not maintained constant, different glow discharge areas may be formed across dicharge gap. The 2D- spatial distribution of migrative electron energy flux (MEF) was recorded at a peak value of $7.79x10^{20}$ V/(m^2s). Figure -13 shows the simulation results for DBD discharges, including (a) total capacitive power deposition (CPD) and (b) electron density (ED) variations in the graphical media in Ar gas system coupled with ZnSe cathodeThe DBDs are unstable and variable discharges. When a voltage is applied to the system, a high electric field is generated along the surface of the dielectric, followed by a gas discharge. This discharge causes electron avalanche from the cathode to the anode by a chain electron multiplication mechanism [33,34]. In Table 3 show that capacitive power deposition (CPD) values are tabulated per each cycle.When a time-varying alternating voltage is applied to the cell module, a discharge is observed across the entire surface of the dielectric, causing electron density (ED) parameter to vary in the range of 1x1014 to 9.7x1014 (1/m3) as shown in Figure 13(b).

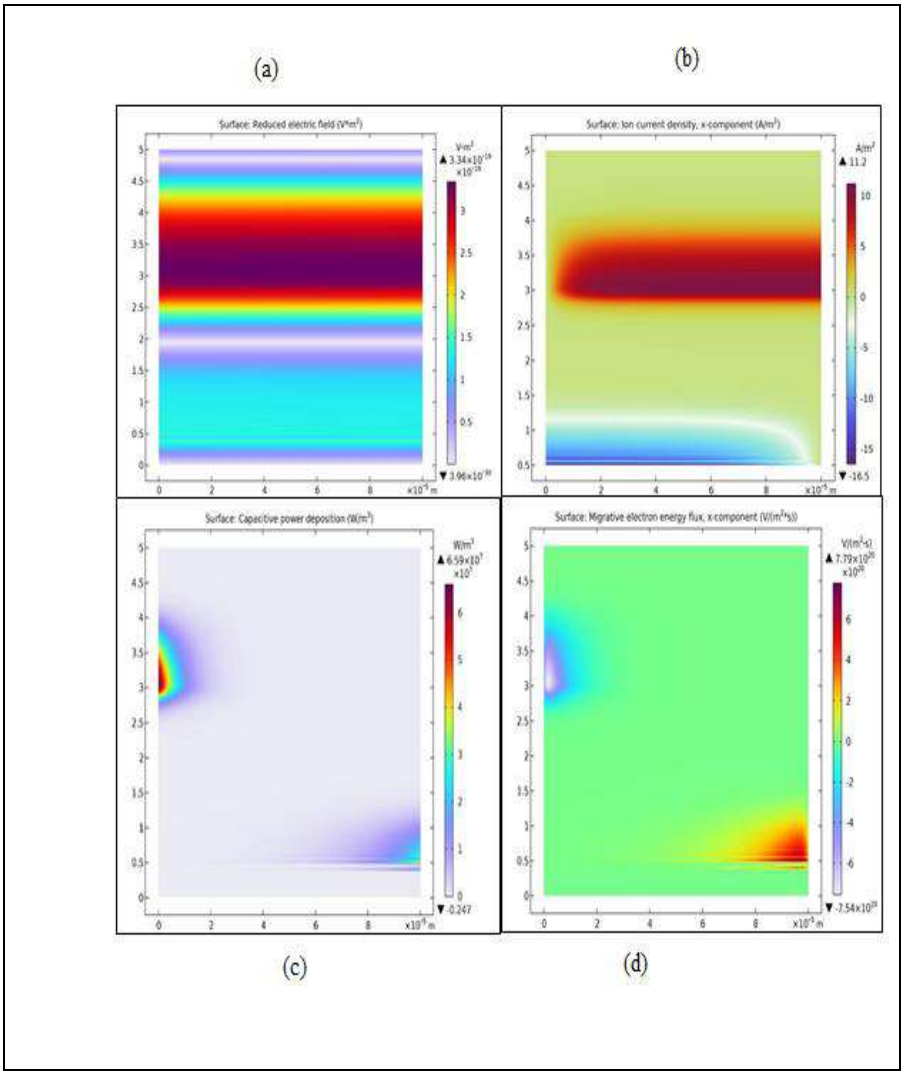

Figure 12. The 2D- spatiotemporal simulation results of DBD discharges: (a) Reduced electric field, (b) Ion current density, (c) Capacitive power deposition, (d) Migrative electron energy flux.

.

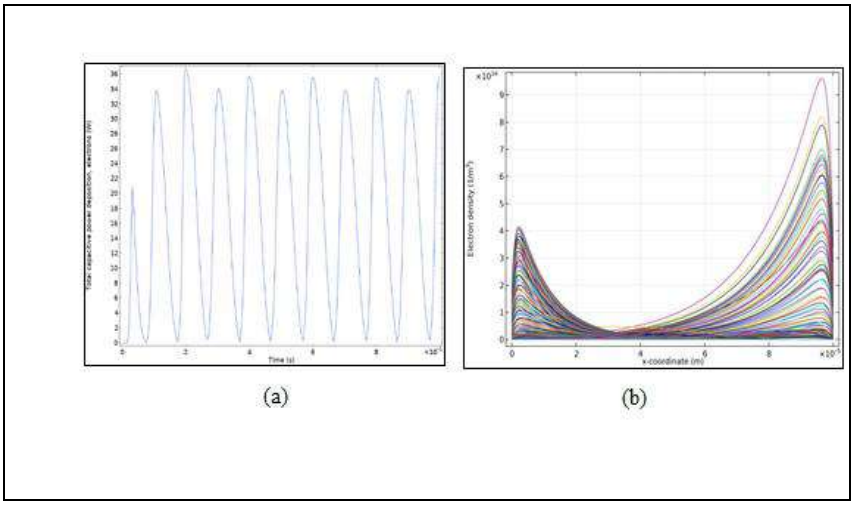

Figure 13. (a) Total capacitive power deposition (CPD), (b) electron density (ED) plots.

Table 3. CPD (W)values per cycles.

Time (s)	Cycle 2 (W)	Cycle 3 (W)	Cycle 4 (W)	Cycle 5 (W)	Cycle 6 (W)	Cycle 7 (W)	Cycle 8 (W)	Cycle 9 (W)	Cycle 10 (W)
1E-4	17.273	17.642	18.07	17.636	18.066	17.677	18.085	17.643	18.101

The DBDs are generated by high-frequency alternating current sources or high-frequency nanopulse sources. However, at atmospheric pressure, the DBDs generally operate in the filamentary mode, which we call microdischarges, or more precisely, the filamentary mode with discrete discharge channels [33-37]. Free charged particles tend to accumulate on the surface of dielectric layers. These charges accumulate on the dielectric surface, causing so-called "memory effects" and an electric field in the discharge area that opposes the initially applied electric field. The inducible electric field (E) plays a crucial role. Being opposite to the external electric field, it prevents the microdischarge channels from arcing. These charges accumulate on the surface, causing a memory effect [33-37].

5.CONCLUSION

The spatio-temporal discharge parameters and operating conditions of the DBD system in the normal glow discharge regime can be effectively controlled. Referring to experimental findings; reactor discharge current increases with increasing gas pressure. Limited operation of the DBD cell modules in the normal glow discharge regime is essential to prevent damage to the semiconductor material. Therefore, care should be taken to limit the reactor discharge current to the range of 1.0–10 mA. As the reactor discharge current shifts towards the arc regime, hot spot regions develop on the surface of cathode electron emission. Ar microplasma module with micro-digitated planar ZnSe cathode would operate more stable and with higher efficiency [38-45]. Referring to numerical analysis; the surface morphology of cathode electron emission can be effectively used to control the discharge parameters and hence the operating conditions of the DBD system. As a result, the effective surface area for cathode electron emission will gradually decrease with use of the cell, thus reducing overall operating performance and optimized service life. However, with an IR-VIS GDSμP system -based device specifically designed for the application requirements; low-energy and low-number infrared light photons can be directly detected and efficiently converted into high-energy and high-number visible light photons. The GDSμP and the DBD systems can be used to design and manufacture devices for potential applications in a wide range of industrial and defense applications.

REFERENCES

1. Schoenbach, K.H., Becker, K. (2016). 20 years of microplasma research: A status report. *The European Physical Journal D*, 70, 29.
2. Chiang, W.-H., Mariotti, D., Sankaran, R.M., Eden, J.G., and Ostrikov, K. (2020). Microplasmas for advanced materials and devices. *Advanced Materials,* 32(18), 1905508.
3. Tabib-Azar, M., Pai, P. (2017). Microplasma field effect transistors. *Micromachines*, 8(4), 117.
4. Baranov, O. O., Xu, S., Xu, L., Huang, S., Lim, J. W. M., Cvelbar U., Levchenko I., and Bazaka, K. (2018). Miniaturized plasma sources: Can technological solutions help electric micropropulsion? *IEEE Transactions on Plasma Science,* 46(2), 230–238.
5. Shivkumar, G., Qiao, L., and Alexeenko, A. A. (2019). Plasma-flow interactions in field-emission discharges with applications in microcombustion. *Journal of Physics D: Applied Physics,* 52, 384001.
6. Takahashi, T., Mori, D., Kawanabe, T., Takao, Y., Eriguchi, K., and Ono, K. (2019). Microplasma thruster powered by X-band microwaves. *Journal of Applied Physics,* 125, 083301.
7. Liangliang, L., and Wang, Q. (2015). Microplasma: A New Generation of Technology for Functional Nanomaterial Synthesis. *Plasma Chemistry and Plasma Processing,* 35, 925–962.
8. Kurt, H.Y., Inalöz, A., Salamov, B.G. (2010). Study of non-thermal plasma discharge in semiconductor gas discharge electronic devices. *Optoelectronics and Advanced Materials-Rapid Communications,* 4(2), 205-210.
9. Kurt, H.H., Koc, E., Salamov, B.G. (2010). Atmospheric Pressure DC Glow Discharge in Semiconductor Gas Discharge Electronic Devices. *IEEE Transactions on Plasma Science,* 38(2), 137-141.
10. Salamov, B.G., Kurt, H. H. (2020). Ar-driven gas discharge system based on dielectric zeolite material. *The Journal of The Minerals, Metals & Materials Society (JOM)*, 72(10), 1-7.
11. Kurt, H.Y., Salamov, B.G., and Mammadov, T.S. (2005). Electrical instability in a semiconductor gas discharge system. *Crystal Research and Technology*, 40(12), 1160-1164.
12. Sadiq, Y., Kurt, H.Y., Albarzanji, A.O., Alekperov, S.D, Salamov, B.G. (2009). Transport properties in semiconductor-gas discharge electronic devices. *Solid-State Electronics*, 53(9), 1009-1015.

13. Kurt, H.H. (2018). Exploration of gas discharges with GaAs, GaP and ZnSe electrodes under atmospheric pressure. *Journal of Electronic Materials,* 47, 4444-4454.
14. Kurt, H.H., Tanrıverdi, E. (2017). Electrical properties of ZnS and ZnSe semiconductors in a plasma-semiconductor system. *Journal of Electronic Materials,* 46(7), 3965-3975.
15. Kurt, H.H. (2018). Exploration of the infrared sensitivity for a ZnSe electrode of an IR image converter. *Journal of Electronic Materials,* 47(8), 4486-4492.
16. Fu, Y., Zhang, P., Verboncoeur, J.P., and Wang, X. (2020). Electrical breakdown from macro to micro/nano scales: a tutorial and a review of the state of the art. *Plasma Research Express,* 2(1), 013001.
17. Garner, A.L., Meng, G., Fu, Y., Loveless, A.M., Brayfield II, R.S., Darr, A.M. (2020). Transitions between electron emission and gas breakdown mechanisms across length and pressure scales. *Journal of Applied Physics,* 128(21), 210903.
18. Go, D.B. and Venkattraman, A. (2014). Microscale gas breakdown: ion-enhanced field emission and the modified Paschen's curve. *Journal of Physics D: Applied Physics,* 47(50), 503001.
19. Garner, A.L., Loveless, A.M., Dahal, J.N., Venkattraman, A. (2020). A tutorial on theoretical and computational techniques for gas breakdown in microscale gaps. *IEEE Transactions on Plasma Science,* 48(4), 808–824.
20. Somayajula, S.K., Sriram, A.T., Shelar, V.M. (2020). Study of argon and xenon gas properties on DC-glow discharge plasma. *Journal of Physics Conference Series,* 1706(1), 012030.
21. Niklaus, F., Vieider, C., and Jakobsen, H. (2008). MEMS-based uncooled infrared bolometer arrays: a review. *Proceedings of SPIE-The International Society for Optical Engineering,* 6838.
22. Rogalski, A. (2011). Recent progress in infrared detector technologies. *Infrared Physics & Technology,* 54(3), 136-154.
23. Norton, P.R. (1999). Infrared detectors in the next millennium. *Proceedings of the SPIE*, 3698, 652-665.
24. Yu, P. Y., Cardona, M. (2010). *Fundamentals of Semiconductors: Physics and Materials Properties. Graduate Texts in Physics*. Fourth Edition, Springer.
25. Nweze, C.I., Ekpunobi, A.J. (2014). Electrodeposition of zinc selenide films on different substrates and its characterization. *International Journal of Scientific & Technology Research,* 3(9), 201-203.

26. Yan, L., Woollam, J.A., Franke, E. (2002). Oxygen plasma effects on optical properties of ZnSe films. *Journal of Vacuum Science & Technology A: Vacuum, Surfaces, and Films,* 20(3), 693-701.
27. Banthí-Barcenas, J.C., Sutara, F., and Hernández-Calderón, I. (2018). Design of a quantum well based on a ZnCdSe/ZnTe type II heterostructure confined type I within ZnSe barriers. *8th International Conference on Low Dimensional Structures and Devices (LDSD 2016), AIP Conference Proceedings*, 1934(1), 030001.
28. Fu, Y., Zhang, P., Krek, J., and Verboncoeur, J. P. (2019). Gas breakdown and its scaling law in microgaps with multiple concentric cathode protrusions. *Applied Physics Letters*, 114, 014102.
29. Naresh, C. Das. (2011). Tunable infrared plasmonic absorption by metallic nanoparticles. *Journal of Applied Physics,* 110, 046101.
30. Zhang, J., Wang, Y., Li, D., Sun, Y. (2022). Engineering Surface Plasmons in Metal/Nonmetal Structures for Highly Desirable Plasmonic Photodetectors. *ACS Materials Letters,* 4(2), 343−355.
31. Brayfield, II R.S., Fairbanks, A.J., Loveless, A.M., Gao, S., Dhanabal, A., Li, W., Darr, C., Wu, W., and Garner A.L. (2019). The impact of cathode surface roughness and multiple breakdown events on microscale gas breakdown at atmospheric pressure. *Journal of Applied Physics,* 125, 203302.
32. Malayter, J. R. and Garner, A. L. (2020). Theoretical assessment of surface waviness on work function. *AIP Advances,* 10(9), 095110.
33. Kogelschatz U. (2003). *Plasma Chem. Plasma Process*.23, 1.
34. Wagner, H.-E., Brandenburg R., Kozlov, K. V., Sonnenfeld, A., Michel, P., and Behnke, J. F. (2003). *Vacuum*, 71,417.
35. Raizer Y. P., Gas Discharge Physics (*Springer*, Berlin, 1991).
36. Roth J. R., Industrial Plasma Engineering: Volume 2: Applications to Nonthermal Plasma Processing
(*CRC Press, Boca Raton*, FL, 2001).
37. Truong Hoa Thi, Uesugi Yoshihiko, Nguyen (2021). Mechanisms of low-frequency dielectric barrier discharge (DBD) plasma driven by unipolar pulses and bipolar pulses. *AIP Advances*, 11, 025022.
38. Ongun, E., Yücel (Kurt), H.H., Utaş, S. (2024). Investigation of direct current micro glow discharge plasma in the modified zinc selenide-argon system. *8th International Conference on Innovative Studies of Contemporary Sciences*. Tokyo, Japan.
39. Ongun, E., Yücel (Kurt), H.H., Utaş, S. (2024). Modeling and simulation of DC glow discharges in the zinc selenide-argon/hydrogen microplasma

system. *8th International Conference on Innovative Studies of Contemporary Sciences*. Tokyo, Japan.

40. Ongun, E., Utaş, S., Yücel (Kurt), H.H. (2023). ZnSe-Ar/H_2 yarıiletken-gaz deşarj mikro plazma sisteminin incelenmesi: Modelleme ve simülasyon. *Yoğun Madde Fiziği Ankara Toplantısı*.
41. Ongun, E., Utaş, S., Yücel (Kurt), H.H. (2024). An investigation of DC - driven micro plasma system with ZnSe coupled Ar/H_2 gas discharge medium at sub atmospheric pressure. *15th China to Adriatic Turkish World International Scientific Research Congress. ANAS Central Library of Science & IKSAD Institute*. Baku, Azerbaijan.
42. Ongun, E., Yücel, H.H., Utaş, S. (2024). DC-driven sub atmospheric glow discharges in the infrared-stimulated. *Journal of Materials Science: Materials in Electronics,* 35, 655-669.
43. Ongun, E., Yücel, H.H. (2024). Spatiotemporal Modeling and Simulation of DC Microplasma Glow Discharges in ZnSe-Ar/H_2 System. *Inspiring Technologies and Innovations,* 3(1), 1-8.
44. Kurt H.Y., Inalöz A., Salamov B.G. (2010). Study of non-thermal plasma discharge in semiconductor gas discharge electronic devices. *Optoelectronics and Advanced Materials-Rapid Communications*, 4 205.
45. Kurt H.Y. (2018). Exploration of the infrared sensitivity for a ZnSe electrode of an IR image converter, *Journal of Electronic Materials* 47 (8), 4486-4492.

Chapter 4

INVESTIGATION OF THE CHARACTERISTICS OF PLASMA CELLS WITH LAB6 AND IRIDIUM CATHODES

Hatice Hilal YÜCEL[1], Yücel Mert KARAOĞLU [2], Tuğçe GÜRSOY [3]

1.INTRODUCTION

The fundamental principle of plasma formation and the search for new alternative sources to address the global energy crisis are the primary motivations for this study. The energy gap that arises in parallel with technological advancements can be addressed through the efficient and reliable use of plasma systems. This study examines the interaction of boride structures in the lanthanum group and metal structures with various low band gaps with inert gases. The system is constructed by placing a thin sheet-shaped cathode surface within a cylindrical area and an anode surface of equal thickness at the other end. The system operates at voltages lower than the band gaps of the materials. The aim is to develop a plasma cell that exhibits battery properties due to its low voltage operation.

process. Masses of hot, ionized gas stabilized by magnetic fields are called plasmoids. Plasmoids have both plasma-induced pressure and internal pressure from magnetic fields. In other words, we can say that plasmoids are coherent structures formed by the combination of plasma and magnetic fields. Plasmoids can also be expressed as plasma cylinders in the direction of the applied magnetic field.The primary particle acceleration mechanism in a magnetized blazar region is generally known as magnetic reconnection. A significant portion of the emitted high-energy radiation originates from plasmoids and their mergers within the reconnection layer. Plasmoid mergers, which cause significant energy concentrations, can cause powerful multi-wavelength flares and consequently large shifts in synchrotron polarization signatures. Given the

[1] Prof. Dr., Gazi University, Institute of Science, Department of Physics, Ankara, hkurt@gazi.edu.tr, (ORCID: 0000- 0002-1277-5204)
[2] Undergraduate student, Gazi University, Institute of Science, Department of Physics, Ankara, ymr.darkson@gmail.com, (ORCID: 0009-0002-1576-652X)
[3] Undergraduate student, Gazi University, Institute of Science, Department of Physics, Ankara, tugce.gursoy@gazi.edu.tr, (ORCID: 0009-0005-0805-7284)

relatively limited number of studies in this area, the radiation properties of plasmoid mergers have not been adequately investigated due to the difficulties in monitoring these recombination processes.Among all ceramic materials produced, LaB6 has the best thermionic emission. This material offers many technological advantages, including low electron emission and good chemical resistance. LaB6 has been identified as possessing many advantageous properties, including low electron emission and good chemical resistance. It has a high melting point, typically exceeding 2200°C. Melting points vary depending on impurities and are therefore sensitive to the B/La ratio. Based on all the properties mentioned, it is clear that LaB6 plays a very important role in industry.[1] LaB6 is a material crystallized with a cubic structure. La atoms occupy the center, while boron atoms occupy the corners of the unit cell. In this arrangement, covalent bonds between boron atoms provide hardness and stability at high temperatures. However, the free electrons of La atoms are responsible for its hot-emission properties.One of the ultimate reasons for choosing lanthanum hexabode as the cathode is that this material can absorb in the near IR region due to its low specific density.[1]

As is known, the need for clean water resources is increasing daily due to the rapid population growth in our world. In areas where freshwater resources are scarce, purification and desalination of salty seawater are being attempted as an alternative to meet this need. Materials that can absorb light, increase vapor production, and convert it into heat are attracting significant interest. Au nanoparticles, due to their very strong light absorption in the NIR region thanks to localized surface plasmon resonance (LSPR), are used as excellent photothermal conversion materials. However, despite all these properties, Au nanoparticles exhibit poor stability under IR illumination when exposed to long-term illumination. Furthermore, their high cost has limited their application. Lanthanum hexaboride (LaB6), a functional ceramic discovered in 2003, emerged as a material with excellent NIR adsorption. Therefore, this material is gaining importance as a stable photoconversion material.[2]Iridium is at the forefront of electrocatalyst development efforts because it is currently the only commercially available catalyst material for use in oxygen evolution reactions (OER) in an acidic environment. Accelerated dissolution of iridium anode in the presence of organic compounds [3]Iridium cathode has been used instead of LaB6. The results show that Lab6 has high plasma activity than that Iridium. That is, migrative electron flux is 3.48 times higher than that of iridium which means that LaB6 provides effective performance thereby increasing surface activity a catalyst. The results give key issues to enhance the device performance with high performance computer simulations. Liang et all have

reported [6, 7] the catalytic performance of iridium-based catalysts in their researh.[4] This study provides important guidance about Iridium and LaB6 materials.

2.THEORETICAL KNOWLEDGE

A glow discharge is a discharge consisting of bright and dark plasma regions with different electric field distributions supported by secondary emission, offering significant advantages in many industrial applications due to its luminous nature. In this discharge, the current density is not stable and electric field domains move from the cathode to the anode which causes a strong potential drop of 100-400 V. Conversely, negative space charge accumulation occurs around the anode.[5] In this discharge, the primary region where secondary electron emission (SEE) dominates is the cathode layer, which has a big amount of positive space charge near the cathode surface. Depending on the gas pressure and gap distance, a strong potential drop of approximately 100-400 V is observed. A negative space charge is present near the anode. The central portion, representing a weakly ionized state, is the positive column.[5] At the outer boundaries of the Aston layer, the electron has enough energy to create the cathode glow. [5]The region following this region, called the negative glow, which is separated by sharp borders from the cathode dark space. The dark region, also called the Faraday dark space, forms immediately after the negative glow due to the loss of energy by the electrons. Although the electric field and electron temperature increase, the electron concentration decreases in this region. As a result of all this, the plasma density of the Faraday dark space decreases and the electric field strength will increase, which leads to the formation of a positive column. An interesting fact is that, even though the positive column shrinks as the anode approaches the cathode, the structure of the cathode layer is preserved. So much so that, as the anode is brought even closer to the cathode, several sharply defined regions emerge, one between the anode glow and the other dark.[5]

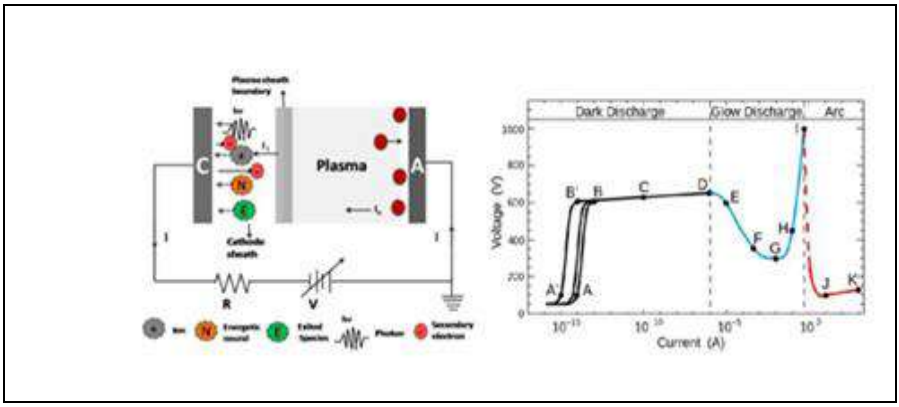

Figure.1 Discharge processes of sytems [7].

negative space is created, and the electric field near the anode increases. The decrease in electron density explains the dark space, while the converse increase in electric field explains the anode glow.[5] Plasma is divided into two categories: thermal and non-thermal plasma. Non-thermal plasma is generally used in industry, medicine, and healthcare, while thermal plasma finds its place in the energy and fuel sectors. Furthermore, while thermal plasma exhibits temperature equilibrium between particles, non-thermal plasma does not.

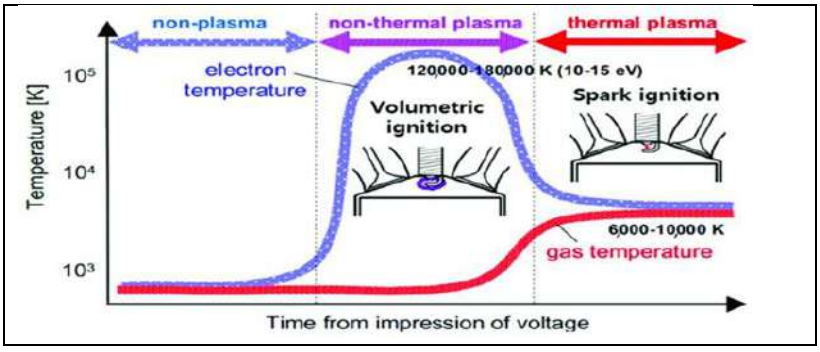

Figure.2 Temperature dependent behavior of plasma in different voltage ranges[13]

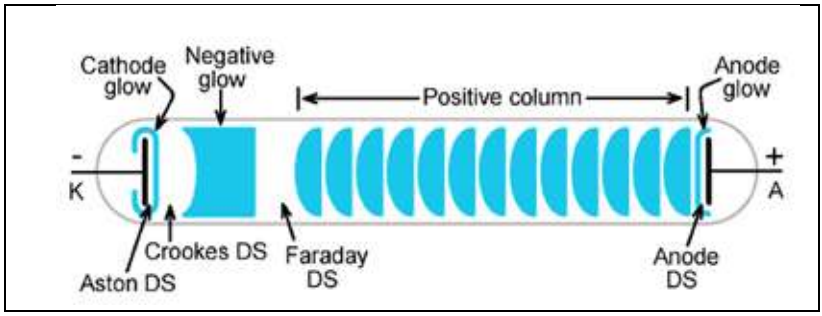

Figure.3 Representative image of glow discharges [15].

We can also classify plasmas as equilibrium and non-equilibrium. While equilibrium plasmas exhibit thermodynamic equilibrium among all plasma types in the plasma environment, non-equilibrium plasmas exhibit different energy conditions for different plasma types. These properties of non-equilibrium plasmas allow for control over plasma characteristics. This is an indispensable feature, especially in the medical field. Thermal plasmas are plasmas above 10,000 K. They have a high electron and radiation density.There are different thermal plasma generation techniques. These can be classified as ICP (inductively coupled plasma), arc discharges, and plasma jets. ICP plasmas generate thermal plasma based on changing magnetic flux via electromagnetic induction, while plasma jets create directed plasma streams. Arc plasmas, on the other hand, generate high-temperature arc discharges using a high-electric arc. Laser-induced plasmas, widely used in technology and medicine, are generated by exposing target materials to intense laser radiation, while laser-induced plasmas are generated by exposing target materials to intense laser radiation. Non-thermal plasmas present a significant temperature difference between electrons and heavy particles. In other words, electron temperatures range from 1 to 10 eV, while the temperature of the gas remains the same as the ambient temperature. They have a much lower ionization rate than thermal plasmas, ranging from 10^{-6} to 10^{-1}. Thermal plasmas have electron densities between 10^{-1} and 10^{-6} m^{-3}. Cold plasmas offer unique advantages in plasma medicine due to their selective reactions. Dielectric barrier discharges (DBDs) create cold plasma with insulating barriers. Corona discharges, an example of cold plasma, create non-thermal plasma localized in high electric field regions.Electrons and other atoms within a plasma have different speed and energy distributions. One of these is the Maxwell-Boltzmann distribution, which describes particles in thermal equilibrium. Non-Maxwellian distributions, on the other hand, are observed in non-equilibrium plasmas and therefore affect plasma reaction kinetics. The Maxwell-Boltzmann distribution describes particle speeds in

thermal equilibrium plasmas. Non-Maxwellian distributions occur in non-equilibrium plasmas and affect reaction kinetics.

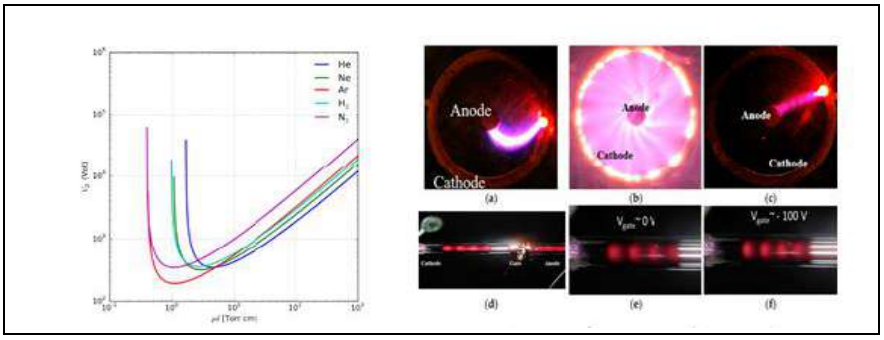

Figure4. (a) Plasma stage of breakdown voltage charcteristic feature (b)Plasma state of the gas after threshold voltage [6,7].

Energy distribution occurs between different degrees of freedom (translation, rotation, vibration). In non-thermal plasmas, ohmic energy transfer from the electric field is transferred to plasma particles through collisions. [6] Figure 1.1 shows breakdown curves for different gases and Fig.1.1.1 shows the stages of plasma formation after breakdown.As can be seen, a sudden glow is observed after a critical voltage (breakdown). This glow then covers the entire cathode surface, and due to the non-homogeneous electric field, distinct glow discharge regions are observed [6,7].

.

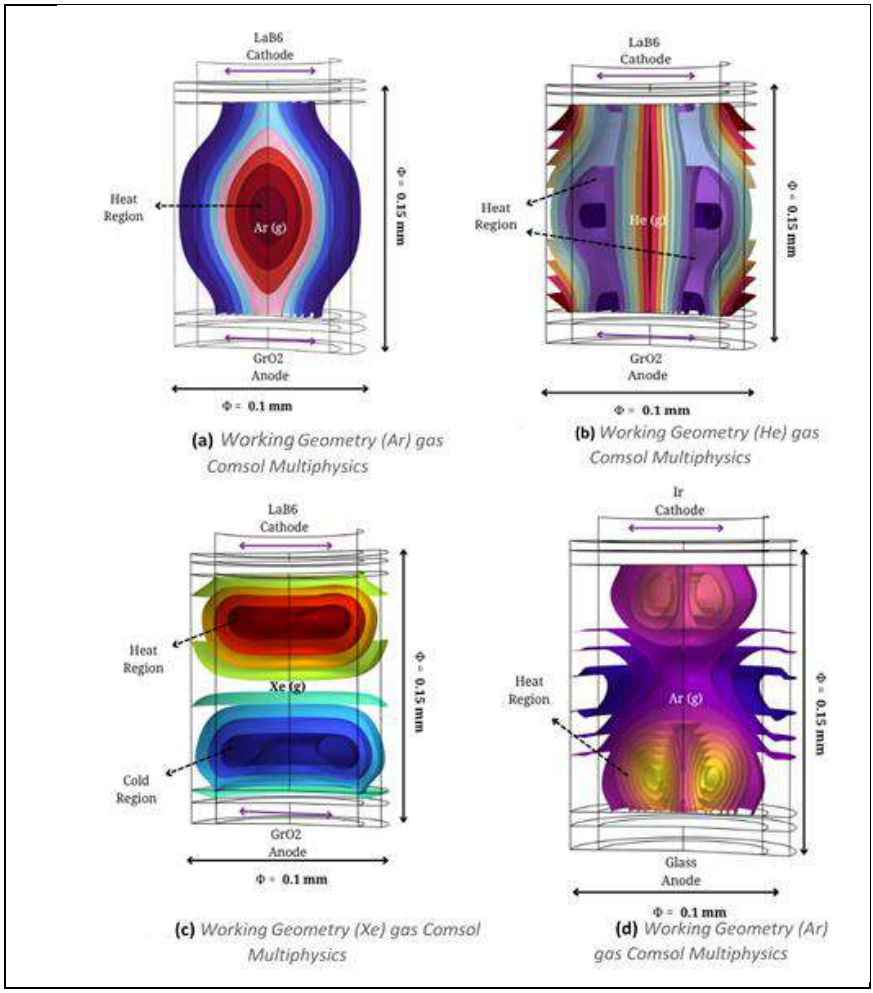

Figure 5. (a)(b)(c)(d) structure contains thin plate surfaces separated [15,16].

3.MATERIAL AND METHODS

In Figure 1.2 (a)(b)(c)(d), structure contains thin plate surfaces separated at two ends. These plates consist of two surfaces: the cathode is lanthanum hexaboride, and the anode is graphite oxide. Various reactive inert gases are contained within the cylinder. In the event of power loss at low voltages, electrons in the valence band of the cathode material are excited to the conduction band, where they collide with gas atoms in the environment, causing ionization, thus making the gas conductive. Consequently, a plasma environment accompanied by radiation is formed [15,16].

3.1 types of gas discharge

There are three types of gas discharges: Townsend, glow, and arc. The following figure shows these gas discharges and their current values at different voltages. A Townsend discharge is a nearly homogeneous and stable discharge. A glow discharge is unstable due to instabilities in the electric field and the accumulation of space charge near the cathode[15,16].However, due to its high current density, it is a luminous discharge, hence its name. An arc discharge is completely unstable, with a filamentary current density.

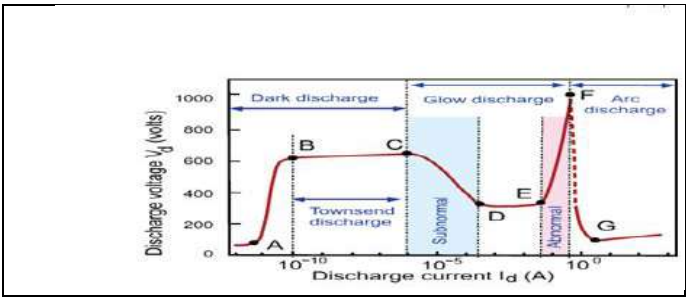

Figure.6 Discharge processes of depented voltage & current[15,16].

3.2 ionization processes

3.2.1 Alfa (α) ionization process

To briefly describe the process, semi-free electrons emerging from the cathode undergo elastic collisions with the surrounding neutral gases. Initially, the electrons' speeds are slow and therefore they cannot sufficiently excite the electrons in the gas atom. Therefore, when no excitation occurs, photons with energy E=h.ν are very few. This corresponds to the Dark Townsend region in the 1st Townsend ionization region [17,18].The emitted radiation is extremely low. The reason for the low radiation is that the semi-free electrons lack sufficient kinetic energy, meaning they cannot accelerate. To be clear, Bremsstrahlung radiation is observed in proportion to the deceleration of these electrons as they pass around the nucleus. Bremsstrahlung radiation is also referred to in the literature as an energy-carrying electromagnetic wave. Considering the weak kinetic energy of the incoming electrons, it is clear that there will not be a significant amount of Bremsstrahlung photon radiation. Because the lack of kinetic energy prevents the electron from approaching the nucleus, it will be slowed down at a certain distance (r).

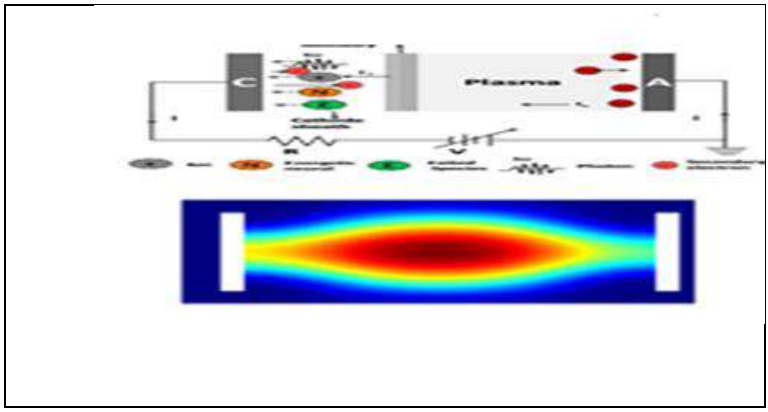

Figure 7. Surface electron density gradient movement at the cathode [7].

As a result, minimal radiation be observed.A small number of bremsstrahlung photons will produce maximum radiation because the radiation rate is proportional to the distance of the electrons from the nucleus. The closer the electrons pass to the nucleus, the more intense the x-ray photons they emit. Considering the Townsend primary ionization process, or (α) process, the bremsstrahlung photon will be less energetic because the electrons have lower kinetic energy. Consequently, some regions of the system will exhibit dark surfaces with little luminescence or luminescence. This is why it is called the Dark Townsend region.Electrons and other carriers in a Maxwellian plasma have different energies. Depending on the distance between them, electrons interact with ions and neutral atoms in the medium according to the Coulomb force.[8] During these collisions, the scattered or decelerated electrons begin to emit Bremsstrahlung photons. In the medium used, Bremsstrahlung photons emitted by a Maxwellian plasma can act as a result of the motion of thermal electrons, causing braking. Bremsstrahlung photons emitted in the medium arise from the radiative power of the photons.[8]

$$P \propto C.n_e.n_i.Z^2\sqrt{T_e} \tag{1.1}$$

Here (P) represents the power of the radiation, (C) is a constant ($1.69x10^{-38}$ w/m^3), the number of electrons (ne), the number of ions (ni), the ionized atomic charge Z and Te are expressed by the electron temperature.

Table1. ion tipleri ve kullanım alanları

ion type	Notation	Charge	Use of place
Ion singly charged ion	Ar^{+}	+1	Glow discharges,
doubly charged ion	Ar^{2+}	+2	low-energy plasmas
Triple charged and more	Ar^{3+}, Ar^{4+}	+3, +4	High-energy plasmas

Bremsstrahlung occurs as a result of the acceleration of an ion in Coulomb field. This can be considered a small inelastic effect on Coulomb scattering. For this phenomenon to occur, the electron must approach the ion within a certain distance. Thermal bremsstrahlung is one of the two important processes in radio astronomy, and this strong absorption provides evidence for the presence of ionized gas in optically inaccessible locations and in the interstellar medium.[9]

The emissivity of the emitted radiation varies with the square of the plasma density, so dense clouds of ionized gas are preferentially visible. In fact, these clouds are only found near strong heat sources, such as young, massive stars with photoionizing radiation flux. Therefore, clouds with high thermal bremsstrahlung emission can be used as tracers of star formation activity in a galaxy in our universe.[9] Thermal bremsstrahlung phenomena are seen in astrophysical plasmas (solar, stellar atmospheres) and laboratory gas discharges, while non-thermal bremsstrallung phenomena are seen in X-ray tubes and tokamaks whose energies are non-Maxwellian (e.g. radiation caused by accelerated electrons as a "beam").[10] The formation of bremsstrahlung radiation from ions generated by the excitation of the cathode material is evidence of its existence. In some cases, despite low electron temperatures, excess intensity can dominate the radiation.

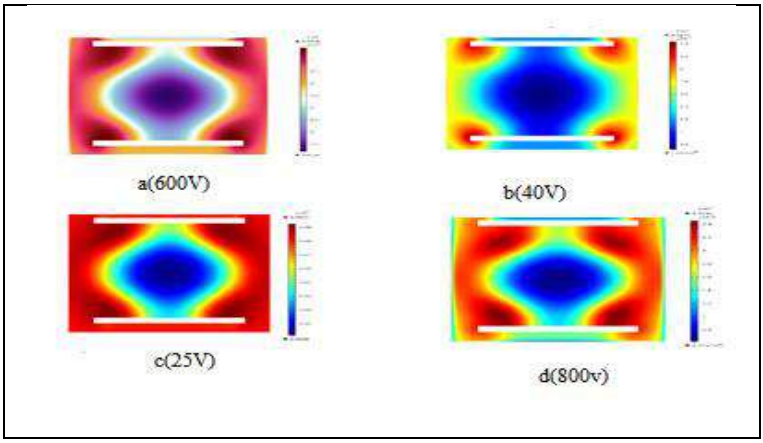

Figure 8. Surface charge distribution gradients of Lab6 in different voltage ranges.

3.2.2Gamma (γ) ionization process

The process of removing electrons from the surface due to positive charges accumulating near the cathode is a gamma-phase process. An electric field is created around the cathode due to the potential difference. Furthermore, the speed of the electrons increases with increasing voltage,

$$W = \vec{F}.\vec{d} \equiv q.\vec{E}.\vec{d} \quad (1.2)$$

$$\Delta V = q.\vec{E}.\vec{d} \quad (1.3)$$

$$\frac{1}{2} m_e.v_e^2 = q.\vec{E} \quad (1.4)$$

$$\vec{v}_e = \sqrt{\frac{2q.\vec{E}}{m}} \quad (1.5)$$

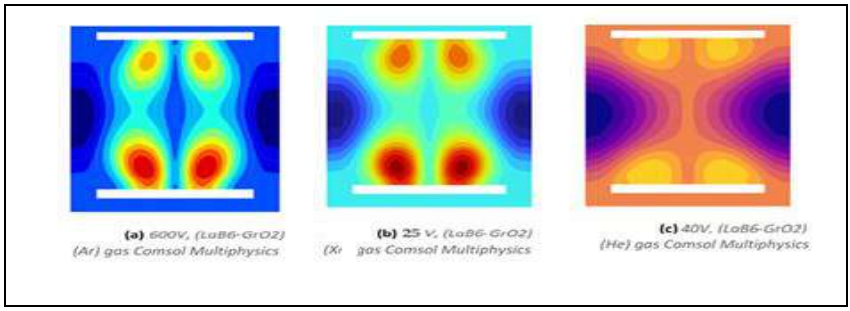

Figure.9 Electron density distributions in different gas environments at different voltages.

In other words, as the probability of inelastic collisions increases and the number of photons with energy (E=h.ν) increases, the radiation will become stronger. Consequently, as a result of these collisions, the electrons in the atom's orbital orbital are elevated to a higher orbital, and at this point, a phase transition is observed. This is called the γ process, which is Townsend's second ionization process. The observed phase transition is called a glow discharge. The positive charges that accumulate around the electron due to its heavy mass are called space charges. This secondary emission process is the basis of the electron avalanche mechanism.The materials used in the simulation are as follows,LaB6 is a very important and special material used in thrust engines and has been tested for a long time. The importance of this material stems from its very low work function. Therefore, its low work function and bandgap create a more intense plasma environment in a shorter time.Lanthanum hexaboride has been compared to tungsten in previous studies and has been found to exhibit a 10-fold brighter effect than tungsten [6]. Due to its low work function, it has a longer lifespan, unlike cathode materials grown with calcium, barium, and aluminum.[11]Graphite oxide has been used in many different ways for long-term energy storage, rechargeable systems, and environmental impacts. More specifically, graphite oxide tends to interact with other materials due to its chemical properties and the presence of oxygen. Furthermore, its electrical conductivity, susceptibility to optical stimulation, and mechanical strength contribute to its longevity.[12]

3.2.3 Ir and Glass systems:

Iridium is a material with low corrosion properties. Due to its high conductivity, it has a wide spectrum. When used it as a cathode material, it can last for long periods without deformation. The glass that forms the anode forms a type of DBD (dielectric barrier discharge) structure, trapping ions within the

cell. Furthermore, because space charges accumulate around the cathode region, the cathode is more prone to damage than the anode. Furthermore, because the band gap varies depending on the cathode material and electrons are released from the cathode, the selection of a durable material is crucial. While iridium, which is electrically conductive, loses electrons, the ions and molecules formed during Townsend remain in the cell without scattering, thanks to the dielectric properties of the glass, increasing efficiency.[13][14]

4.CONCLUSION

Due to the scarcity of fossil fuels and their environmental pollution, alternative energy sources are being sought to replace traditional energy consumption. Energy storage research has accelerated in parallel with the growth of the human population and the increasing energy demand. Therefore, there is an urgent need to develop new green energy systems, including supercapacitors and batteries, to meet the growing need for energy storage. This study contains crucial and valuable information regarding the need for alternative energy sources today. Clean and reliable energy sources will be achieved by using technology effectively and efficiently for the benefit of humanity.

Knowledge: *This work was funded by the Scientific and Tecnological Research Council of Türkiye (Tübitak 2209-A)*

REFERENCES

[1]Demirskyi D. Tohru S., et al., (2022). Consolidation and high-temperature strength of monolithic lanthanum hexaboride, J ACeramSoc.105, 4277–4290.

[2] Chaofan Z., Baohua Y., , et,al (2020). J Am Ceram Soc.103, 3466–3472

[3] Seohyeon K., Youngrok L., et al., (2025).Communications.16, 8946.

[4] Yao L.,Hongzhong C.,Jiushuai D.,at al.(2020).Iridium surface treatment by glow plasma treatment and ıts application as electrocatalyst for methanol and co oxidation, j. electrochem. sci.15, 4953 – 4963.

[5] https://www.sciencedirect.com/topics/engineering/glow-discharge

[6]https://fiveable.me/plasma-medicine/unit-1/types-plasmas-thermal-nonthermal/study-guide/ekjxlghwyvueganchttps://fiveable.me/plasma-medicine/unit-1/types-plasmas-thermal-non-thermal/study guide/ekjxlghwyvueganc)

[7]Tabib A.M,Pai.P.,(2017).Microplasma field effect transistors micromachines, Micromachines. 8 (4), 117.

[8] Massey, H.S.W ,McDaniels E.W.,Bederson B.,(1984).applied atomic collision physics ,barnrt and m.fa. harrison 2 plasmas academic press ınc.

[9] https://www-zeuthen.desy.de/~pohlmadq/teach/405-505-f05/sess18.pdf

[10] Chen, Francis F. – Introduction to Plasma Physics and Controlled Fusion - Radiation losses

[11] Warner, D. J., Branam, R. D., & Hargus, W. A., (2009). Ignition and plume characteristics of Low-Current cerium and lanthanum hexaboride hollow cathodes, Journal of Propulsion and Power. 26(1), 130–134 .

[12] Li, F., Jiang, X., Zhao, J., & Zhang, S., Graphene oxide: A promising nanomaterial for energy and environmental applications. Nano Energy. 16, 488–515 (2015).

[13] Li, J., Ma, C., Zhu, S., Yu, F., at al., (2019). A review of recent advances of dielectric barrier discharge plasma in catalysis., Nanomaterials. 9(10), 1428 (

[14] UniversityWafer Inc. (n.d.),(2025). ITO glass substrates—technical data sheet. Retrieved from https://www.universitywafer.com/ito-glass.html.

[15]https://physics.stackexchange.com/questions/266010/alternate-light-and-dark-regions-in-cathode-ray-tube

[16] Raizer Yu. P.,(2010). Gas-Discharge Physics , Nauka, Moscow (1987)]

[17] Kurt HY, Inalöz A, Salamov BG, (2010).Study of non-thermal plasma discharge in semiconductor gas discharge electronic devices, Optoelectronics and Advanced Materials-Rapid Communications.4, 205-210.

[18] Kurt HY,(2018).Exploration of the infrared sensitivity for a ZnSe electrode of an IR image converter Exploration of the infrared sensitivity for a ZnSe electrode of an IR image converter, Journal of Electronic Materials. 47 (8), 4486-4492.

Chapter 5

RADIOACTIVITY AND RADIOLOGICAL HEALTH RISK ASSESSMENT

Aslı KURNAZ[1], Aybaba HANÇERLİOĞULLARI[2], Şeref TURHAN[3]

1.INTRODUCTION

Radioactivity is fundamental physical phenomenon resulting from decay processes of elements such as uranium, thorium, and potassium [1-4]. Humankind has been constantly and inevitably exposed to radiation since its existence. As a part of life, we are exposed to radiation from natural sources such as cosmic rays from outer space and the sun, radionuclides found in the Earth's crust, soil and building materials, water, and food, as well as from artificial sources. Long-lived radioactive elements, which have been present in nature since the formation of the Earth, constitute a natural radiation level in our environment that is considered normal and un avoidable[3,4-6]. Natural sources play a significant role in radiation dose assessments because people receive substantial doses from radiation emitted from natural sources throughout their lives. There are two main contributors to the level of natural radiation exposure;(i) High-energy cosmic rays entering the Earth's atmosphere, (ii)Radioactive elements formed in the Earth's crust, which are ubiquitous in our environment and even in the human body. Humans are exposed to both internal and external radiation from these sources. Cosmic rays and radiation emitted from naturally occurring radioactive substances in the Earth's crust, building materials, and air cause external radiation, while naturally occurring radioactive atoms found in the air and foodstuffs cause internal radiation through respiration and ingestion [5,7,10-16].The largest contributor to natural radiation comes from naturally occurring radioactive elements such as ^{238}U and ^{232}Th, and their decay products, ^{226}Ra, ^{222}Rn, and ^{235}U and ^{40}K[8-15].While human exposure to natural sources varies depending on living standards, the physical characteristics of their environments, and geographical conditions, the annual

[1] Prof. Dr., Department of Physisc/Faculty of Science, Kastamonu University, Turkey, akurnaz@kastamonu.edu.tr ,(ORCID: 0000-0002-7910-3461)
[2] Prof.Dr.,Department of Physisc/Faculty of Science, Kastamonu University, Turkey, aybaba@kastamonu.edu.tr, (ORCID: 0000-0000-1700-8480)
[3] Prof.Dr.,Department of Physisc/Faculty of Science, Kastamonu University, Turkey, serefturhan63@gmail.com, (ORCID: 0000-0005-5303-3680)

dose is approximately 2.4 mSv. A large portion of this dose (approximately 1.3 mSv per year) is comprised of radon gas and its short half-life decay products[1,9].Radon comes from all rocks and soil where uranium is present, and because it is gaseous, it travels through the interstitial spaces of the environment and spreads into the atmosphere. Radon enters the lungs through inhalation and, as a result of its decay, increases the risk of lung cancer . However, this does not mean that everyone exposed to high doses of radon develop lung cancer [2,4,10-14].Because people generally spend approximately 90% of their time indoors, radon exposure poses a significant problem. The amount of radon in the environment is affected by the natural uranium found on the land where buildings are built, the infiltration of radon resulting from the decay of uranium into the building, and the release of radon from building materials into the air. A large portion of the radon source in buildings is the soil and rocks at the foundation of the building. Indoor radon concentrations vary significantly between countries and even between different regions of the same country [4,5].These differences depend on the geological structure of the soil, climate parameters, and building characteristics. e also released radioactive elements into the environment. However, these radiations can also be called back ground radiation, and the geology and geography of the region, and therefore the mineralogical structure of the soil and rocks, as well as geographical elevation, affect the baseline radiation level [5,6]. This requires determining the environmental concentrations of radionuclides that constitute natural radiation sources and the effects of radiation on biological systems, particularly humans. Furthermore, the relationship between radionuclides present in the environment and the radiation dose humans receive from these sources must be determined. Only after such an investigation can a decision be made whether a region is suitable for healthy living in terms of natural radiation. Studies conducted for this purpose have been conducted by the international commission on radiological protection (ICRP), the united states national committee on radiation protection and measurement [1,23-27].

In this study we resercahed of basic radioactivity, artificial and natural radioactivity, radioactivity units, annual effective dose, and activities of U-238, Th-232, and K-40 naturally occurring in volcanic and sedimentary minerals of Turkey measured using HPGe gamma spectrometry and compared with the world literature.Mineralogy is the branch of geology that studies minerals: their chemical composition, crystal structure, and physical properties (color, hardness, density, luster). Mineralogy helps scientists understand how rocks are formed, the resources they contain (such as uranium, thorium, and potassium), and how these minerals affect the Earth's crust and radiation environment. In

mineralogy, radioactivity refers to the natural emission of radiation from unstable isotopes in certain minerals.HPGe gamma spectrometer detectors, due to their high energy resolution, are the most reliable method for detecting natural radionuclides. Measurements were made using a 40,000-second counter time, radon-equilibrated samples, and Marinelli containers.The results show that all of Turkey's minerals are below IAEA limits[1].The physical and chemical properties of minerals affect natural radionuclide concentrations. Zeolite exhibits a crystalline structure, while pumice is highly porous. Perlite, due to its volcanic glass structure, contains high K-40 [7-9].Turkey holds more than half of the world's perlite and pumice reserves. It also holds a significant place in bentonite and zeolite reserves.The levels of U-238, Th-232, and K-40 in Turkish minerals are generally found to be equivalent or lower compared to the world literature. Turkey's geology, particularly its volcanic rocks, zeolite, perlite, pumice, and bentonite deposits, serves as an important laboratory for the study of natural radionuclides.

1.1 Radioactivity

Radioactivity discovered in 1896, following Rontgen's discovery of X-rays in 1895, when Henry Becquerel determined that some uranium salts spontaneously emitted interstitial rays, which passed through paper, glass, and other substances and impacted photographic film. Radioactivity is the spontaneous decay of atomic nuclei by emitting electromagnetic radiation, α and β particles. This process continues until the nucleus becomes stable. Except for hydrogen, the simplest nucleus, all other nuclei are composed of protons (p) with a +e charge and uncharged neutrons (n), called nucleons, the fundamental unit of charge in nature. Nucleons are held together within the nucleus by Coulomb and nuclear interactions. Unless Coulomb forces are taken into account, optimum stability within a nucleus is achieved when the number of protons and neutrons is approximately equal. This is the case in light nuclei, where Coulomb repulsion is negligible compared to short-range nuclear forces. Coulomb forces become increasingly significant as the atomic number exceeds 20. Significant increases in these repulsive forces within the nucleus will disrupt the stability of the nucleus, and as the atomic number increases, an excess of neutrons is required for the nucleus to remain stable. If the number of neutrons in the atomic nucleus of any substance exceeds the number of protons, such matter exhibits instability. Unstable nuclei are called radionuclides, and these nuclei with this excess energy disintegrate by emitting radiation. In the periodic table, elements with a ratio of neutron numbers (N) to proton numbers (Z) (the N/Z ratio) of approximately 1 are considered stable. As the atomic number

increases above 20, the N/Z ratio required for stability gradually increases, reaching a value of 1,5 at atomic number 83. Above this atomic number, there are no stable nuclei in the periodic table; in other words, all nuclei with N/Z >1,5 are unstable. An unstable element decay by releasing particles or emitting radiation, and this process continue until the nucleus becomes stable. Because not all nuclei are unstable, radioactivity is distinctive physical property

1.2 Radioactive Decay Processes

Radioactive decay is the process by which an unstable atomic nucleus emits radiation to transition to a more stable state. Nuclei attempt to return to a more stable state by emitting alpha particles (helium nuclei), beta particles, and gamma rays. Gamma rays are usually emitted along with beta particles and sometimes with alpha particles.

1.2.1 Alpha Decay

Alpha particles (${}^{4}_{2}He_{2}$) are helium nuclei composed of two protons and two neutrons. The spontaneous emission of an alpha particle (α) can be described by the following reaction.

$$ {}^{A}_{Z}X_{N} \rightarrow {}^{A-4}_{Z-2}Y_{N-2} + {}^{4}_{2}He_{2} \qquad (1) $$

Here, A represents the mass number of the nucleus, Z represents the atomic number. X represents the parent nucleus and Y represents the product nucleus. An example of alpha decay is,

$$ {}^{226}_{88}Ra_{138} \rightarrow {}^{222}_{86}Rn_{136} + \alpha \qquad (2) $$

Alpha particle emission is a phenomenon observed in isotopes with high atomic numbers. When alpha particles pass through a substance, they cause ionization within the substance due to their electric charge, and therefore, they quickly lose their energy. Furthermore, because alpha particles are ejected from a radioactive nucleus at a speed of 1.6 x 10^7 m/s, they have high energy, but their mass is relatively large compared to other particles, resulting in a short range. Furthermore, alpha particles emitted by naturally occurring radioactive substances have energies below 9 MeV and short wavelengths, making them interceptable with very small thickness of material. Therefore, they do not pose an external radiation hazard. However, the ionization they cause if they enter

the body through ingestion, inhalation, or other routes can pose a significant internal radiation hazard [10,31-33].

1.2.2 Beta Decay

The nucleus can rid itself of its excess proton or neutron by converting a proton into a neutron or a neutron into a proton. This process can occur in three different ways. In all three cases, another charged particle is required to maintain the electric charge (it was later shown that the charged particle, initially called the particle, is identical to the known electron).Because beta particles have a specific charge and mass, they cause ionization during their interaction with matter. However, because beta particles are lighter and more penetrating than alpha particles, the ionization they produce is less than that caused by alpha particles. Due to their smaller mass and charge compared to alpha particles, although their stopping power is not as high as that of alpha particles, they cannot penetrate matter very far unless they possess very high energies.Their penetrability varies depending on their energy and the properties of the material they interact with. While their range within matter is not very long, they can propagate through air for quite long distances. Radioisotopes that emit beta particles can pose an external radiation hazard, but they also pose a serious internal radiation hazard if taken into the body. β^+ *decay*, radiation is the ejection of an electron from an unstable nucleus. This process is known as negative beta decay and involves the creation and emission of an electron. Although there are no electrons in the nucleus of an atom, the conservation of electric charge in the β^- emission process requires that the excess neutron in the unstable nucleus convert into a proton and an electron, thus increasing the atomic number by one. In β^- decay, the proton remains in the nucleus while the electron is ejected. In this decay, the atomic number increases by one, while the mass number remains unchanged. β^- rays are composed of electrons. Therefore, because β^- rays are negatively charged particles, they are deflected by electric and magnetic fields. The decay equation is,

$$n \rightarrow p + e^- + \bar{\upsilon} \tag{3}$$

$$^{A}_{Z}X \rightarrow {}^{A}_{Z+1}Y + {}^{0}_{-1}e(\beta^-) + \bar{\upsilon} \tag{4}$$

This expression shows that the neutron decays to form a proton, an electron, and an antineutrino particle. Because the neutrino has no electric charge, its

presence does not affect the identity of the other final particles [11,19,29-35].An example of β^- decay is,

$$^{131}_{53}I_{78} \rightarrow {}^{131}_{54}Xe_{77}\ t_{1/2} = 8{,}0\ \text{d} \tag{5}$$

β^+decay, this process is called positive beta decay, or positron decay, and positively charged electron is emitted. The decay is the transformation of a proton into a neutron. If the number of protons in the nucleus is high, one of the protons transforms into a neutron, a positively charged electron (positron), and a neutrino. The positron is ejected from the nucleus, while the neutron remains in the nucleus [10,11]. Thus, the atomic number of the nucleus decreases by one, and the decay equation becomes,

$$p \rightarrow n + e^+ + \nu \tag{6}$$

$$^{A}_{Z}X \rightarrow {}^{A}_{Z-1}Y + {}^{0}_{1}e(\beta^+) + \upsilon \tag{7}$$

β^+ decay occurs when the rest mass difference between the parent nucleus and the product nucleus is greater than the rest mass of two electrons. An example of β^+ decay is,

$$^{25}_{13}Al_{12} \rightarrow {}^{25}_{12}Mg_{13} \qquad t_{1/2} = 7{,}2\ \text{sn} \tag{8}$$

1.2.3. Electron Capture

In nuclei with more protons than neutrons [n/p < 1], an electron from the orbital closest to the nucleus (1S) is captured by the nucleus, transforming a proton into a neutron. This is also called the alternative form of positron emission. The atomic number decreases by 1, while the mass number remains unchanged. In this process, the element's isobar is formed [1,14-16] decay equation is,

$$p + e^- \rightarrow n + \upsilon \tag{9}$$

$$^{A}_{Z}X + {}^{0}_{-1}e \rightarrow {}^{A}_{Z-1}Y + \upsilon + \gamma \tag{10}$$

1.2.4. Gamma Decay

Radioactive gamma ray emission is similar to atomic radiation emission, such as optical or x-ray transitions. The emission of a particle, such as an alpha (α) or beta (β) particle, from a nucleus usually leaves the nucleus in an excited state. An excited state transitions to a lower excited state, or ground state, by emission of a gamma ray with an energy equal to the difference between the nuclear states (less the recoil energy of the emitted nucleus) [11,12]. After the gamma ray emission, the atom does not transform into another atom.

The decay equation is,

$$ {}^{A}_{Z}X^{*} \rightarrow {}^{A}_{Z}X + \gamma \tag{11} $$

Gamma rays, known as short-wavelength electromagnetic radiation, are not subject to the Coulomb force, unlike charged particles, because they lack an electrical charge. This does not mean they do not ionize atoms within matter. Gamma rays are not directly ionizing, but they are carriers of the electromagnetic force, interacting with matter through ionization and energy deposition in the environment. In short, the behavior of gamma rays in matter is quite different from that of charged particles. In particular, they can lose a significant portion, or even all, of their energy when interacting with an atom's electrons. Gamma rays do not have the range of charged particles. They are more penetrating than alpha and beta rays, and because they are uncharged, they are not deflected by electric or magnetic fields. Gamma rays generally undergo the following interactions as they pass through matter; photoelectric effect, compton scattering (includes thomson and rayleigh scattering), pair production. These interactions explain two important properties of gamma rays. First, gamma rays can penetrate longer distances through matter compared to charged particles, and second, gamma rays do not lose energy when they pass through a certain thickness of material, only their intensity. In summary, the photoelectric effect, compton scattering, and pair production contribute to the interaction of gamma rays with matter [12,13].The half-life of gamma (γ)-emissions is very short, usually less than 10^{-9} s, but gamma (γ)-emissions with half-lives on the order of hours or even days do occur. These transitions are known as isomeric transitions.

2. NATURAL RADIATION SOURCES

Natural radioactivity is determined by three main radionuclides: U-238, Th-232, and K-40. These isotopes are a natural result of geological processes and

can be found in minerals at varying concentrations. During the $10'x10^9$ years between the Big Bang and the condensation of the solar system, hydrogen and helium, along with the heavy elements in stars, novae, and supernovae, were formed. Most of the elements formed are radioactive, and unstable nuclei have been decaying ever since. Several radioactive elements have long half-lives compared to the age of the Earth, and their radioactivity can still be observed today. This is called natural radioactivity. All elements with a proton number greater than 83 are radioactive, and the number of radioactive nuclei known in nature is approximately 340. Most of the naturally occurring radioactive elements observed today are composed of very heavy nuclei and have no stable isotopes. These nuclei decrease their Z and A numbers by emitting alpha and beta until they reach a stable, light nucleus. Alpha decay changes A by four units, while beta decay does not change A, and thus we obtain four independent decay series with mass numbers 4n (Thorium), 4n+1 (Neptinium), 4n+2 (Uranium), and 4n+3 (Actinium), where n is an integer [12].The decay process tends to drive the nucleus to the longest-lived member of the chain, and if this nucleus' lifetime is at least on the order of the age of the Earth, this activity will still be observed today.The largest contributor to human radiation exposure comes from naturally occurring radioactive elements. Natural radioactivity is found in abundance in our environment, in soil, air, water, and plants. Natural radioactive elements are generally divided into two groups: terrestrial and space-based. Cosmic rays originate from sources throughout space and beyond the solar system. A large portion of these rays are captured as they attempt to pass through the Earth's atmosphere. Only a small amount reaches the Earth's surface. A person on a mountaintop or in an airplane traveling overhead is exposed to significantly more cosmic rays than a person at sea level. In our daily lives, the global average radiation dose from cosmic rays is 0.39 mSv/year. The main sources of terrestrial gamma radiation are ^{238}U, ^{235}U, ^{232}Th, and ^{40}K. The vast majority of radionuclides in nature are in the ^{238}U decay chain. Radon (^{222}Rn), a decay product of the element ^{238}U, has the greatest impact, accounting for 55%. Fossil fuels contain natural, long-lived radioactive elements. When these fossil fuels are burned, these elements are released into the atmosphere and then return to the soil, causing a slight increase in natural radiation levels. The global average radiation dose we are exposed to from soil, including the gamma rays emitted by short-lived radioactive elements present in nature, is 0.46 mSv/year. Natural radiation originates from both sources outside the body and from naturally occurring radioactive substances within the body. External radiation sources include cosmic rays reaching the Earth from space, radioactive substances such as uranium and thorium found in the Earth's crust,

radon gas in the air we breathe, and gamma rays emitted from building materials. Internal radiation sources are primarily potassium and radium [11-13,15]. Internal radiation originates from ^{40}K and ^{14}C within the body, as well as radon and its decay products inhaled into the lungs. We are exposed to a certain dose of radiation due to the radioactive elements found in our bodies (especially the ^{40}K radioactive element). The global average annual internal radiation dose is approximately 0.23 mSv. Because building materials are sourced from the earth, they contain these radioactive substances. Although building materials provide some shielding against external radiation, the radiation level inside buildings constructed from these materials is generally higher than the external radiation level. The average radiation dose inside a building made of brick or concrete is around 80 mrad per year, while the dose intensity inside a granite-type structure is around 100 mrad per year. Radon and thoron are gaseous products of the uranium and thorium decay chain and are emitted into the air to some extent. While thoron is not particularly significant due to its very short half-life, radon, with its 3.8-day half-life, can be emitted at sufficient levels to create a significant airborne concentration. Due to radon released from plaster and other building materials, indoor radon concentrations are generally higher than outdoor radon concentrations. The global average dose we are exposed to from food, beverages, and the air we breathe is approximately 0.25 mSv/year. Shellfish, in particular, contain higher levels of radioactive material, and people who consume large amounts of these products receive a higher than average radiation dose. One of the most significant factors increasing natural radiation levels is radon gas, released during the decay of the radioactive element radium (^{226}Ra), a common component of the Earth's crust.

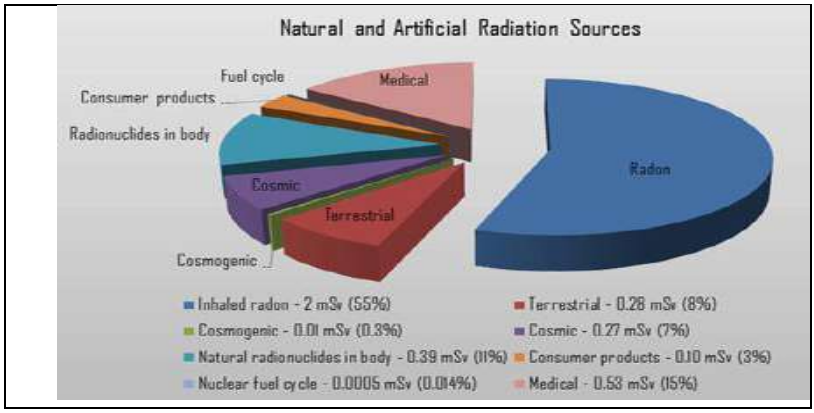

Figure.1 Natural radioactivity and natural radiation sources[11-15].

While other radioactive materials formed during this decay remain in the soil, radon unfortunately rises to the soil surface. Without such ventilation, radon gas be hundreds or even thousands of times more concentrated inside the home than outside. If inhaled, this gas can temporarily settle in the lungs and cause radiation exposure to all tissues. The global average dose from radon gas is 1.3 mSv/year [11,13,14]. If this gas is diluted by emissions, it does not pose a problem. However, homes located on surfaces where radon gas is emitted must have a good ventilation system.

3. ARTIFICIAL RADIATION SOURCES

New elements formed when stable or unstable elements are bombarded with particles such as alpha, neutrons, and protons in nuclear reactors or accelerators are also radioactive. This property of radioactive elements obtained through bombardment is called artificial radioactivity. Artificial radiation sources, like natural radiation sources, cause exposure to a certain amount of radiation dose. However, although this dose increases depending on the method and amount of use, it is much lower than the dose received from natural sources. Unlike natural radiation sources, their ability to be controlled is also important in terms of the amount of exposure [14,15]. Some artificial radiation sources and the proportional distribution of radiation emitted from these sources are shown in Figure-1 [11-15].

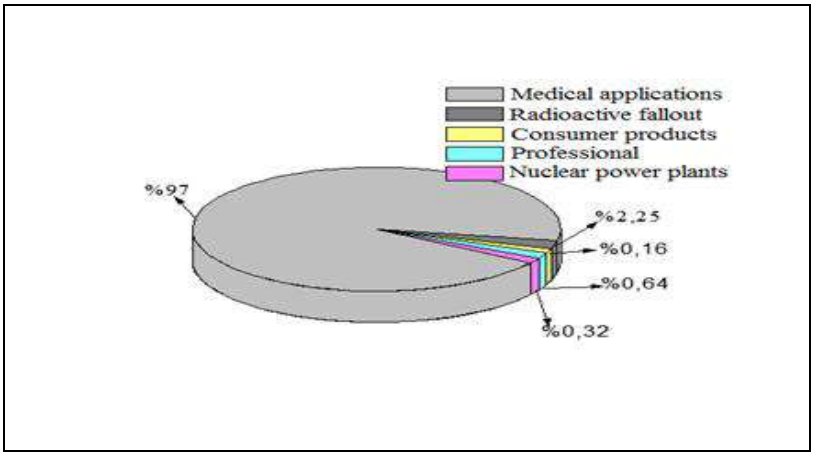

Figure 2. Artificial radiation source % distribution [15].

3.1 Radiation dose units

Dose refers to the amount of any substance used or consumed over a period of time. Radiation dose is the amount of radiation absorbed or received by a

target population over a period of time[1,15]. All harmful substances generally cause some biological damage to the body. The extent of this damage depends on the type of substance, the method, duration, and amount of exposure. Furthermore, the total amount ingested over a lifetime is a significant factor in determining the potential harm. Unless necessary precautions are taken, some harmful effects will inevitably occur in living beings that absorb more than a certain amount of radiation energy over a period of time, i.e., receive a radiation dose. The magnitude of this effect can only be determined when the type of radiation, the amount of radiation absorbed and the amount of radiation not absorbed, are known. When all these factors are known, the impact of radiation on human health and other living and non-living things can be easily determined. Since the discovery of radioactivity by Henrie Becquerel in 1896, the growing interest in radioactivity and its applications has highlighted the importance of understanding the doses humans receive from radiation. It has become clear that calculating radiation dose requires first examining natural radioactivity. The effects of radiation depend on the ionization it creates in the environment through which it passes, and ionization, in turn, depends on the energy of the radiation absorbed by that environment. The international committee on radiation units (ICRU) defined the units Curie (Ci), Roentgen (R), Rad, and Rem for activity, irradiation dose, absorbed dose, and dose equivalent, respectively. These specialized units were discontinued in 1986, and replaced by the international system of units (SI) to ensure uniformity of units used worldwide. The SI units for these concepts are the Becquerel (Bq), Coulomb/kg (C/kg), Gray (Gy), and Sievert (Sv). Activity unit is the number of decays a radioactive substance undergoes per second. The SI unit of activity is the Becquerel, symbolized by Bq (decay/second). The old unit of activity is known as Curie (1 Curie (Ci) = 3,7 x 10^{10} decays/second. The old dose unit is Roentgen (R), which is the amount of X or γ radiation that produces positive and negative ions with an electric charge of 2,58x10^{-4} Coulombs in 1 kilogram of air under normal air conditions . The new radiation unit is exposure which is determined as (C/kg). The advancement of nuclear technology, high-energy X-rays, such as α, β, and neutron radiation, have become insufficient to measure the absorbed energy of any object. Therefore, the gray is defined as the unit of absorbed dose for all types of radiation and matter. Radiation released by a radioactive substance releases energy into the materials it interacts with. Absorbed dose is any amount of radiation that produces 1 Joule of energy absorbed per kilogram of the irradiated substance and is symbolized by Gy.The old unit of absorbed dose is rad,(1rad = 100 erg/gr = 0,01 J/kg = 10^{-5} J/gr),(100 rad =1,Gray =1J/kg). Equivalent dose unit is to determine the harmful biological

effects that may occur in humans exposed to radiation, a measurable unit of radiation dose is needed. When energy packets and particles ejected by radiation strike living cells, they deposit their energy. However, even if different radiation particles release the same amount of energy, their biological effects on living cells vary. The harmful biological effects caused by the absorbed dose vary depending on both the ionization density and the type of radiation (α, β, γ and n). In other words, the resulting biological effect depends on the amount of energy lost by ionizing radiation (linear energy transfer, LET) per unit length of the medium they pass through, as increases. Therefore, the equivalent dose unit should be a measure of the harmful biological effects caused by radiation [11-16].The SI unit of dose equivalent is the Sievert (1Sv =100 rem), defined as the product of the absorbed dose and the quality factor.

4. RADIOLOGICAL RISK HEALTH ASSESSMENT

Radiological health risk assessment is a scientific method used to determine the short and longterm health effects of individuals or populations exposed to ionizing radiation. This assessment combines exposure measurements, dose calculations, risk modeling, and epidemiological data. The aim is to quantify the potential effects of both environmental and medical radiation sources on human health. Equivalent Dose and Effective Dose (mSv/year) are given by the following equation,

$$E=\sum(D\times WR\times WT) \tag{12}$$

Here, D is the absorbed dose, WR is the radiation weighting factor, $WT$is the tissue factor. Radiological Risk Health Assessment is a critical process for establishing safety standards in the environment, industry, and medical practices. Dose measurements, risk indices, and epidemiological data are combined to determine safe limits for public health.

4.1. Annual Effective Dose

The annual effective dose is an important radiological quantity used to estimate the radiation dose an individual receives from natural or artificial radioactive sources over the course of a year. It considers both the absorbed dose and the biological effects of the radiation type on human tissues. This value is defined as the radiation dose a person would receive in a year, whether from external exposure to radiation from various radiation sources or from internal exposure to radiation from various radionuclides in the food they eat and the air they breathe. Its unit is the Sievert. Using the type and energy of

radiation emitted by each radionuclide, dose conversion factors are determined for each radionuclide, which emits radiation per unit of activity. The annual effective dose equivalent is calculated by multiplying the activity concentration per unit of volume or weight by the dose conversion factors [8,16-21].To calculate absorbed gamma dose rate (D) (nGy/h)given by,

$$D(nGy/h)=0.462A_u+0.604A_{Th}+0.0417A_k \quad (14)$$

This equation is used to calculate the environmental gamma dose rate of samples containing natural radioactivity, such as soil, rocks, minerals, building materials, etc. A_u,U-238 activity concentration of the series (bq/kg);A_{Th},Th-232 activity concentration of the series (bq/kg),A_K, K-40 activity concentration (Bq/kg) [1,19].

4.2 Lifetime Cancer Risk (LCR)

Lifetime Cancer Risk is a radiological risk parameter that expresses the increase in the probability of an individual developing cancer throughout their life as a result of exposure to ionizing radiation. Cancer risk for low doses is according to the linear nothreshold model [1,8,19]. LCR is given by the following equation,

$$LCR= (AEDE)x (DL)x(RF) \quad (15)$$

Where, (AEDE annual effective dose(Sv/year,(DL Lifetime for 70 years) ,(RF fatal cancer risk factor 0.05 Lv^{-1} [1,8,19].

8.CONCLUSION AND DISCUSSION

Today, natural radioactivity remains the dominant factor in public exposure,while exposure from artificial radioactivity appears to be under control and at acceptable levels for general public health.This study examines and interprets the activity concentrations of these radionuclides in commercially important industrial minerals in mineralogy and compares them to global reference values [8,22-30]. Radioactivity is a fundamental physical phenomenon resulting from the natural decay processes of elements such as uranium, thorium and potassium. The comparison includes global average activity concentrations defined by Unscear. Naturally occurring industrial minerals such as perlite, zeolite, bentonite, and sepiolite are widely used in various engineering, construction, and environmental technologies. Their structural and physicochemical properties make them ideal for use in composite

materials, filtration, and industrial waste recycling. However, these materials may contain natural radionuclides such as Uranium-238 (U-238), Thorium-232 (Th-232), and Potassium-40 (K-40), which can pose potential radiological health risks to workers and end users. Methodology and data source (U-238, Th-232, and K-40) activity concentrations were compiled from peer-reviewed literature and international standards[1,8-9,23].In terms of radiological risk effects, mining, quarrying, or processing facilities, ceramics and composites industries, and cement and insulation sectors may be chronically exposed to above-background gamma radiation, particularly when working with zeolite, bentonite, or perlite.Environmental and end-use effects, when these materials are used in buildings or filters, can contribute to indoor radiation dose, particularly due to K-40 in volcanic materials and Th-232 in bentonite [13,17,24-27].

In terms of safety measures and recommendations, routine monitoring of activity concentrations in raw material batches, the use of personal dosimeters for workers in high-exposure areas, material selection criteria based on radiological safety for indoor applications, and the inclusion of radon mitigation strategies where appropriate are important. Consequently, industrial minerals are essential for the development of innovative materials, but their radiological properties must be carefully evaluated. Materials such as bentonite, zeolite, and volcanic tuff exhibit activity above the global average, which can impact occupational safety and material regulations. Integrating radioactivity screening into quality control will ensure both the protection of human health and the sustainable use of these materials in industrial applications. [11,29,33-35].

REFERENCES

1-UNSCEAR.(2001).Heredıtary effectsof radıatıonunited nations scientific committee on the effects o., *Atomic Radiationunscear With Scientific Annex*.

2-IARC .(1988). International Agency for Research on Cancer, In Man-made mineral fibres and radon. In: IARC Mono-graphs on the Evaluation of Carcinogenic Risks to Humans. *43 (Lyon, France: IARC).*

3-ICRP.(1990). The International Commission on Radiological Protection, ICRP Publication 60. Recommendations of the International Commission on the Radiological Protection, *Pergamon Press Inc., ICRP,* USA.

4-Enflo, A. (2002). Where are the radon-induced lung cancer cases? Is it time for a re-evaluation of the radon problem? *International Congress Series,* 1236, 23-25.

5-Köksal, E. M., Çelebi, N., Ataksor, at al. (2004). A survey of ^{222}Rn concentrations in dwellings of Turkey, *Journal of Radioanalytical and Nuclear Chemistry*, 259, 2, 213-216.

6-Bozkurt, A., Yorulmaz, N.(2007).Assessment of environmental radioactivity for Şanliurfa region of Southeastern Turkey., *Radiation Measurements*, 42, 8, 1387-1391.

7-Tzortzis, M., Svoukis, E. ve Tsertos, H. (2004). A comprehensive study of natural gamma radioactivity levels andassociated dose rates from surface soils in Cyprus. *Radiation Protection Dosimetry*, 109, 3, 217-224.

8-Turhan Ş, Tokat S, Kurnaz A, Altıkulaç A. (2022). Distribution of elemental compositions of zeolite quarries and calculation of radiogenic heat generation. *International Journal of Environmental Analytical Chemistry*, 109(19), 7851–7862.

9-Yaroshevsky AA. (2006). Abundances of chemical elements in the Earth's crust. *Geochemistry International* 44(1), 48–55

10-BEIR VI. (1999). Health Effects of Exposure to Radon. Committee on Health Risks of Exposure to Radon. Board on Radiation Effects Research (BEIR VI). *National Academy Press.*

11-Krane, K. S., (1988). *Introductory Nuclear Physics*, Canada.

12-Krane, K. S., (20019, Nuclear physics, volume 1, *Palme Publishing,* Ankara.

13-Kurnaz,A.(2009).Trabzon determination of natural radioactivity levels and annual effective dose equivalents in the province and şebinkarahisar district. karadeniz technical university, institute of science, department of physics, phd thesis.14-*Taek*, 2002.Ankara.

15-Turhan Ş, Garad A.M.K, Hançerlioğulları A.,at al. (2020). Ecological assessment of heavy metals in soil around a coal-fired thermal power plant in Turkey. *Environmental Earth Sciences* 79(6), 1–15.

16- Poh SC, Tahi NM. (2017). The common pitfall of using enrichment factor in assessing soil heavy metal pollution. *Malaysian Journal of Analytical Sciences* 21(1), 52–59.

17- Parvez MS, Nawshin S, Sultana S, Hossain MS, at,al. (2025). Analysis of nigella sativa l. (black cumin) seeds for levels of heavy metals using faas: *Geospatial Profiling And Regional Safety Implications,2* (223),

18-IAEA, (1996). International Atomic Energy Agency, *Radiation Safety IAEA Division of Public Information, 9*6-00725 IAEA/PI/A47E.

19-Unscear, (2000). United Nations Scientific Committee on the Effect of Atomic Radiation to the General Assembly, Sources, Effects and Risk of Ionizing Radiation, United Nations, New York, USA.

20-Li R, Yuan Y, Li C, Sun W, Yang M, Wang X. (2020). Environmental health and ecological risk assessment of soil heavy metal pollution in the coastal cities of Estuarine Bay-A case study of Hangzhou Bay, China. *Toxics*,8(75), 1–19.

21-Majid SN, Sheikh-Abdullah SM. (2016). Spatial distribution of some alkali and alkaline earth metals of selected locations in Sulaimani Governorate, Kurdistan Region, Iraq (KRI). Journal of Zankoy Sulaimani Part-A- *Pure and Applied Sciences,* 18, 7–23.

21-Msaky JJ, Calvert R. (1990). Adsorption behaviour of copper and zinc in soils: influence of pH on adsorption characteristics, *Soil Science* 150(2), 513–522.

Muller G. (1969). Index of geoaccumulation in sediments of the Rhine River. Geological Journal 2, 108–118.

22-Özkara A, Akyıl D.(2018). Environmental pollution and pollutants on the ecosystem: A review. Turkish Journal of Scientific Reviews 11 (2), 11–17.

23-Özkul C. (2016). Heavy metal contamination in soils around the Tunçbilek thermal power plant (Kütahya, Turkey). *Environmental Monitoring and Assessment* 188(284), 1–12.

24- Miletić A, Lučić M, Onjia A. (2023). Exposure factors in health risk assessment of heavy metal(loid)s in soil and sediment. *Metals* 13(7), 1–28.

25- United States Environmental Protection Agency (USEPA), (2011). Exposure Factors Handbook (Final Report). Chapter 5: Soil and Dust Ingestion. U.S. *Environmental Protection Agency*, Washington, DC.

26-Mitra S, Chakraborty AJ, Tareq AM, Emran TB, Nainu F, Khusro A, Idris AM, Khandaker MU, Osman H, Alhumaydhi FA, Simal-Gandara J.(2022). Impact of heavy metals on the environment and human health: Novel therapeutic insights to counter the toxicity. *Journal of King Saud University – Science*. 34(3), 1–23.

27-Rudnick RL, Gao S., (2014).Composition of the continental crust. The crust (ed. R.L.Rudnick), Treatise on geochemistry (eds. H.D. Holland and K.K. Turekian) , *2nd4. Elsevier-Pergamon, Oxford.*

28-Sall ML, Diaw AKD, Gningue-Sall D, Aaron SE, Aaron JJ. (2020). Toxic heavy metals: impact on the environment and human health, and treatment with conducting organic polymers, a review. *Environmental Science and Pollution Research*, 27, 29927–29942.

29-Turhan Ş, Tokat S, Kurnaz A, Altıkulaç A.(2020). Distribution of elemental compositions of zeolite quarries and calculation of radiogenic heat generation. *International Journal of Environmental Analytical Chemistry*, 102(19), 7851–7862.

30-USEPA.(2024). Updated dermal exposure assessment guidance. region 3 technical guidance manual, risk assessment. web page: *https://www.epa.gov/risk/updated-dermal-exposure-assessment-guidanc*.

31-Haghighizadeh A, Rajabi O, Nezarat A, Hajyani Z, Haghmohammadi M, Hedayatikhah S, Asl SD, Beni AA. (2024). Comprehensive analysis of heavy metal soil contamination in mining environments: impacts, monitoring techniques, and remediation strategies. *Arabian Journal of Chemistry,* 17(6), 1–26.

32-DPT.(2007). Ninth five-year *Development Plan- Mining Specialized Commission Report, Dpt*: 2739 – öik, 690, ankara

33-Karn, R, Ojha N, Abbas S, Bhugra S.(2021).A review on heavy metal contamination at mining sites and remedial techniques. iop conf. series: *Earth And Environmental Science*, 796, 1–30.

34- Rybach L, edited by Haenel R, at al.(1988). Handbook of terrestrial heat-flow density determination. kluwer academic publishers, dordrecht, 125–142.

35. Imperl J, Kolar M, Petrova P, Chochkova M. (2023).Mineral content Estimation of black Cumin seeds. *J Chem Technol Metall.* ,58(5),859–64.

Chapter 6

MICROORGANISMS AS THE VITAL RECYCLERS OF URANIUM

Oktay BIYIKLIOĞLU[1], Selin ÇETER[2], İdris YAZGAN[3]

1. INTRODUCTION

Uranium ($^{92}U^{238.029}$) is by far the most used actinide element in industry, which was discovered in 1789 with same year of the Revolution in France. Even though it is known for nuclear energy production, such fields as nuclear medicine, catalysis, radiometric dating, industrial X-rays, food processing and materials [1]. Uranium has mainly U^{238} (~ 97.3%) and U^{235} (~ 0.7%) isotopes [2], but in nature there are up to 27 isotopes [3]. Even though Uranium is among the rare element elements, it is accepted as one of the most problematic contaminants worldwide [2] since it can cause a variety of health problems including bones and kidneys, and it can contaminate foods (e.g. honey) in addition to soil and water [4]. Apart from acute toxicity, Uranium accumulation can cause cancer as shown by Basheer *et al* (2024) that blood Uranium level is significantly higher in leaukemia patients compared to heatlhy individuals [5]. Besides, it is critical to note that Uranium can reach to human through food chain, so its contamination in soil and water becomes very critical [6]. In soil, the Uranium contamination is mostly present on the surface (top layer used for agriculture), so agricultural crops are potentially exposed to Uranium when there is contamination [7]. It should not be confused that chemotoxic Uranium is related to natural isotopes while radiotoxic Uranium is related to the enriched Uranium (U^{234} and U^{235}) [3]. Today, the exact mechanism of Uranium is still unknown despite of the fact that accumulation of U^{6+} is known through food-chain [8]. Besides, inhalation of Uranium contaminated air is also another way of triggering Uranium toxicity [9].

[1]MSc, Department of Biology, Faculty of Science, Kastamonu University, Turkiye, oktayman@gmail.com, (ORCID: 0000-0003-4238-931X)

[2]MSc, Department of Biology, Faculty of Science, Kastamonu University, Turkiye, akdoganselin@gmail.com, (ORCID:0000-0003-4379-7411)

[3]Prof. Dr., Department of Biology, Faculty of Science, Kastamonu University, Turkiye, iyazgan@kastamonu.edu.tr, (ORCID: 0000-0002-0264-1253)

2. URANIUM CONTAMINATION THROUGH FOOD CHAIN

Food-chain is probably the most prominent way of Uranium ion enrichment, which is caused by human activity. Its accumulation and enrichment (refers to quantity increases throughout the text) within the soil and plants show close relation with the microbial colony, soil characteristics (e.g. acidity, presence of clay, humic acid content, ionic concentration etc.) and organic matter of the contaminate site [10]. In addition to the vegetables directly collected from the farms, the processed food can contain Uranium ions that show close relation with the phosphate content since it is one of the compound that precipitate and increase the available Uranium within the foods [11]. Therefore, remediation of its pollution becomes a need to deal with. The concentration is generally higher for the plats grown nearby the Uranium mining area [12]. The level of Uranium has been reported up to ~17.5 mg/kg for radishes, which is way beyond the acceptable level [13].

Plants can absorb and store radionuclides through their roots, leaves, and flowers. Honey can become contaminated with these radionuclides when honeybees collect nectar and pollen from flowers [14]. Uranium contamination in honey largely originates from nectar. However, correlations have also been reported between the amount of uranium in honey and soil, plant, and flower samples [15]. This allows radioactive isotopes in honey to be used as an important bioindicator of environmental pollution. Radioactive elements such as uranium can be transferred to humans through honey consumption [16]. However, many studies have reported that the uranium intake in honey is well below the level that would cause health concerns [14–17]. Furthermore, uranium contained in the pollen of some wind-pollinated plants can be transmitted to humans through the respiratory tract [18].

3. URANIUM POLLUTION AND BIOLOGICAL REMEDIATION

Uranium pollution in soil is classified into light, medium and heavy pollutions. The enrichment factor is used to evaluate quantitative level of pollution level and source. Besides, geological accumulation index and pollution load index are also used to evaluate the level of Uranium pollution (details can be found in *Ref* [6]). Remediation of Uranium waste is carried out by chemical, physical and biological methods. Physical methods can only be used for smaller liquid systems while chemical methods are efficient and cheaper for soil and liquid small size plants. In contrast to this biological approaches can be applied to larger soil and water plants for lower Uranium concentrations [19]. Among the biological approaches, bacterial and fungal communities have been proposed as valuable Uranium recyclers for their

unique mechanisms and adaptation [20]. Current microbial approaches have alerted that even remediation of higher Uranium concentration is possible, such as sulfate reducing bacterial species was shown to be effective even in 0.5 mM U^{VI} concentrations [21].

One of the major mechanisms of diminishing and/or preventing Uranium contamination is to convert the soluble form of Uranium (U^{VI}) into the precipitated form U^{IV} (U^{6+} and U^{4+} are the two common ionic form in nature [3]) while certain bacterial species can oxidize U^{4+} to U^{6+}, which is precipitated with such anioic groups present in the treatment environment [22] (**Figure 1**). A variety of bacterial species can perform this task using different mechanisms including energy gain mechanism and independent from energy gain. Particularly sulfate reducing bacterial species, Fe^{III} reducing bacteria and the bacterial species that can convert U^{VI}-carbonate into U^{IV}-oxide are among the most common bacterial species that can serve as Uranium waste recyclers. For example, Cardenas *et al* (2008) reported that *Desulfovibrio* spp. (a sulfate reducing bacterium), *Ferribacterium* spp. and *Geothrix* spp. (Fe^{3+} reducing bacteria) were capable of reducing the soluble Uranium level (from 60 mg/L to <30 μg/L) in the field application that took place in Oak Ridge (Tennessee, the US) with a two-year study [23]. Bacterial species can reduce and oxidize Uranium ions along with that the species can produce complexing agents that can appear as biosorption, intracellular accumulation and precipitation [24]. It is proposed that co-culture of sulfate-reducing and phosphate-solubilizing bacteria can be beneficial for Uranium detoxification; where simultaneous biological reduction, adsorption and precipitation take place [25]. It should be noted that sulfate reducing bacterial species require oxygen while phosphate solubilizing bacteria do not require oxygen, so they can also be used in oxygen-free environment [26]. Bacterial species can particularly use different types of cytochromes during Uranium bioremediation, for instance *Geobacter sulfurreducens* use periplasmic c_7-type cytochrome PpcA while c-type cytochrome A is highly active during Uranium reduction by *Geobacter* sp.. It was also tested for such species as *Shewanella oneidensis* MR-1 strain lost its Uranium detoxification when cytochrome deficiency is present. Iron containing enzymes and certain FAD and NAD utilizing enzymes (e.g. thioredoxin reductase) can also reduce U^{IV} into solid Uranium ion [20]. Production of lactic acid by the bacterial species can solubilize the phosphate precipitated Uranium ions, where external phosphate resources are needed to decrease the available soluble Uranium levels [7]. In addition to these, the functional groups on the bacterial species including amino, carbonyl and hydroxyl groups can complex

with UO_2^{2+} [21] that cause adsorption of Uranium as of the first step, which undergoes to biomineralization later on.

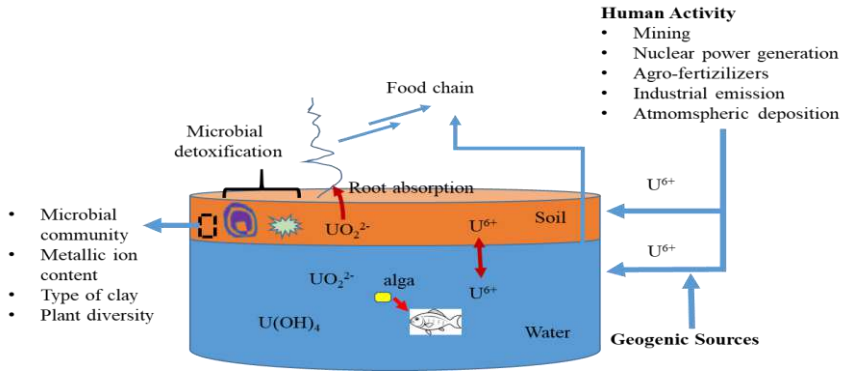

Figure 1: Main sources of Uranium contamination, remediation by microorganisms and flow of food chain accumulation.

Different fungal species can follow distinct pattern for the detoxification of Uranium as shown by *Schizophyllum commune*, *Pleurotus ostreatus* and *Leucoagaricus naucinus*, which affects the location of the crystalized Uranium ions. For instance, *Schizophyllum commune* can accumulate the Uranium crystals within the cytoplasms and outer layer of the cell wall while that happens within the cytoplasm on the subcellular bodies [27]. Figueiredo *et al* (2024) showed that Uranium as the waste in mine affluent can be captured by white rot fungi species (e.g. *Trametes versicolor*) that can trigger increased production of industrially important enzymes (e.g. laccases) and molecules (e.g. the metabolites melanin and oxalic acid) [28]. Biosorption studies were performed for Uranium in water and soil to understand the precipitation mechanisms. Celik *et al* (2018) reported that the stability of Uranyl ions and formation of Uranium oxides show close relation with the treatment pH [2]. Since Uranium can adopt valance values ranging from III to VI that allows it to coordinate with such groups through 5f-/6d-orbitals [1] and its coordinating groups show relation with the pH, Uranium oxides carbonates ($UO_2(CO_3)_2^{2-}$ and $UO_2(CO_3)_3^{4-}$) can occur in the treatment environment, so the pH must be optimized in order to increase the biosorption of uranium contaminants [2]. During microbial remediation, microorganisms can release chelating agents (e.g. siderophores) into the media that cause precipitation of U^{IV} [20]. *Aeromonas veronii* and *Bacillus cereus* species isolated from Uranium mines were exposed to carbonate containing Uranium waste, and Uranium was captured by the bacterial species as of biosorption in the form of Uranium

oxides carbonates and Uranium hydrates [29] as reported for the chemical precipitation. However, altering the electron donors and extracellular phosphates can trigger biomineralization of Uranium ions [30]. Therefore, it is clear that utilization of external agents along with altering the pH can alter the fate of Uranium ions. In contrast to this, certain microorganisms including *Penicillium simplicissimum* can produce phosphorylated amino acids that can interact with Uranium ions to contribute precipitation [31].

Enrichment of the treatment plants with key compositions contribute microbial Uranium detoxification. Qi *et al* (2021) showed that biochar introduction to the treatment media increased the stabilization of Uranium ions through ion-ion exchange (biochar contains a variety of chelating agents) and dehydrogenase activity, that turned into elevated Uranium detoxification [32]. Similar findings were reported by Zhang *et al* (2025), where combination of *Psedumonas* and *Bacillus* species were also introduced to the system in order to advance the treatment performance. The comparative study also revealed that each bacterial species contributes with a dedicated mechanism (i.e. adsorption, bioreduction, and biomineralization) via enzymatical activity, cell surface properties and metabolic activity [33]. Besides biochar, Fe^{2+} rich clay mineral nontronite combined with siderophore desferrioxamine B enhances the adsorption and reduction of U^{IV} with the help of *Shewanella putrefaciens* [34]. The clay-ligand change facilitates the conversion of Uranium oxidation level [35]. Similarly, Ohnuki *et al* (2010) U^{6+} can be directly absorbed by *Bacillus subtilis* species while combination with kaolinite clay enhanced the treatment efficiency [36]. **Figure 1** depicts the sources of Uranium contamination sources and biological remediation pathways.

Microorganism can also be immobilized on such surfaces as graphene oxide to enhance Uranium removal from the media. Zhao *et al* (2019) reported that immobilization of *Lysinibacillus* sp. on graphene oxide layers, which enabled reusable surface with high load of Uranium removal capacity from the treatment environment [37]. *Yarrowia lipolytica* was entrapped within alginate beads to remove Uranium from waste aqueous systems using batch and regenerative approach, and high success was obtained [38]. Similarly, placing fungal cells on the cathode electrodes can increase the speed of U^{VI} conversion to U^{IV} [39]. Microorganisms can serve as major bio-fighters in remediation of industrial chemical waste, there is only limited studies for Uranium remediation in large fields, so further improvements are needed to offer microorganisms as the most practical approach in Uranium detoxification. Current studies reveal that sulfate reducing bacterial species can adapt to different environmental conditions [40]

but genetic engineering might be needed to design a perfect Uranium recycler. It is suggested that new technologies that enhance microbial performance in Uranium detoxification and co-utilization of microorganisms with plants need to be explored to obtain the desired performance from the microorganisms [6]. For example, recent studies have shown that arbuscular mycorrhizal fungi species enhance Uranium uptake by plants that help elevate the remediation [41]. Zhu *et al* (2026) reported that Proteobacteria and Ascomycota can resist stress and can speed up production of Krebs cycle metabolites (e.g. oxalic acid, glutamic acid), which in turn the enhancement of Uranium intake by plant species [42]. The plant-microbe interaction is not limited to fungal species, bacterial species can also perform this type of activity, which might use different signaling pathways [43].

REFERENCES

[1] B. Maria, T. Costa, E. Kraka, Uranium : The Nuclear Fuel Cycle and Beyond, Int. J. Mol. Sci. 23 (2022) 4655.

[2] F. Celik, M. Camas, K. Kyeremeh, Microbial Sorption of Uranium Using Amycolatopsis sp . K47 Isolated from Uranium Deposits, Water Air Soil Pollut. 229 (2018) 212.

[3] A.M. Rathod, S. Verpaele, M. Kelvin, K. V. Sullivan, M.I. Leybourne, Uranium: an overview of physicochemical properties, exposure assessment methodologies, and health effects of environmental and occupational exposure, Environ. Geochem. Health 45 (2023) 1183–1200. https://doi.org/10.1007/s10653-022-01293-x.

[4] V. Georgiev, I. Dakova, I. Karadjova, Uranium Determination in Waters , Wine and Honey by Solid Phase Extraction with New Ion Imprinted Polymer, Molecules 27 (2022) 5516.

[5] N. Basheer, Z. Abdelkafi, M.S. Aswood, Quantitative of uranium levels in blood samples of cancer patients collected from different regions in Iraq, Radiat. Phys. Chem. 223 (2024) 111975. https://doi.org/10.1016/j.radphyschem.2024.111975.

[6] C. Cheng, L. Chen, K. Guo, J. Xie, Y. Shu, S. He, F. Xiao, Progress of uranium-contaminated soil bioremediation technology, J. Environ. Radioact. 241 (2022) 106773. https://doi.org/10.1016/j.jenvrad.2021.106773.

[7] Z. He, L. Dong, K. Zhang, D. Zhang, X. Pan, Lactic acid bacteria induce phosphate recrystallization for the in situ remediation of uranium-contaminated topsoil: Principle and application, Environ. Pollut. 314 (2022) 120277. https://doi.org/10.1016/j.envpol.2022.120277.

[8] Z. Li, P. Sun, C. Zhang, N. Zhu, N. Xu, D. Li, Y. Gao, J. Zhao, Translocation and transformation of uranium along the aquatic food chain: New insights into uranium risks to the environment, J. Hazard. Mater. 478 (2024) 135499. https://doi.org/10.1016/j.jhazmat.2024.135499.

[9] W. Li, L. Yu, B. Fu, J. Chu, C. Chen, X. Li, J. Ma, W. Tang, Protective effects of Polygonatum kingianum polysaccharides and aqueous extract on uranium-induced toxicity in human kidney (HK-2) cells, Int. J. Biol. Macromol. 202 (2022) 68–79. https://doi.org/10.1016/j.ijbiomac.2022.01.043.

[10] Q. Cui, Z. Zhang, J. Beiyuan, Y. Cui, L. Chen, H. Chen, L. Fang, A critical review of uranium in the soil-plant system: Distribution, bioavailability, toxicity, and bioremediation strategies, Crit. Rev. Environ.

Sci. Technol. 53 (2023) 340–365. https://doi.org/10.1080/10643389.2022.2054246.
[11] S. Haneklaus, H. Windmann, M. Maekawa, L. Zhang, E. Schnug, Diet Controls Uranium Intake and Aggravates Health Hazards, Med. Res. Arch. 9 (2021). https://doi.org/10.18103/mra.v9i8.2484.
[12] B. Yang, Q. Zhou, J. Zhang, Z. Li, F. Tuo, Evaluation of the natural radioactivity in food and soil around uranium mining region, J. Radioanal. Nucl. Chem. 329 (2021) 127–133. https://doi.org/10.1007/s10967-021-07794-w.
[13] S. Sachdeva, M.A. Powell, G. Nandini, H. Kumar, R. Kumar, P.K. Sahoo, Uranium and Fluoride Accumulation in Vegetable and Cereal Crops: A Review on Current Status and Crop-Wise Differences, Sustain. 15 (2023) 13895. https://doi.org/10.3390/su151813895.
[14] Ž. Mihaljev, S. Jakšić, M.Ž. Baloš, N. Popov, RADIOACTIVE RESIDUE IN HONEY, Arch. Vet. Med. 14 (2021) 49–60. https://doi.org/10.46784/eavm.v14i2.290.
[15] M.A. Misdaq, A. Mortassim, The influence of the nature of soil and plant and pollution on the 238U, 232Th, 222Rn and 220Rn concentrations in various natural honey samples using nuclear track detectors: Impact on the adult consumers, Pramana 73 (2009) 859–879. https://doi.org/10.1007/s12043-009-0154-0.
[16] S. Dizman, G. Hodolli, S. Kadiri, H. Aliu, S. Makolli, Radioactivity in Kosovo Honey Samples, Polish J. Environ. Stud. 29 (2019) 1119–1127. https://doi.org/10.15244/pjoes/105968.
[17] M.A. Meli, D. Desideri, C. Roselli, L. Feduzi, C. Benedetti, Radioactivity in honey of the central Italy, Food Chem. 202 (2016) 349–355. https://doi.org/10.1016/j.foodchem.2016.02.010.
[18] Ş. Turhan, T. Çeter, E.M. Altuner, S. Karabıcak, S. Çeter, O. Bıyıklıoğlu, Ş. Aktaş, A. Kurnaz, Determination of potentially toxic metals and natural radionuclides in airborne pollens produced different urban environments in Turkey and health risk assessment, Int. J. Environ. Health Res. (2024) 1–18. https://doi.org/10.1080/09603123.2024.2391460.
[19] J. Li, Y. Zhang, Remediation technology for the uranium contaminated environment: a review, Procedia Environ. Sci. 13 (2012) 1609–1615. https://doi.org/10.1016/j.proenv.2012.01.153.
[20] T. Rogiers, R. Van Houdt, A. Williamson, N. Leys, N. Boon, K. Mijnendonckx, Molecular Mechanisms Underlying Bacterial Uranium Resistance, Front. Microbiol. 13 (2022) 822197.

https://doi.org/10.3389/fmicb.2022.822197.
[21] X. Wang, F. Li, R. Wu, S. He, P. Li, P.L. Show, Y. Zhang, J. Chen, Mechanism of direct treatment of high concentration uranium using sulfate reducing bacteria, Chem. Eng. J. 520 (2025) 166265. https://doi.org/10.1016/j.cej.2025.166265.
[22] A.E. Ray, J.R. Bargar, V. Sivaswamy, A.C. Dohnalkova, Y. Fujita, B.M. Peyton, T.S. Magnuson, Evidence for multiple modes of uranium immobilization by an anaerobic bacterium, Geochim. Cosmochim. Acta 75 (2011) 2684–2695. https://doi.org/10.1016/j.gca.2011.02.040.
[23] E. Cardenas, W.M. Wu, M.B. Leigh, J. Carley, S. Carroll, T. Gentry, J. Luo, D. Watson, B. Gu, M. Ginder-Vogel, P.K. Kitanidis, P.M. Jardine, J. Zhou, C.S. Criddle, T.L. Marsh, J.M. Tiedje, Microbial communities in contaminated sediments, associated with bioremediation of uranium to submicromolar levels, Appl. Environ. Microbiol. 74 (2008) 3718–3729. https://doi.org/10.1128/AEM.02308-07.
[24] M.L. Merroun, S. Selenska-pobell, Bacterial interactions with uranium : An environmental perspective, J. Contam. Hydrol. 102 (2008) 285–295. https://doi.org/10.1016/j.jconhyd.2008.09.019.
[25] Y. Lv, C. Tang, X. Liu, B. Chen, M. Zhang, X. Yan, X. Hu, S. Chen, X. Zhu, Stabilization and mechanism of uranium sequestration by a mixed culture consortia of sulfate-reducing and phosphate-solubilizing bacteria, Sci. Total Environ. 827 (2022) 154216. https://doi.org/10.1016/j.scitotenv.2022.154216.
[26] X. Yu, F. Xiong, C. Zhou, Z. Luo, Z. Zhou, J. Chen, K. Sun, Uranium bioprecipitation mediated by a phosphate-solubilizing Enterobacter sp. N1-10 and remediation of uranium-contaminated soil, Sci. Total Environ. 906 (2024) 167688. https://doi.org/10.1016/j.scitotenv.2023.167688.
[27] A. Wollenberg, J. Kretzschmar, B. Drobot, R. Hübner, L. Freitag, F. Lehmann, A. Günther, T. Stumpf, J. Raff, Uranium(VI) bioassociation by different fungi – a comparative study into molecular processes, J. Hazard. Mater. 411 (2021) 125068. https://doi.org/10.1016/j.jhazmat.2021.125068.
[28] G. Figueiredo, J.P. da Costa, T. Rocha-Santos, T. Caetano, R. Pereira, S. Mendo, J. Lourenço, Uranium mining effluents: What about the re-use of mining wastes to improve the bioproduction of industrially relevant bioactive compounds?, Chemosphere 363 (2024) 142982. https://doi.org/10.1016/j.chemosphere.2024.142982.
[29] U.K. Banala, N.P.I. Das, R.K. Padhi, S.R. Toleti, Alkaliphilic bacteria retrieved from uranium mining effluent: Characterization, U

sequestration and remediation potential, Environ. Technol. Innov. 24 (2021) 101893. https://doi.org/10.1016/j.eti.2021.101893.

[30] G. Wang, Y. Liu, J. Wang, J. Xiang, T. Zeng, S. Li, J. Song, Z. Zhang, J. Liu, The remediation of uranium-contaminated groundwater via bioreduction coupled to biomineralization with different pH and electron donors, Environ. Sci. Pollut. Res. 30 (2023) 23096–23109. https://doi.org/10.1007/s11356-022-23902-z.

[31] S. Schaefer, R. Steudtner, R. Hübner, E. Krawczyk-Bärsch, M.L. Merroun, Effect of Temperature and Cell Viability on Uranium Biomineralization by the Uranium Mine Isolate Penicillium simplicissimum, Front. Microbiol. 12 (2021) 802926. https://doi.org/10.3389/fmicb.2021.802926.

[32] X. Qi, J. Gou, X. Chen, S. Xiao, I. Ali, R. Shang, D. Wang, Y. Wu, M. Han, X. Luo, Application of mixed bacteria-loaded biochar to enhance uranium and cadmium immobilization in a co-contaminated soil, J. Hazard. Mater. 401 (2021) 123823. https://doi.org/10.1016/j.jhazmat.2020.123823.

[33] J. Zhang, N. Li, R. Guo, X. Guo, X. Li, X. Chen, Y. Dong, Q. Wang, Y. Zhu, W. Zhu, High-efficient immobilization of uranium by biochar loaded mixed microorganisms composed of Bacillus and Pseudomonas, J. Hazard. Mater. 496 (2025) 139296. https://doi.org/10.1016/j.jhazmat.2025.139296.

[34] L. Zhang, H. Dong, R. Li, D. Liu, L. Bian, Y. Chen, Z. Pan, M.I. Boyanov, K.M. Kemner, J. Wen, Q. Xia, H. Chen, E.J. O'Loughlin, G. Wang, Y. Huang, Effect of Siderophore DFOB on U(VI) Adsorption to Clay Mineral and Its Subsequent Reduction by an Iron-Reducing Bacterium, Environ. Sci. Technol. 56 (2022) 12702–12712. https://doi.org/10.1021/acs.est.2c02047.

[35] R. Li, L. Zhang, Y. Chen, Q. Xia, D. Liu, Y. Huang, H. Dong, Oxidation of Biogenic U(IV) in the Presence of Bioreduced Clay Minerals and Organic Ligands, Environ. Sci. Technol. 58 (2024) 1541–1550. https://doi.org/10.1021/acs.est.3c07385.

[36] T. Ohnuki, N. Kozai, F. Sakamoto, T. Ozaki, T. Nankawa, Y. Suzuki, A.J. Francis, Association of actinides with microorganisms and clay: Implications for radionuclide migration from waste-repository sites, Geomicrobiol. J. 27 (2010) 225–230. https://doi.org/10.1080/01490450903456715.

[37] C. Zhao, J. Liu, Y. Deng, Y. Tian, G. Zhang, J. Liao, J. Yang, Y. Yang, N. Liu, Q. Sun, Uranium(VI) adsorption from aqueous solutions by

microorganism-graphene oxide composites via an immobilization approach, J. Clean. Prod. 236 (2019) 117624. https://doi.org/10.1016/j.jclepro.2019.117624.

[38] N. Kolhe, S. Zinjarde, C. Acharya, Removal of uranium by immobilized biomass of a tropical marine yeast Yarrowia lipolytica, J. Environ. Radioact. 223–224 (2020) 106419. https://doi.org/10.1016/j.jenvrad.2020.106419.

[39] F. Chen, B. Fan, C. Wang, J. Qian, B. Wang, X. Tang, Z. Qin, Y. Chen, Bin Liang, W. Liu, A. Wang, Y. Ye, Y. Wang, Weak electro-stimulation promotes microbial uranium removal: Efficacy and mechanisms, J. Hazard. Mater. 439 (2022) 129622. https://doi.org/10.1016/j.jhazmat.2022.129622.

[40] R. Xiao, Z. Liu, M. Xu, G. Jiang, Y. Peng, C. Li, J. Wang, H. Yin, L. Xu, Microbial mechanisms of sulfate reduction for low-temperature bioremediation of acid-mined uranium sandstone groundwater, J. Water Process Eng. 69 (2025) 106627. https://doi.org/10.1016/j.jwpe.2024.106627.

[41] J. Rosas-Moreno, C. Walker, K. Duffy, C. Krüger, M. Krüger, C.H. Robinson, J.K. Pittman, Isolation and identification of arbuscular mycorrhizal fungi from an abandoned uranium mine and their role in soil-to-plant transfer of radionuclides and metals, Sci. Total Environ. 876 (2023) 162781. https://doi.org/10.1016/j.scitotenv.2023.162781.

[42] K. Zhu, Z. Yang, M. Li, Q. Deng, F. Xiao, Y. Wang, D. Ding, H. Yu, N. Hu, Synergistic enhancement of phytoremediation efficiency and mechanisms of uranium-contaminated soil by oxalic acid and endophytic fungus Fusariumsp. A-2 withMacleaya cordata, J. Environ. Radioact. 291 (2026) 107844. https://doi.org/10.1016/j.jenvrad.2025.107844.

[43] Y. Liu, G. He, T. He, M. Saleem, Signaling and Detoxification Strategies in Plant-Microbes Symbiosis under Heavy Metal Stress: A Mechanistic Understanding, Microorganisms 11 (2023). https://doi.org/10.3390/microorganisms11010069.

Chapter 7

CHARACTERISTICS AND USAGE AREAS OF INDUSTRIAL MINERALS

Gamze SAVACI SELAMET[1], Temel SARIYILDIZ[2]

1. INTRODUCTION

Industrial minerals are defined as naturally occurring, non-metallic, and non-renewable minerals and rocks with unique chemical compositions [1]. In comparison with ore minerals, industrial minerals are inexpensive due to their abundance, wide distribution on the Earth's surface, and ease of processing [2].

Asbestos, barite, bentonite, kaolinite, smectite, talc, mica, vermiculite, diatomite, feldspar, gypsum, hormite, limestone, nepheline, perlite, silica sand, wollastonite, and zeolite minerals are all essential industrial minerals due to their characteristic physicochemical properties and their variety of applications in different industrial sectors (Figure 1). Those minerals are used in several industries, such as glass and ceramics (feldspar, silica, kaolinite, nepheline, and talc), pharmaceuticals and cosmetics (talc, kaolinite, mica, and silica), electronics (mica, silica, and feldspar), construction (limestone, gypsum, barite, talc, vermiculite, and zeolite), metallury and foundry (bentonite, wollastonite, and silica), chemical industry (limestone, barite, zeolite, gypsum, and felspar), agriculture and horticulture (diatomite, zeolite, vermiculite, and bentonite), automotive and aerospace (talc, mica, wollastonite, and kaolinite), energy and environmental remediation (zeolite, bentonite, diatomite, and vermiculite), food packaging (kaolinite, diatomite, and zeolite), clothing and paints (kaolinite, talc, calcium carbonate, and mica), polymers and rubber (talc, kaolinite, mica, and silica), radioactive waste disposal (barite).

[1] Assoc. Prof. Dr., Department of Forest Engineering/Faculty of Forestry, Kastamonu University, Türkiye, gsavaci@kastamonu.edu.tr, (ORCID: 0000-0003-4685-2797)

[2] Prof. Dr., Department of Forest Engineering/Faculty of Forestry, Bursa Technical University, Türkiye, temel.sariyildiz@btu.edu.tr, (ORCID: 0000-0003-3451-3229)

Figure 1. Applications of industrial minerals in different sectors.

This section of the book provides a detailed examination of the physicochemical properties of some industrial minerals and their applications in the industrial sector.

2. SIGNIFICANCE OF PHYSICAL AND CHEMICAL PROPERTIES

The physical properties of industrial minerals, including hardness, density, particle size, colour, luster, specific surface area, and thermal stability are critical determinants of their industrial applications and economic values [3]. Therefore, the physical properties such as brightness (kaolinite), hardness (silica), or platy habit (talc, mica) are more critical than the chemical compositions in defining their industrial and economic values. The chemical properties of industrial minerals are crucial because they determine how these materials react, interact, or remain stable in industrial processes [4]. Industrial minerals are often selected based on their chemical composition and stability rather than their metal content. For example, the purity of $CaCO_3$ in limestone or SiO_2 in silica (quartz) is critical for most applications [5].

The industrial minerals and rocks are used as raw materials or after processing due to their important physical and chemical properties [6]. Special

processes have the capacity to endow certain industrial minerals and rocks with novel physical properties. For instance, the processing of bentonite with inorganic acids, a process known as acid activation [7], produces materials with numerous acid sites and high sorption capacity. These materials are capable of adsorbing coloring compounds, thereby colorizing and stabilizing crude edible oils. In a similar manner, the expansion of perlite or the flaking of vermiculite produces lightweight aggregates with significant insulation properties. These properties are not found in unprocessed raw materials [8].

3. MAJOR INDUSTRIAL MINERALS AND THEIR USES

3.1. Asbestos

Asbestos is a fibrous silicate mineral that occurs naturally and can be released when ultramafic or serpentine rocks undergo mechanical disruption such as fracturing or crushing [9]. It possesses a fibrous habit, lacks electrical conductivity, and shows exceptional resistance to heat, acids, and physical stress [10]. In terms of composition, asbestos comprises various silicate types including iron–magnesium silicate, calcium–magnesium silicate, magnesium silicate, and complex sodium–iron silicate minerals [10]. Naturally, six main asbestos minerals are recognized and grouped under two categories: serpentine (chrysotile) and amphibole (tremolite amosite, crocidolite, anthophyllite, and actinolite) [11].

Chrysotile deposits generally occur at tectonic boundaries between peridotite and gabbroic rocks, and may also appear as veins within serpentinites, serpentinized ultramafic bodies, and serpentinized dolomitic marbles [12, 13]. Representing about 90% of global asbestos use, chrysotile is the predominant industrial variety [14]. It belongs to the serpentine group and is a hydrated magnesium silicate mineral characterized by a white color, silky luster, soft texture, and fibrous form [10]. The chemical formula of chrysotile is $Mg_3Si_2O_5(OH)_4$, and its hardness on the Mohs scale ranges between 2.5 and 4 [15]. The 1:1 ratio of these two types of layers and these properties make chrysotile fibers processable, resulting in a versatile material [11]. The amphibole group is a harmful type of asbestos and has a hard, needle-like structure [16]. It contains magnesium, sodium, calcium silicate, and iron in its fiber structure [17]. These exhibit a linear form with rigid and tight characteristics [18].

Asbestos fibers are resistant to heat, chemical corrosion, and friction. They are also impermeable to heat, sound, and electricity, and are relatively inexpensive [19-21]. The addition of chrysotile asbestos fibers to rubber produces materials that are commonly used for packings and gaskets [13].

Asbestos has been widely applied in construction materials, including ceilings, walls, floors, pipes, beams, and columns [22]. Asbestos minerals can contain toxic elements that pose health risks [23]. Due to their harmful effects on human health, most asbestos facilities stopped operating by the late 1990s, and asbestos production and trade are now banned worldwide [10].

3.2. Barite

Barite ($BaSO_4$) is a non-metallic mineral characterized by a specific gravity of 4.2–4.7, a stable crystal structure [24], and a Mohs hardness of 3.0 [25]. Barite deposits occur in sedimentary, metamorphic, or igneous environments depending on geological conditions [26]. It has been reported that barite in the Earth's crust forms through the mixing of two fluids - one containing barium derived from silicate minerals and the other containing sulfate [27].

Barite is a vital industrial mineral used in petroleum and gas drilling, as well as in the production of paints, papers, rubbers, plastics, glasses, leathers, tobaccos, fertilizers, radiological materials, and pharmaceuticals [28, 29]. Owing to its softness, chemical inertness, insolubility in water, low solid content, and ability to increase mud density, it is widely used in the oil and gas sector. Barite serves as a drilling weighting agent, filler, and radiation-shielding material [30-32]. It is also employed in the chemical industry for producing barium compounds and in the paint and glass industries [33].

3.3. Diatomite

Diatoms are a major component of phytoplankton in marine ecosystems [34] and accumulate in various aquatic environments, including wetlands, lakes, and oceans [35]. Diatomites are sedimentary silica rocks mainly composed of opal and cristobalite [36]. They are light, fine-grained, and formed primarily from the opaline skeletons or fragments of diatoms (diatom algae). Diatomites can appear in several colors, such as white, light grey, dark grey, brownish-grey, and yellowish-grey [36].

Diatomite is a siliceous material with high porosity, low thermal and acoustic conductivity, chemical inertness, and resistance to acids and heat. It also has a large surface area, high absorption capacity, and low bulk density [37]. These properties allow its use in pharmaceuticals [38], cosmetics [39], food [36], and nanotechnology [40]. It is also applied as a soil conditioner with inorganic fertilizers [41] and as insulation in furnace covers, pipe linings, and walls [36].

3.4. Clay Minerals, Classifications and Structures

Clay minerals are hydrous aluminium silicates that play an important role in both natural processes and industrial applications [42]. They are mainly formed through the weathering of igneous and metamorphic rocks and are characterized by fine particle size, plate-like morphology, and layered structures [43]. The classification of clay minerals depends on how their tetrahedral and octahedral silicate layers are arranged and stacked. Groups include kaolinites with a 1:1 ratio structure (e.g., halloysite, kaolinite), limited-expanding 2:1 clays (e.g., vermiculite), non-expanding 2:1 clays (e.g., mica, illite), uncharged 2:1 clays (e.g., talc, pyrophyllite), strongly expanding 2:1 clays (e.g., montmorillonite), 2:1:1 clays containing a brucite layer (e.g., chlorites), and fibrous silicates (e.g., sepiolite, palygorskite) [44]. The clay minerals classified above are nanoscale materials and are represented in Figure 2 [45].

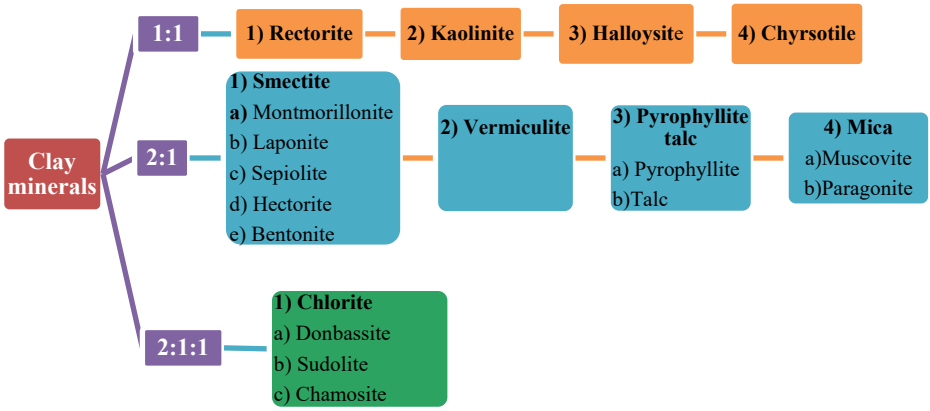

Figure 2. Different types of clay minerals and their classifications

Clay minerals (bentonite, kaolinite, smectite, talc, mica, and vermiculite) are important industrial minerals due to their wide range of applications across various sectors (Figure 3). They are used in industries such as construction, cosmetics, ceramics, paper, biomedicine, textiles, energy, food packaging, healthcare, paint, environmental remediation, radioactive waste management, and soil improvement.

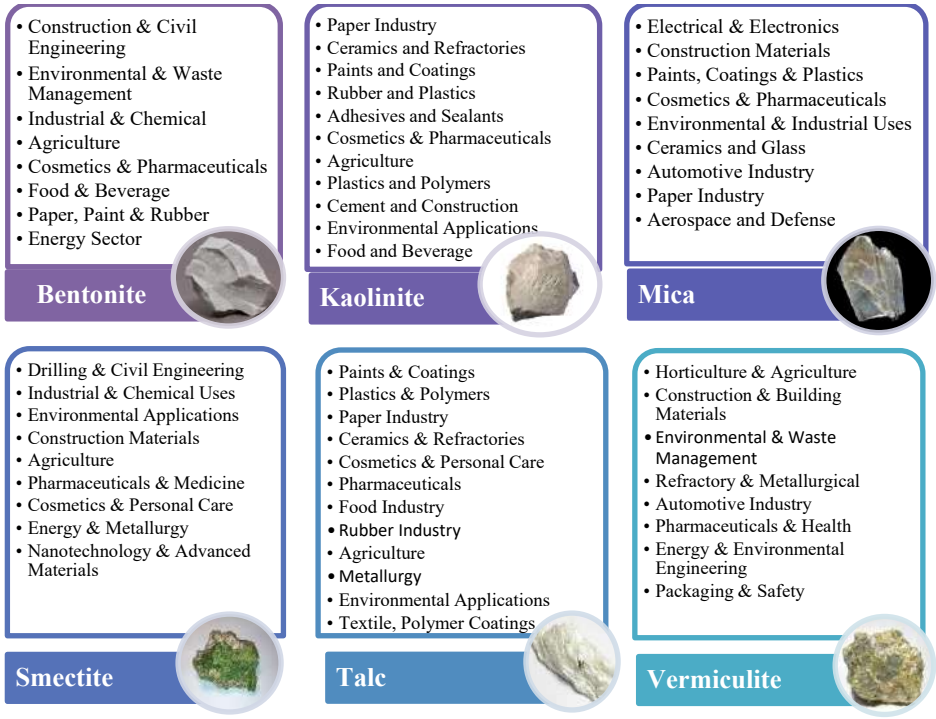

Figure 3. Applications of Clay Minerals

3.5. Feldspar

Feldspars constitute the most abundant minerals in the crusts of many terrestrial planets, such as Earth, the Moon, and Mars, and are also commonly found in asteroids and meteorites [46]. They are aluminosilicate minerals containing calcium, sodium, and potassium, and occasionally cesium or barium, forming isomorphous mixtures [47]. Feldspars are chemically classified into alkali feldspars and plagioclases and exhibit anisotropic crystal chemistry. Most feldspar minerals have a specific gravity of 2.5–2.8, a Mohs hardness of 6–6.5, and a glassy luster that appears pearly on cleavage surfaces [48]. Feldspars, including alkali feldspar and plagioclase, are chemically and optically complex [46]. They are important in various industrial applications, particularly as fluxing agents in glass and ceramic production due to their high alkali and alumina content [49,50]. Feldspar is widely used in glass manufacturing, plastics, paper, ceramics, enamel frits, polymers, paints and glazes, welding electrodes, and as a filler or extender in rubber [51]. In glass production, alumina from feldspar enhances hardness, durability, and chemical resistance, making high alumina content and alkali presence critical for the industry [52].

3.6. Gypsum

Gypsum, composed of calcium sulfate dihydrate ($CaSO_4 \cdot 2H_2O$), is a mineral commonly found in nature as a white powder. Its hardness is 1.5-2, and its density is 2.3-2.4. It is colorless or white. They are the first minerals formed by the evaporation of seawater in salt beds. They usually form together with halite, calcite, dolomite, anhydrite, sulfur, pyrite, and Quartz [53]. Gypsum is a sedimentary mineral found in deposits worldwide, particularly in evaporite sources. In its purest form, it consists of calcium sulfate dihydrate, though most naturally occurring gypsum is found alongside anhydrite, clay, dolomite and limestone [54]. Gypsum is a significant material, and it is one of the oldest materials still in use in the construction industry [55]. Gypsum is utilised in a variety of products, including plaster, plasterboard, interior coatings, cement retarders, ceramics, and medical supplements or implants [55-57]. Gypsum is widely used as a soil acidity improver in surface applications [58].

3.7. Calcium Carbonate (Limestone)

Calcium carbonate exists in three polymorphs: orthorhombic aragonite, hexagonal vaterite, and hexagonal calcite [59]. Calcite is the stable form, while vaterite and aragonite are metastable and convert readily to calcite. Vaterite is the least stable, slowly dissolving in water and recrystallizing as calcite [60].

The Earth's crust contains calcite as the most common form of calcium carbonate, whereas aragonite and vaterite are less widespread, and dolomite is relatively uncommon. Most calcite is relatively pure, with common impurities including manganese, iron, and magnesium. Calc-silicate rocks form through the metamorphism of impure carbonates or from the accumulation of calcareous shells, and weathering of these rocks produces calcite [53,61]. Calcite is used in the chemical industry, cement, lime production, and construction. Aragonite precipitates from seawater and is found in mollusk and coral shells; its orthorhombic structure provides enhanced stability and durability [62]. Aragonite is applied in building facades, sculpture, and decorative items. Vaterite may form as an initial phase in the exoskeletons of some invertebrates under specific conditions [63].

3.8. Nepheline

The chemical formula of the nepheline mineral, which belongs to the feldspathoid group, is (Na, K) ($AlSiO_4$) and it crystallizes in a hexagonal system [53]. Chemically, it is close to alkali feldspars, but they are deficient in silica [64]. It is a major mineral in alkaline rocks, primarily syenite and its pegmatites, phenolites, and nepheline basalts. Nepheline is relatively enriched in alkalies

and alumina than the alkali feldspars and hence it is known to be a better natural substitute for feldspar in all industries [65].

Nepheline syenite serves as a fluxing agent in glass and ceramics, similar to feldspar, by providing alkalis that lower the melting temperature, reduce viscosity, accelerate the formation of the glassy phase, and enhance reactivity with quartz. In glass manufacturing, it also contributes alumina, which increases mechanical strength, thermal stability, and chemical durability [64].

3.9. Perlite

This definition underscores the dominance of SiO_2 and Al_2O_3 in its composition, which contribute to its low density, high surface area, and chemical inertness [66]. Perlite consists predominantly of principal oxides: SiO_2, Al_2O_3, K_2O, Na_2O; minor constituents: TiO_2, CaO, MgO, Fe_2O_3, water, and small amounts of unburned carbon. Because of its high silica and alumina content, especially in its finely ground form, perlite exhibits pozzolanic activity (the capacity to chemically react with calcium hydroxide in the presence of moisture, forming cementitious compounds). This property is attributed to its amorphous (non-crystalline) glassy structure [67]. Perlite is a naturally occurring volcanic glass that contains water within its structure and expands into a lightweight, porous material when rapidly heated. Although classified as an industrial mineral, its composition can vary because it is a rock rather than a true mineral [68]. The expanded form of perlite is widely used in construction, horticulture, insulation, and various industrial applications due to its low density and high porosity [69].

3.10. Wollastonite

Wollastonite belongs to the pyroxene group and is a naturally occurring calcium metasilicate ($CaSiO_3$). It is a non-metallic, needle-like crystal structure, alkaline (pH 9.8), white-colored mineral. The main reason for the commercial use of wollastonite is its crystal structure and chemistry [70]. It generally contains magnesium, manganese, iron, and strontium. It occurs in contact metamorphic limestones and volcanic rocks together with quartz, garnet, diopside, plagioclase feldspar, tremolite, sphene, calcite, apatite, epidote, and andradite [13, 70].

Wollastonite is mostly used in the ceramic industry. Its needle-like crystals increase the strength of ceramics and raise the drying rate [53]. Wollastonite has a fibrous, needle-like crystal structure, allowing its use as a filler in paints [71]. It is also employed in the production of heat-insulating packaging materials, ceramics, foundry linings, and as a filler in paints and polymers for the

metallurgical and automotive industries [72]. Wollastonite is used in a new way in the bioactive ceramics industry and acts as a biocompatible material used as a bone substitute, covering its applications [72, 73]. With its low-temperature melting properties, wollastonite is an important additive for the continuous casting process used in sheet metal production [70].

3.11. Zeolite

Zeolites are hydrated aluminum silicates with a crystalline structure composed of alkali and alkaline earth elements [53]. Zeolites form in gneiss, amphibolite, serpentinite, hornfels, quartzite, and marble rocks. Zeolites are minerals that form at low pressure and temperature depending on the presence of water (H_2O) and have a porous structure. Zeolites have an open lattice structure, which gives them a lower density [74]. Zeolites, which are low in weight, highly porous, homogeneous, compact, and robust, can be easily cut and processed [75] Anorthite, hollandite, lömantite, natrolite, sabazite, stilbite, and phillipsite are the most common minerals in the zeolite group. Zeolites are industrially important due to their catalytic, adsorptive, and ion-exchange properties [76]. They are applied as fertilizer additives and soil conditioners, in construction and cement production, for oil spill cleanup, as drying agents, and in water treatment. Additionally, zeolites serve as carriers for pesticides, herbicides, and animal feed additives, as well as in binding toxins, controlling odors, and managing hazardous and nuclear wastes. They are also utilized in biochemical processes, including enzyme and antibiotic production, and as components in food supplements [77-79].

4. CONCLUSION

The industrial minerals play a crucial role in modern industry due to their wide range of physical and chemical properties, which determine their suitability for various technological and environmental applications. Understanding the characteristics of these minerals - such as particle size, purity, hardness, and chemical composition - is essential for optimizing their use in industries ranging from construction and ceramics to pharmaceuticals and electronics.

The diversity of industrial minerals, including sulfate, feldspar, clay minerals, carbonates, and zeolites, provides unique functional advantages such as thermal stability, adsorption capacity, and mechanical strength. As technology advances, the demand for higher purity and more specialized forms of industrial minerals continues to increase, highlighting the importance of mineral beneficiation and sustainable resource management.

In conclusion, the industrial minerals are indispensable raw materials for modern industry and sustainable development. The relationship between the properties and applications of industrial minerals underscores their indispensable role in industrial development and innovation. Continued research on mineral processing, substitution, and recycling will be vital for ensuring sustainable and efficient utilization of these non-metallic resources.

REFERENCES

1. Garg, V. (2018). A review about minerals and power resources and their uses. *Journal of Advances and Scholarly Researches in Allied Education 15*(12), 1-4.
2. Garcia-Valles, M. (2021). Editorial for Special Issue "Industrial Minerals". *Minerals*, *11*(2), 129.
3. Phipps, J. S. (2014). Engineering minerals for performance applications: an industrial perspective. *Clay Minerals*, *49*(1), 1-16.
4. Harben, P. W. (1999). The Industrial Minerals Handbook. Industrial Minerals Information Ltd.
5. USGS (U.S. Geological Survey). (2023). Mineral Commodity Summaries – Industrial Minerals. *U.S. Department of the Interior*.
6. Bates, R.L. (1969): Geology of the industrial rocks and minerals. *Dover, NY*, 459 p.
7. Christidis, G., Scott, P.W. & Dunham, A.C. (1997): Acid activation and bleaching capacity of bentonites from the islands of Milos and Chios, Aegean, Greece. *Appl. Clay Sci*. 12: 329-347.
8. Christidis, G. E. (2010). Industrial minerals: significance and important characteristics. 9: *Mineralogical Society of Great Britain and Ireland*, 1-12.
9. Van Gosen, B. S. (2007). The geology of asbestos in the United States and its practical applications. *Environmental & Engineering Geoscience*, *13*(1), 55-68.
10. Atabey E. 2014. Türkiye asbest haritası (Çevresel asbest maruziyeti akciğer kanseri-mezotelyoma). *Tuberk Toraks*., *63*(3), 199-219.
11. Durczak, K., Pyzalski, M., Sujak, A., Juszczyk, M., Sala, D., & Ustinovichius, L. (2024). Efficient Management of Asbestos Waste Through Utilization as Mineral Additives in Portland Cement Production. *Materials*, *17*(23), 5793.
12. Heikal, M. T. S., Surour, A. A., & Said, A. A. (2024). Chemical, thermal and infra-red characterization of chrysotile modes from the Wadi Daftah serpentinite (Semail ophiolite), United Arab Emirates. *Discover Geoscience*, *2*(1), 87.
13. Virta, R. L. (2002). Asbestos: Geology, mineralogy, mining, and uses (p. 28). Washington, DC, USA: *US Department of the Interior*, US Geological Survey.
14. Kusiorowski, R., Gerle, A., Kujawa, M., Antonovič, V., & Boris, R. (2024). Structural Characterisation of End-of-Life Cement–Asbestos Materials from Lithuania. *Fibers*, *12*(4), 37.

15. Skinner, H. C. W. (2003). Mineralogy of asbestos minerals. *Indoor and Built Environment*, *12*(6), 385-389.
16. Bağcı, Ö., & Özmıhçı, S. (2023). Evaluation of Asbestos in Terms of Occupational Safety in Urban Renewal. *Artvin Çoruh Üniversitesi Mühendislik ve Fen Bilimleri Dergisi*, *1*(1), 51-61.
17. Karaağaç, R. A., & Aydın, Ş. D. (2024). The Mineral That Leads to Death: Asbestos Impacts on Biodiversity and Environmental Sustainability. *Kastamonu Üniversitesi Sağlık Bilimleri Fakültesi Dergisi*, *3*(3), 219-230.
18. Kumagai-Takei, N., Lee, S., Srinivas, B., Shimizu, Y., Sada, N., Yoshitome, K., ... & Otsuki, T. (2020). The effects of asbestos fibers on human T cells. *International Journal of Molecular Sciences*, *21*(19), 6987.
19. Lemen, R. A. (1997). Introduction: history of the use of asbestos. *La Medicina del Lavoro*, *88*(4), 288-292.
20. Harris, L. V., & Kahwa, I. A. (2003). Asbestos: old foe in 21st century developing countries. *Science of the total environment*, *307*(1-3), 1-9.
21. Frank, A. L., & Joshi, T. K. (2014). The global spread of asbestos. *Annals Of Global Health*, *80*(4), 257-262.
22. Akbel, E. and Özdemir, K. (2020). Investigation of Dust Factor in terms of Occupational Health and Safety in Construction Sector, *Uşak University Journal of Science and Natural Sciences*, *4*(2), 139 –150.
23. Punturo, R., Ricchiuti, C., Mengel, K., Apollaro, C., De Rosa, R., & Bloise, A. (2018). Serpentinite-derived soils in southern Italy: Potential for hazardous exposure. *J. Mediterr. Earth Sci*, *10*, 51-61.
24. You, C., Wang, C. L., Liu, D. H., Yu, X. C., Yan, K., Liu, S. H., & Zhou, B. W. (2022). REE geochemistry of fluorite from Kantian fluorite deposit and its geological implications in Ningdu area, Jiangxi Province. *Acta Geoscientica Sinica*, *43*(3), 359-370.
25. Nzeh, N. S., & Popoola, P. A. (2023). Exploration and characterization of barite mineral from Azara-Nassarawa ore deposits from suitabiity in industrial applications. Physicochemical Problems of Mineral Processing, 59.
26. Kolawole, F. O., Bergerman, M. G., Ulsen, C., & Kolawole, S. K. (2019). a Global Review of Barite Beneficiation Processes: a Case Study of Azara Barite Ores in Nigeria. *Nigerian Journal of Engineering*, *26*(1).
27. Bulatovic, S. M. (2007). Handbook of flotation reagents: chemistry, theory and practice: Volume 1: flotation of sulfide ores. *Elsevier*.

28. Akpan, A. E., Ebong, E. D., Ekwok, S. E., & Joseph, S. (2014). Geophysical and geological studies of the spread and industrial quality of Okurike Barite deposit. *American Journal of Environmental Sciences*, *10*(6), 566-574.
29. Aladesanmi, A. O., Ogundana, A. K., Olowookere, A. A., & Jenakumo, L. (2018). Geological characterization of azara barite mineralization, Middle Benue Trough Nigeria. *J Environ Earth Sci*, *8*(3), 44-46.
30. Amin, M. N., Ahmad, I., Iqbal, M., Abbas, A., Khan, K., Faraz, M. I., ... & Ullah, S. (2022). Computational AI models for investigating the radiation shielding potential of high-density concrete. *Materials*, *15*(13), 4573.
31. Turhan, MF, Akman, F., Kaçal, MR, Polat, H. ve Demirkol, İ. (2023). Barit dolgulu polimer kompozitlerin gama ışını zayıflatma performanslarına yönelik bir çalışma. Uygulamalı Radyasyon ve *İzotoplar*, *191*, 110568.
32. Salimi, A., Beni, A. H., & Bazvand, M. (2024). Evaluation of a water-based spacer fluid with additives for mud removal in well cementing operations. *Heliyon*, *10*(4).
33. Tanko, I. Y., Adam, M., & Shettima, B. (2015). Petrology and geochemistry of barite mineralisation around Azara, North Central Nigeria. *International Journal of Scientific and Technological Research*, *4*, 44-49.
34. Zahajská, P., Opfergelt, S., Fritz, S. C., Stadmark, J., & Conley, D. J. (2020). What is diatomite?. *Quaternary Research*, *96*, 48-52.
35. Clarke, J., 2003. The occurrence and significance of biogenic opal in the regolith. *Earth-Science Reviews 60*, 175–194.
36. Ivanov, S. É., & Belyakov, A. V. (2008). Diatomite and its applications. *Glass & Ceramics*, *65*.
37. Temirova, S., Fischer, D., & Kuldeyev, Y. E. (2024). The use of diatomites in industrial production technologies. *Challenges of Science*, *7*, 46-51.
38. Engh, K. R. (1993). Kirk-Othmer Encyclopedia of Chemical Technology. *M. Howe Grant* (Ed.), 8.
39. Tang, Y., Zhang, Z., Yang, S., Smith, G. J., & Liu, L. (2021). Diatomite encapsulated AgNPs as novel hair dye cosmetics: Preparation, performance, and toxicity. *Colloids and Surfaces B: Biointerfaces*, *200*, 111599.
40. Villani, M., Onesto, V., Coluccio, M. L., Valpapuram, I., Majewska, R., Alabastri, A., ... & Gentile, F. (2019). Transforming diatomaceous earth

into sensing devices by surface modification with gold nanoparticles. *Micro and Nano Engineering*, *2*, 29-34.
41. Kulikova, A. H. & Yashin, E. A. (2015). The role of silicon and high-silicon rocks in the protection of crops. *Bulletin of Ulyanovsk State Agricultural Academy*, *4*, 30-35.
42. Jacob, A. G., Alisi, I. O., & Surajo, J. M. (2025). Kaolinite clay as green and sustainable raw material for zeolites production: A review. *FUDMA Journal of Sciences*, *9*, 18-35.
43. Ajibola, A.A, Omoleye, J.A, Efeovbokhan, V.E. (2018). Catalytic cracking of polyethylene plastic waste using synthesized zeolite Y from Nigerian kaolin deposit. *Applied Petrochem Resource*, *8*(4):211-217.
44. Singh, N. B. (2022). Clays and clay minerals in the construction industry. *Minerals*, *12*(3), 301.
45. Ma, Y., Shi, C., Lei, L., Sha, S., Zhou, B., Liu, Y., & Xiao, Y. (2020). Research progress on polycarboxylate based superplasticizers with tolerance to clays-a review. *Construction and Building Materials*, *255*, 119386.
46. Pickersgill, A. E., Jaret, S. J., Pittarello, L., Fritz, J., & Harris, R. S. (2021). Shock effects in feldspars: An overview, in Large Meteorite Impacts and Planetary Evolution VI, W. U. Reimold, C. Koeberl, Eds. (*Geological Society of America*, 2021), *550*, 507–535.
47. Kyonka, J. C., & Cook, R. L. V. (1954). The properties of feldspars and their use in whitewares. Bulletin/University of Illinois, *Engineering Experiment Station*; no. 422.
48. Zhang, Y., Hu, Y., Sun, N., Liu, R., Wang, Z., Wang, L., & Sun, W. (2018). Systematic review of feldspar beneficiation and its comprehensive application. *Minerals Engineering*, *128*, 141-152.
49. Wu, J., Li, Z., Huang, Y., Li, F., & Yang, Q. (2014). Fabrication and characterization of low temperature co-fired cordierite glass–ceramics from potassium feldspar. *Journal of alloys and compounds*, *583*, 248-253.
50. Zawrah, M. F., Khattab, R. M., El-Kheshen, A. A., & El Fadaly, E. (2017). Sintering and properties of borosilicate glass/Li-Na-K-feldspar composites for electronic applications. *Ceramics International*, *43*(17), 15068-15073.
51. Akkal, R., & Ouldhamou, M. (2015). Comparative study of mineral processing applied to the local feldspar's assessment. In Proceedings of the *24th International Mining Congress of Turkey*, 1135-1143.

52. Skorina, T., & Allanore, A. (2015). Aqueous alteration of potassium-bearing aluminosilicate minerals: from mechanism to processing. *Green Chemistry*, *17*(4), 2123-2136.
53. Kurt, H., & Arık, F. (2015). Mineraloji. *Nobel Yayın* No.29677, Ankara, 1-258.
54. Crangle, R. D. (2011). Mineral resource of the month: gypsum. *Earth*, *56*(8), 27.
55. Coquard, P., Boistelle, R., Amathieu, L., & Barriac, P. (1994). Hardness, elasticity modulus and flexion strength of dry set plaster. *Journal of Materials Science*, *29*(17), 4611-4617.
56. Arikan, M., & Sobolev, K. (2002). The optimization of a gypsum-based composite material. *Cement and concrete research*, *32*(11), 1725-1728.
57. Sievert, T., Wolter, A., & Singh, N. B. (2005). Hydration of anhydrite of gypsum ($CaSO_4$. II) in a ball mill. *Cement and concrete research*, *35*(4), 623-630.
58. Meriño-Gergichevich, C., Alberdi, M., Ivanov, A. G., & Reyes-Díaz, M. (2010). Al^{3+}-Ca^{2+} interaction in plants growing in acid soils: al-phytotoxicity response to calcareous amendments. *Journal of soil science and plant nutrition*, *10*(3), 217-243.
59. Addadi, L., Raz, S., & Weiner, S. (2003). Taking advantage of disorder: amorphous calcium carbonate and its roles in biomineralization. *Advanced Materials*, *15*(12), 959-970.
60. Svenskaya, Y., Parakhonskiy, B., Haase, A., Atkin, V., Lukyanets, E., Gorin, D., & Antolini, R. (2013). Anticancer drug delivery system based on calcium carbonate particles loaded with a photosensitizer. *Biophysical chemistry*, *182*, 11-15.
61. Ikoro, D. O., Okereke, C. N., Agumanu, A. E., Isreal, H. O., & Ekeocha, N. E. (2012). Geochemistry of the calc-silicate rocks of Igarra, southwestern Nigeria. *Inter J Emerging Trends Eng Dev*, *2*(2), 35-46.
62. Lee, S. Y., Chang, B., Kang, S. A., Seo, J., & Lee, Y. J. (2021). Effects of temperature and saturation on the crystal morphology of aragonite ($CaCO_3$) and the distribution coefficient of strontium: study on the properties of strontium incorporation into aragonite with respect to the crystal growth rate. *Korean Journal of Mineralogy and Petrology*, *34*(2), 133-146.
63. Kamhi, S. R. (1963). On the structure of vaterite $CaCO_3$. *Acta Crystallographica*, *16*(8), 770-772.

64. Tait, K. T., Sokolova, E., Hawthorne, F. C., & Khomyakov, A. P. (2003). The crystal chemistry of nepheline. *The Canadian Mineralogist*, *41*(1), 61-70.
65. Nalluri, S., & Ragi, M. R. (2020). Nepheline Syenite: A Potential Alternative for Feldspar in the Mineral Industry—A Case Study from SE India. *J. Indian Geophys. Union*, *24*, 33-38.
66. Skenderi, K., Memedi, H., Berisha, A., Thaçi, V., Aggrey, P., Haziri, V., & Reka, A. A. (2025). Perlite: characterization, modification and applications. *Journal of Natural Sciences & Mathematics*, *10*.
67. Erdem, T. K. (2005). Investigation on the pozzolanic property of perlite for use ın producing blended cements. Doctoral dissertation, Middle East Technical University, Turkey.
68. Kogel, J. E. (Ed.). (2006). Industrial minerals & rocks: commodities, markets, and uses. *SME*.
69. Angelopoulos, P. M. (2024). Insights in the physicochemical and mechanical properties and characterization methodology of perlites. *Minerals*, *14*(1), 113.
70. Kogel, J.E., Trivedi, N.C., Barker, J.M., Krukowski, S.T., 2006. Industrial Minerals & Rocks (7^{th} Edition). Published by Society for Mining, Metallurgy, and Exploration, Inc., Colorado, 1507 p.
71. Virta, R. L., & Revette, D. (2006). Wollastonite. *Mining Engineering*, *58*(6), 61-62.
72. Nour, W. M. N., Mostafa, A. A., & Ibrahim, D. M. (2008). Recycled wastes as precursor for synthesizing wollastonite. *Ceramics International*, *34*(1), 101-105.
73. Long, L. H., Chen, L. D., & Chang, J. (2006). Low temperature fabrication and characterizations of β-$CaSiO_3$ ceramics. *Ceramics International*, *32*(4), 457-460.
74. Armbruster, T., & Gunter, M. E. (2001). Crystal structures of natural zeolites. *Reviews in Mineralogy and Geochemistry*, *45*(1), 1-67.
75. Dikmen, Z., & Orhun, Ö. (2013). Manyetik modifiye edilmiş sentetik ve doğal zeolitlerin hazırlanması ve bazı fiziksel özelliklerinin kıyaslanması. *Anadolu University of Sciences & Technology A: Applied Sciences & Engineering*, 14(1).
76. Fertu, D. I. T., & Gavrilescu, M. (2012). Application of natural zeolites as sorbents in the clean-up of aqueous streams. *Environmental Engineering & Management Journal*, *11*(4).

77. Muga, H. E., & Mihelcic, J. R. (2008). Sustainability of wastewater treatment technologies. *Journal of environmental management*, *88*(3), 437-447.
78. Mumpton, F. A. (1985). Using zeolites in agriculture. *In Congress of the US, Office of Technology Assessment: Washington*, 144-149.
79. Ozaydin, S., Kocer, G., & Hepbasli, A. (2006). Natural zeolites in energy applications. *Energy Sources*, Part A, *28*(15), 1425-1431.

Chapter 8

FUTURE DIRECTIONS IN COMPOSITE MATERIALS AND THEIR INTEGRATION WITH GREEN TECHNOLOGIES

Almusa ATAMALİYEV[1] , Altunay İSKENDERLİ[2], Temel Kan BAKIR[3]

1. INTRODUCTION

One of the primary tasks facing materials science and engineering in the 21st century is the creation of material systems that are efficient both technologically and ecologically [1,2]. In parallel 4.0 industrial revolution, materials technologies have oriented themselves toward smart, sustainable, and green production models. Against this backdrop, composite materials assume particular strategic importance. Unlike conventional metals and ceramics, composite materials by virtue of their multiphase structure-combine high mechanical strength with low mass density. Their key advantages include corrosion resistance, shape stability, tunable thermal and electrical properties, and energy efficiency. In recent years, global industry has focused not only on product performance, but also on its environmental footprint . Concepts such as the green economy, sustainable manufacturing, and the circular economy have entered the everyday lexicon of engineering laboratories and industrial enterprises alike. According to statistical forecasts, the global composites market exceeded USD 95 billion in 2023 and is expected to reach USD 140 billion by 2030 (Market Research Future, 2024). The main drivers of this growth are, the use of composites in the renewable energy sector (wind turbines, solar panels) [3] shift to lightweight materials in transportation to reduce fuel consumption the expanding adoption of bio-based raw materials and recycling technologies [4]. For industrially developing countries such as Azerbaijan and Türkiye, the ecological integration of composite technologies is doubly significant: on the one hand, it ensures the efficient use of local resources

[1] Phd. Student, Department of Chemistry/Faculty of Science, Kastamonu University, Türkiye, almusa.atamaliyev@adpu.edu.az ,(ORCID: 0009-0009-8887-6149)
[2] Lecturer, Department of Education/Faculty of Management, Azerbaijan State PedagogicalUniversity,Bakü,Azerbaijan,altunayi155@sabah.edu.az,(ORCID:0009-0000-1904-6250)
[3] Prof.Dr.Department of Chemistry/Science Faculty, Kastamonu University, Kastamonu/Türkiye,temelkan@kastamonu.edu.tr,(ORCID : 0000-0002-7447-1468)

(basalt, clay, petro-polymers); on the other, it supports the formation of new industrial models aligned with green energy policy. Accordingly, the aim of this study is to analyze, on a scientific basis, contemporary development trends in composite materials, their integration with green technologies, and a comparative view of Azerbaijan with Türkiye scientific and applied experience .A composite material is a multiphase heterogeneous system obtained by combining two or more components with distinct physical, chemical, and mechanical properties . In such systems, the components complement each other to yield new, superior properties [5-7]. Reinforcing phase (fiber, particle, or powder) enhances mechanical strength and elasticity .The interfacial interaction between these phases determines the overall behavior of the material. Ideally, the interface optimizes stress distribution and prevents deformation.Historical milestones antiquity, Humans produced primitive composites from natural combinations (clay and straw, wood and pitch, sand and bitumen). Many elements of Egyptian pyramids and Mesopotamian architecture used such composites. Engineering structures emerged from combinations of metal and wood (iron bridges, ship hulls) . 20th century: Polymer-based fiber composites (fiberglass, kevlar, carbon fiber) revolutionized industry, gradually replacing metals in aerospace structures . 21st century: Advances in nanotechnology enabled composite design at the molecular level. Nanoscale particles and biopolymers impart both excellent mechanical performance and biocompatibility. Historical evolution shows that composites have accompanied all phases of human technological creativity [7]. Whereas mechanical durability was the primary goal in antiquity, today the focus is sustainability, recyclability, and ecological responsibility .The scholarly literature emphasizes that reliable measurement, statistical modeling, and systematic optimization are foundational to sustainable technological progress. Applied to materials science, each new composite system is tested not only for mechanical metrics, but also for ecological indicators. Contemporary materials engineering therefore foregrounds the notion not merely of strong material, but of responsible material.

2. PROPERTIES OF MODERN COMPOSITE MATERIALS

Based on the matrix type, modern composites are divided into four main groups, each with specific technological and ecological advantages [7]. Polymer matrix composites (PMCs) matrices include epoxies, polyesters,polyamides, and thermoplastics; reinforcement typically comprises glass, carbon, or aramid fibers. Advantages, low weight and high elasticity; ease of forming (lay-up,

vacuum bagging, etc.); lower production costs and broad applicability. Applications, aerospace, automotive, marine engineering, sporting goods .

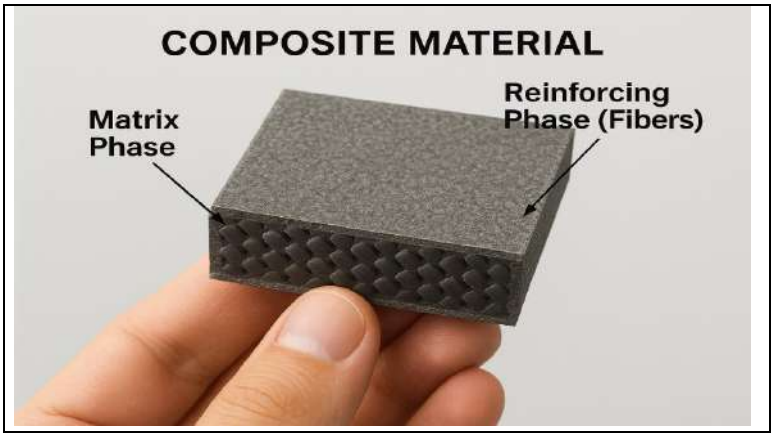

Figure .1 Classification and types of modern composites[3,7,9].

2.1 Metal matrix composites (mmcs)

Matrices are aluminum, magnesium, and titanium alloys; reinforcements include SiC, Al_2O_3, or carbon nanotubes [7]. Advantages: capability at high temperatures; high strength-to-density ratio; oxidation resistance.Applications: aerospace technologies, defense industry, high-speed transport systems .

2.2 Ceramic matrix composites (cmcs)

Matrices are ceramicbased (SiC, Al_2O_3, ZrO_2) and remain stable at very high temperatures [7]. Advantages: resistance to wear and erosion; thermal stability and dimensional constancy [8,9].Applications:gas turbines, combustion chambers, thermal protection panels of spacecraft .

2.3. Biocomposites and nanocomposites

Reinforcements include plant-derived fibers (flax, bamboo, sisal, kenaf) or nanometer-scale particles (graphene, nanotubes, nanoclays). Their advantages include biodegradability, dependence on natural resources, reduced carbon footprint, and ecological compatibility. These systems are at the core of green production and are aligned with the UN sustainable development goals (SDGs). Additional scientific aspects rheology: flow, viscosity, and control of molding processes; thermal behavior, conductivity, thermal expansion, and flammability [7,9]; Microstructure analysis by using SEM, XRD, and EDS to study phase morphology .

2.4. Industrial application areas of composite materials

The wide industrial adoption of composites is explained by their unique multiphase structure and adaptability to varied engineering demands Thanks to high strength to weight ratios, corrosion resistance, and thermal chemical stability, composites have gradually displaced metals and ceramics across numerous technological domains [9]. Their use carries strategic importance not only for technical efficiency but also for energy savings and environmental responsibility.

2.4.1. Aerospace

Since the late 20th century, carbon fiber reinforced polymers (CFRPs) have defined a transformative era . In modern aircraft such as the Boeing 787 Dreamliner and Airbus A-350, composites account for more than 50% of structural content. This reduces overall aircraft mass by 20–25%, yielding substantial fuel savings and improving passenger comfort via vibration damping and sound insulation .

2.4.2. Automotive and Energy

Composite panels, bumpers, engine covers, and structural components enhance safety, aerodynamics, and fuel efficiency. Companies like Tesla, BMW, and Toyota have transitioned to hybrid structures built from carbon- and glass-fiber composites, thereby lowering CO_2 emissions and optimizing thermal management of battery systems [10]. Composites spearhead the green energy transition . Wind, blades of 80–100 meters are feasible only with high-modulus composites . Solar, polymer-composite frames are light and corrosion-resistant, extending photovoltaic panel lifetimes beyond 25 years [10]. Hydrogen, carbon-fiber tanks offer reliable storage at pressures up to 700 bar .

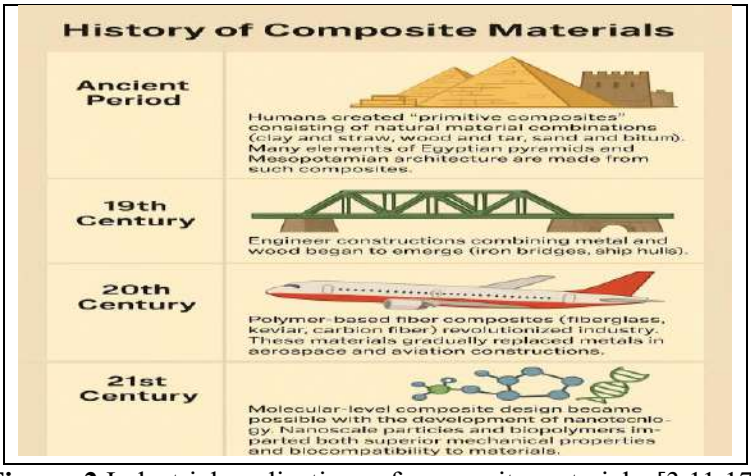

Figure .2 Industrial applications of composite materials. [3,11,17]

Figure.3 Sustainable material flow and circular economy concept[13,14]

2.4.3. Medical engineering and biotechnology

Biocompatible composites (PLA, chitosan, hydroxyapatite systems) are used in orthopedic implants, artificial joints, and prosthetics, combining biocompatibility with tissue integration .Thus, industrial adoption of composites is grounded not only in strength and lightness, but also in the principles of sustainable production and the green economy [11-17].

3. THE CONCEPT AND PRINCIPLES OF GREEN TECHNOLOGIES

Green technologies are set of technological systems that enhance industrial productivity while preserving ecological balance, ensuring resource efficiency and zero-waste production . This concept is one of the main vectors of the UN 2030 Agenda for sustainable development .Five core principles of green technologies; As follows;energy efficiency and resource conservation minimizing energy use in production ,use of renewable energy sources integrating solar, wind, and bioenergy into technological cycles, recycling and circular economy returning used products to the production loop as raw material. Reduction of harmful emissions and waste minimizing CO_2 and VOC releases,use of eco-friendly materials prioritizing biopolymers, natural fibers, and water-based resins .In the composites industry these principles manifest as: adoption of bio-based polymers (PLA, chitosan, lignin, starch) as ecological alternatives to petro-polymers ; utilization of secondary raw materials (e.g., micronized metal/ceramic waste as fillers) [12];low-temperature molding and microwave-assisted synthesis (up to 30 % energy reduction); CO_2-based polymerization (carbon capture and utilization). Green technologies thereby optimize the balance among ecological responsibility, economic efficiency, and technological innovation [17].

3.1. The role of composites in the green economy

A green economy is an economic model that enables ecosystem restoration and efficient use of natural resources [17,18]. Materials science, and composite technologies in particular, play a crucial role in this model [17,18].Composites enable energy savings, emission reductions, and sustainable production cycles across many sectors; Automotive, lightweight composite panels reduce average CO_2 emissions by 90 kg per ton of vehicle mass. Construction, panels made from recycled fibers and biopolymers improve building thermal insulation by 15–20 %. Energy, composites in wind and solar systems extend service life and reduce maintenance costs.The world economic forum (WEF, 2024) estimates that widespread deployment of composite-based technologies could reduce industrial waste (18–22)% by 2035 significant both economically and environmentally. Composites align directly with the SDGs: SDG 7 (Affordable and Clean Energy), SDG 9 (Industry, Innovation and Infrastructure), SDG 12 (Responsible Consumption and Production), SDG 13 (Climate Action) .Thus, composite production is not merely a technological process; it is a core component of an ecological economy [17,18].

3.2. Zero-Waste Technologies and the Importance of Recycling

A key challenge in composites is the difficulty of recycling multiphase systems, as separating polymer, metal, and ceramic components requires complex physical/chemical processes . Yet, the past decade has seen notable progress through zero-waste manufacturing Main approaches[14].

Mechanical recycling: end-of-life parts are milled and the powder is reused as fillers-low cost and environmentally safe thermochemical recovery, pyrolysis and gasification decompose the matrix while preserving fiber integrity-effective for carbon and glass fibers Chemical depolymerization: polymer matrices are broken down to monomers for repolymerization .Bio-processing: enzymatic conversion of natural polymers the cleanest approach [17]. Economic and ecological benefits (10-15%) reduction in production costs decreased emissions and energy use [17]; returning secondary raw materials to industrial circulation minimizing impacts on land and water [17] Accordingly, the industry is transitioning from make and dispose paradigm to waste-to-resource concept, positioning materials science as a driver of the ecological economy [17,18].

3.3. Rare earth elements(RREs) and role of ecological

Rare-earth elements (REEs) the lanthanides plus scandium (Sc) and yttrium (Y) are indispensable in modern technologies and high-performance materials.They optimize the mechanical, electrical, and magnetic properties of composites. Functional roles in composites;adding REEs to composite matrices (especially metal and ceramic systems) can increase corrosion resistance by 25–35 %[22], improve thermal stability up to 30 % optimize electrical conductivity and magnetic behavior, for instance, cerium (Ce) and neodymium (Nd) improve structural stabilityin Al- and Mg-matrix composites. CeO_2 promotes passivation of oxide films, substantially reducing corrosion rates; Nd_2O_3 can enhance magnetic properties and thermal conductivity [8],applications in ecological engineering;catalysts REE oxides (CeO_2, La_2O_3) reduce NO_x and CO in automotive exhaust, Energy storage and renewables: Nd-Fe-B magnets with high energy density are used in wind turbines and electric motors, Photocatalysis: TiO_2–CeO_2 composites activated under UV are applied in water and air purification, recovery and bio-extraction;. Although REE recycling is challenging, recent progress in bio-leaching using microorganisms (*Aspergillus niger*, *Bacillus subtilis*) enables environmentally safer extraction from natural sources and residues, forming key line of green metallurgy [20-26].

3.4. Energy Efficiency and Principles of Sustainable Production

Energy efficiency is fundamental to the economic and ecologicalsustainability of composite manufacturing.Traditional methods often require high temperatures and pressures, increasing energy use and carbon emissions. Modern approaches prioritize low-energy, low-emission technologies . Key directions;Low-temperature synthesis and molding,sol-gel, microwave and ultrasonic-assisted techniques can reduce energy consumption by 30–40 %, while improving matrix homogeneity and particle dispersion. Heat recovery systems: process heat is recuperated for use in other stages, improving LCA metrics, Energy audits and life cycle assessment (LCA): energy use, waste volume, and carbon footprint are quantified at each stage to optimize production [23,24], Local raw materials: leveraging regional resources (basalt, clay, plant fibers) reduces import dependence, transport distances, and strengthens local economies [27,28].Regional İnitiatives Azerbaijan: new polymer–composite production line at Sumgait Chemical Industrial Park is powered by renewables; waste heat is recirculated, achieving up to 28 % energy savings [28]. Türkiye: Under Tübitak and Aselsan’s Eco-Compositesinitiative, biopolymer-based,

thermally robust, and energy-efficient materials are being developed [26, 27-31].These initiatives underpin a green industrial transformation in the region [27].Biocomposites are natural fibers and biobased matrices, biodegradable, environmentally benign, and aligned with the circular economy plant fibers (flax, bamboo, jute, sisal, coir); matrices (PLA, starch, chitosan, lignin). They enable the reintroduction of agricultural waste into industrial cycles, thereby reducing energy consumption and minimizing carbon footprints. Biocomposites see broad use in thermal and acoustic insulation, and in medical and packaging industries, embodying the "green materials" ethos of ecological engineering Nanocomposites Incorporating 1–100 nm particles (graphene, CNTs, SiO_2, Al_2O_3, TiO_2,.) dramatically improves performance due to high surface-area-to-volume ratios . Even 1–2 % nano-additives can: reduce weight by 20 %; increase mechanical strength by up to 50 %; raise thermal conductivity by 30–40 % . Nanocomposites are valued as high-performance, multifunctional materials in defense, aerospace, electronics, and biomedicine [32, 34].Next-generation graphene–polymer systems are already deployed in energy-storage devices (supercapacitors, Li-ion batteries) [34, 36].Thus, bio and nanocomposites define the next stage of green technologies at the nexus of ecological, economic, and technological efficiency [32].Experimental setup for 3d composite research and additive manufacturing.Digital transformation has opened a new era in materials engineering [31].Additive manufacturing (3D printing) maximizes flexibility, economy, and precision in composite production [4]. Processes once reliant on molding, pressing, and sintering are now executed layer-by-layer. Advantages of 3d composites,zero-waste production using only required material quantities , 40–60% increases in production speed [31],mass customization of shapes and dimensions reduced capital expenditure by eliminating molds and tooling [31].Materials include carbon-fiber-reinforced thermoplastics, nano-additive resins, and biopolymer composites, yielding optimal structural stability and energy savings [33].Regional research collaborations.The "3D-BioComp" project between Azerbaijan Technical University (AzTU) and Middle East Technical University (METU, Türkiye) has achieved notable results in modeling mechanical and thermal behavior of 3D biocomposites, including development of biopolymer systems using local natural fibers pilot production via 3D printers AI-based performance prediction [34].Such collaborations provide a scientific foundation for localizing green technologies and advancing digital manufacturing in the South Caucasus.The rapid expansion of the composites industry raises critical environmental issues: energy-intensive processes; CO_2 and other emissions; recycling challenges due

to multiphase structures; dependence on petro-based polymers; and long-term waste accumulation . Thus, the next phase involves not only inventing new materials, but also managing their ecological life cycles. Eco-design and Life Cycle Assessment (LCA) Products are no longer judged sufficient merely for mechanical robustness; instead, life-cycle thinking quantifies stages from raw-material sourcing through synthesis, shaping, service, repairability, and end-of-life reuse or recycling.

LCA measures carbon, water, and energy footprints, toxicity, and waste burden. Early integration of LCA compels ecologically acceptable choices from the outset, making materials science a component of eco-technological policy as well as mechanics. Bio-based and biodegradable materials A strong recent trend is the phased substitution of petro-based resins and matrices with biopolymers-especially PLA, PHA, natural structural fibers (flax, bamboo, jute, sisal), and lignin-starch-based fillers. Bio-matrix natural fiber architectures offer biodegradability without toxic residues under appropriate conditions and reduced waste volumes [37]. Studies show biocomposites can cut industrial waste by 40–60 % versus conventional polymer composites for the same function, especially in packaging, automotive interiors, and building insulation [39] Recycling and Zero-Waste Manufacturing The target is to eliminate the very notion of "waste."In practice: off-cuts, excess resin, and fiber remnants are immediately reincorporated as fillers mechanical milling creates secondary raw materials in thermoset epoxies, chemical depolymerization recovers reusable resin fractions This is the circular economy applied to composites: resources do not disappear; they change form and recirculate within the system. Energy and emissions management Composite production (autoclaves, high-pressure molding, high-temperature sintering) is energy-intensive.Industry advances along two parallel lines: powering parts of production with solar and wind energy digitalizing energy monitoring in workshops [33].IoT-based systems track real-time consumption, identify losses, and flag anomalies-reducing energy waste by ~25–30 % while VOC emissions control expedites green certification. These strategies recast the composites sector as a responsive environmental management system, not merely a materials factory.

The next decade prioritize intelligent, ecological, self-managing, and economically justified composite systems over merely "stronger materials" . Four focal areas emerge,Expansion of biocomposites Research targets: improving mechanical stability of natural fibers (flax, bamboo, hemp, jute), mitigating aging and moisture uptake; enhancing thermal/oxidative stability of biopolymer matrices to enable load-bearing uses. Bio-nano hybrids-natural fiber

matrices with CNTs, graphene, or nano-SiO_2 approach the balance of “fully ecological high mechanics” [32, 36].Smart and functional composites Active systems that: monitor structural health via embedded sensor fibers; “sense” load distribution; provide early warnings of damage or microcracking [34].These underpin predictive maintenance in aerospace, critical transport infrastructure (bridges, pipelines), medical implants, and defense [31, 34].Environment-responsive materials Self-healing composites: microencapsulated resins or self-healing phases restore integrity upon microcrack formation [34]. Biodegradable composites: designed to degrade without toxic legacy-relevant for medical implants, single-use industrial structures, and “trace-free” defense infrastructure [37, 39]. The objective is to pre-program the ecological fate of the material. Digitalization and AI, high-dimensional modeling, and big-data analytics shorten the design–test cycle by ~40 %: algorithms pre-optimize matrix–reinforcement ratios, nano-additive loadings, and processing temperatures; mechanical behavior is predicted prior to lab testing; models auto-calibrate from discrepancies with experiments-saving resources and accelerating time-to-market [34, 38].Azerbaijan and Türkiye are parallel-developing regional hubs in composites and green technologies, differing primarily in institutional approach. In both countries, composites have become part of national industrial strategy. Azerbaijan Industrial infrastructure: At the Sumgait Chemical Industrial Park and enterprises producing polymer- and aluminum-based semifinished products, composite structural elements and coating systems are manufactured, with a portion of raw materials sourced locally (petro-polymers, aluminum powders, etc.) . Scientific base: Research under ANAS has yielded results in ceramic-matrix composites and phases modified with rare-earth elements, chiefly for defense, high-temperature coatings, and energy systems [35]. Policy and priorities: For 2025–2030, state industrial programs explicitly prioritize “green industry,” “zero-waste manufacturing,” and the “circular economy,” aimed at environmental protection and reduced dependence on imported high-tech materials.Türkiye Research–engineering integration: Institutions such as Tübitak Mam, Aselsan, and the Sabancı University Composite Technologies Center of Excellence operationalize university-industry partnerships, rapidly transferring lab results to defense, aerospace, automotive, and energy sectors . Biocomposites and energy storage: Green composites are developed not only with bio-based matrices but also for energy-storage components (high-density battery casings, thermal management).Programs such as “GreenMAT” and “BioCompTech” co-optimize mechanical and functional (thermal, electrical,

magnetic) roles . Regulatory framework: Since 2023, the “Green Deal Action Plan” has embedded carbon neutrality, emissions management, and resource efficiency in binding industrial regulation, elevating green composite production from scientific initiative to state-regulated standard.

Figure. 5 Comparative ınitiatives in green composite technologies[10,31,32].

Azerbaijan is strengthening its resource and materials base (raw materials, energy, geostrategic position), while Türkiye focuses on commercialization and industrial-scale deployment .The ideal regional model merges these strengths: Azerbaijan leads in raw materials and foundational research; Türkiye advances applied engineering and market scaling-together forming a unified South Caucasus–Anatolia “green composites ecosystem” .

4. CONCLUSIONS AND RECOMMENDATIONS

Our analysis shows that composites are not merely structural solutions to technical problems; they embody the ideological core of future industry low carbon economy, resource security, zero-waste production, ecological responsibility, and high-tech sovereignty. Composites are pivotal to energy efficiency, Lightweight structures reduce fuel use in transport and extend service life in renewable systems (wind, solar), directly lowering CO_2 emissions. Rare-earth elements and functional additives elevate performance to a new tier, enhancing mechanics and thermal stability while enabling high-value ecological-engineering applications (catalysis, water treatment, energy storage) [35].Biocomposites and nanocomposites are becoming mainstays of green industry biodegradability and valorization of agricultural waste reinforce the circular economy; nanocomposites deliver maximum mechanical functional

performance at minimal mass. Digitalization, 3D printing, and AI are reshaping manufacturingadditive processes realize zero-waste concepts. Azerbaijan–Türkiye collaboration can accelerate green composite technologies via joint labs, common material standards, and harmonized environmental norms positioning the South Caucasus Anatolia corridor as a high-tech green manufacturing hub. Azerbaijan with Türkiye “Green Composites Research Center” specializing in biocomposites, REE-modified composites, and zero-waste manufacturing. Industrial-scale recycling lines: Create regional parks for mechanical milling, chemical depolymerization, and bio-recovery of composite waste-generating ecological and economic value chains. Education and workforce: Integrate ecological materials science, LCA, circular economy, and green engineering modules into university curricula to train a new generation that unites classical materials engineering with environmental responsibility Regulatory framework: Develop unified regional standards for composite-waste management that both limit industrial waste volumes and assign life-cycle responsibility to producers. Local raw-materials strategy: Prioritize local basalt fibers, polymer resources, REE components, and agro-fiber feedstocks to reduce import dependence and ensure raw-material security . As result ,the development trajectory of composites now extends beyond creating new materials; it articulates a new industrial philosophy lightweight, intelligent, clean, and responsibl supporting regional economic sovereignty and addressing global ecological challenges [40].

REFERENCES

1. Ashby, M. F. (2013). Materials and the environment: Eco-informed material choice (2nd ed.). Elsevier.
2. Binnemans, K., Jones, P. T., Blanpain, B. (2013). Recycling of rare earths: A critical review. *Journal of Cleaner Production, 51*, 1–22.
3. Brøndsted, P., Lilholt, H., & Lystrup, A. (2005). Materials for wind turbine blades. *Annual Review of Materials Research, 35,* 505–538.
4. Caminero, M. A., Chacón, J. M. (2019). Additive manufacturing of polymer-matrix composites: *A review. Polymers, 11*(3), 1–32.
5. Das, S. (2015). Life cycle assessment of carbon fiber manufacturing processes. *Journal of Cleaner Production, 102*, 461–472.
6. Faruk, O., Bledzki, A. K. (2012). Biocomposites reinforced with natural fibers: 2000–2010. *Progress in Polymer Science, 37*(11), 1552–1596. https://doi.org/10.1016/j.progpolymsci.2012.04.003.
7. Gibson, R. F. (2016). Principles of composite material mechanics (4th ed.). CRC Press.
8. Gupta, C. K., & Krishnamurthy, N. (2005). Extractive metallurgy of rare earths (2nd ed.). CRC Press.
9. Hull, D., & Clyne, T. W. (1996). An introduction to composite materials (2nd ed.). Cambridge University Press.
10. Koronis, G., Silva, A., Fontul, M. (2013). Green composites: A review of adequate materials for automotive applications. *Composites Part B: Engineering, 44*(1), 120–127.
11. Mohanty, A. K., Misra, M., Drzal, L. T. (2005). Natural fibers, biopolymers, and biocomposites. CRC Press.
12. Oliveux, D., Dandy, L. O.,Leeke, G. A. (2015). Current status of recycling of fibre reinforced polymers: Review of technologies, reuse and resulting properties. *Progress in Materials Science, 72,* 61–99.
13. Pimenta, S., & Pinho, S. T. (2011). Recycling carbon fibre reinforced polymers for structural applications. *Composites Part A: Applied Science and Manufacturing, 42*(6), 1116–1123.
14. Pickering, S. J. (2016). Recycling technologies for thermoset composite materials Current status. *Composites Part A: Applied Science and Manufacturing, 91,* 167–188.
15. Shahzad, M. (2017). Hemp fiber composites A review. *Journal of Cleaner Production, 144*, 394–406.

16. Tekinalp, H. L., Kunc, V. (2014). Highly oriented carbon fiber–polymer composites via additive manufacturing. *Composites Part B: Engineering, 56*, 241–245.
17. UNEP (united nations environment programme), (2023). Circular economy and green technology outlook 2023. Nairobi: UNEP Publishing. https://www.unep.org/resources/report.
18. World Economic Forum (WEF). (2024). Circular transformation of industries: The role of partnerships. Geneva: WEF Publications. https://www.weforum.org/publications.
19. Zhang, Y., Wang, L.,Kim, S. H. (2022). Biocompatible polymer composites for orthopedic applications: Recent progress and challenges. *Materials Today Bio, 15*, 100–122.
20. Zhu, X., Li, J., & Chen, Y. (2023). Bioleaching and recovery of rare-earth elements from e-waste and red mud: A sustainable approach. *Journal of Hazardous Materials, 445*, 130562.
21. ASTM International. (2017). Astm d3039/d3039m-17: Standard test method for tensile properties of polymer matrix composite materials. ASTM International.
22. IEC (International electrotechnical commission), (2019). IEC 61400-1: Wind energy generation systems Part 1: Design requirements. Geneva: IEC Publications.
23. ISO(International organization for standardization), (2006a). ıso 14040: environmental management life cycle assessment -principles and framework. geneva: ıso.
24. ISO(International organization for standardization), (2006b). ıso 14044: environmental management life cycle assessment - requirements and guidelines. geneva: ıso.
25. Sabancı University composite technologies center of excellence, (2023). greenmat and biocomptech project summaries. İstanbul: Sabancı Publications.
26. Aselsan research center. (2023). Eco-composites and lightweight structures annual report, Ankara: Tübitak press.
27. Tübitak Marmara Araştırma Merkezi (MAM), (2024). Türkiye'de yeşil kompozit ve biyokompozit teknolojilerinin gelişimi raporu. Ankara: Tübitak Yayınları.
28. Government of Azerbaijan,(2021). Azerbaijan 2030: National priorities for socio-economic development. Baku: cabinet of ministers of the Republic of Azerbaijan. https://president.az/articles/50474.

29. Republic of Türkiye ministry of trade, (2021). Yeşil mutabakat eylem planı (green deal action plan), Ankara: TicaretBakanlığı. https://ticaret.gov.tr/yesilmutabakat
30. European Commission. (2019). The european green deal (com(2019) 640 final). brussels: publications office of the european union. https://eur-lex.europa.eu/legal-content/en/txt/?uri=celex:52019dc0640.
31. Fidan, I., Imeri, A. (2019). The trends and challenges of fiber reinforced polymer composite 3D printing. Composites Part B: Engineering, 169, 318–326. https://doi.org/10.1016/j.compositesb.2019.04.048.
32. Jiang, L., Koltzenburg, S.,Mezzenga, R.. (2021). Advances in sustainable composites and nanocomposites for green energy technologies. Progress in Materials Science, 118, 100777. https://doi.org/10.1016/j.pmatsci.2021.100777.
33. Li, Y., Zhang, Z., Liu, W. (2022). Energy-efficient manufacturing of polymer composites: A review of recent advances. Journal of Cleaner Production, 380, 135073. https://doi.org/10.1016/j.jclepro.2022.135073.
34. Liu, Y., Xie, X., Zhang, H. (2023). Artificial intelligence-assisted materials design for next-generation composites,materialstoday, 57, 1–14. https://doi.org/10.1016/j.mattod.2023.02.007.
35. Mamedov, S., & Sadigova, L. (2021). Applications of rare-earth elements in materials engineering. baku: anas ınstitute of materials science press.
36. Maqsood, M., Shah, S. A., Kausar, A. (2020). Nanocomposite materials for sustainable energy applications. Renewable and sustainable energy reviews, 132, 110-123.
37. Nguyen, Q. T., Dao, P. H. (2022). Biodegradable polymer nanocomposites for environmental applications: A review. E*nvironmental Nanotechnology, Monitoring & Management, 18*, 100743.
38. Niazi, A., Asghar, A. (2023). Machine learning in composite manufacturing: Optimization of process parameters for energy efficiency. *Computational Materials Science, 220*, 112 432.
39. Sabir, M. I., Xu, X.,Li, L., (2020). A review on biodegradable polymeric materials for environmental applications. *Materials, 13*(22), 4995.
40. World economic forum (2024). Circular industry solutions for a global plasticstreaty.geneva:worldeconomicforum.https://www.weforum.org/publications/circular-industry-solutions-2024.